UNIVERSITÀ DI PISA
FACOLTÀ di
INGEGNERIA

D.E.S.T.eC.

The University of
Nottingham

Electromagnetic and thermal modelling, sizing and design refinement of a permanent magnet synchronous motor

Supervisors:

Prof. Dr. P.Bolognesi - *University of Pisa*

Prof. Dr. C.Gerada - *University of Nottingham*

Student:

Stefano Nuzzo

Academic Year 2012/2013

Contents

Table of Figures

PREFACE

With the development of permanent magnet materials and the techniques of driving an electrical machine, the use of permanent magnet motors (PMM) has rapidly increased in many industrial areas by replacing induction motors because of the following benefits: no electrical energy is absorbed by the field excitation system and thus there are no excitation losses which means substantial increase in the efficiency; higher torque and/or output power per volume than when using electromagnetic excitation; better dynamic performance than motors with electromagnetic excitation (higher magnetic flux density in the air gap); simplification of construction and maintenance; reduction of prices for some types of machines. Moreover, the improvements made in the field of semiconductor drives have meant that the control of brushless motors has become easier and cost effective, with the possibility of operating the motor over a large range of speeds and stil maintaining a good efficiency.

According to [8], permanent magnet motors are classified into: d.c. commutator motors, d.c. brushless motor and a.c. synchronous motors. The construction of a PM d.c. commutator motor is similar to a d.c. motor with the electromagnetic excitation system replaced by PMs. PM d.c. brushless and a.c. synchronous motor designs are practically the same: with a polyphase stator and PMs located on the rotor. The only difference is in the control and shape of the excitation voltage: an a.c. synchronous motor is fed with more or less sinusoidal waveforms which in turn produce a rotating magnetic field. In PM d.c. brushless motors the armature current has a shape of a trapezoidal waveform.

This thesis work will focus on the design of permanent magnet synchronous motors. A synchronous machine is an electrical machine that operates at synchronous speed meaning the speed at which the magnetic field rotates. The synchronous speed depends on the frequency of the applied voltage and the number of poles in the machine.

The basic components are stator and rotor. The stator is also the armature of the synchronous machine. The stator core is made of thin laminations of highly permeable steel. The stator core is placed inside an aluminium frame. The main purpose of the frame is to provide mechanical support for the synchronous machine. Inside the stator core there is a plurality of slots. The coils that form a polyphase winding are arranged symmetrically in these slots. Synchronous machines usually operate at three phase power and the armature winding is thus made of three separate windings. The three phase windings may be connected to either star (Y) or delta (Δ) connection. The winding can be a single layer or a double layer winding. In a double layer winding there are two coil sides in a slot whereas in a single layer winding there is only one. The winding is an integer slot winding if the

number of slots per pole per phase is an integer, otherwise the winding is called a fractional slot winding.

The armature winding of the synchronous machine produces a revolving magnetic field. When the north pole of the field is just above the south pole of the rotor, the force attraction between the two poles starts to move the rotor. Because the rotor is heavy, it takes time before it can start moving, and by the time it starts to move, the revolving field has changed its polarity. Now there are poles with alike polarity close to each other and the repulsive force tries to move the rotor to the other direction. This means that the synchronous machine is typically not self-starting without a frequency converter [10].

The rotor is rotated at synchronous speed. In permanent magnet synchronous machines the main magnetic field is created by permanent magnets that are mounted to the rotor. The rotor core is either solid iron, or made of laminations. The permanent magnets can be mounted to the core in several ways. In surface permanent magnet machines, the magnets are mounted on the surface of the outer periphery of rotor laminations. The surface-mounted permanent magnet motor is commonly used for its simplicity for manufacturing and assembling. Since the relative permeability of the magnet material is close to one, this kind of structure has a large effective air gap, and the d-axis inductance is thus low.

Because the permanent magnets produce a constant flux in the air gap, the field weakening properties of a surface magnet machine are poor. Most of the current would go to demagnetization, and very little current would be left to produce torque. If high operation speed is needed, the nominal rotation speed of the surface mounted PMSM should thus be close to the needed operation speed. The surface magnet construction might also need a fibre glass band to make the construction mechanically robust enough in order to avoid the effects of the centrifugal force. One drawback is also that the frequency converter produces higher order harmonics. An advantage of the surface magnet construction is that the leakage flux is low, because there is no ferromagnetic path for the flux at the edges of the magnet. Reduced quadrature axis inductance decreases the armature reaction which leads into a smaller pole angle and higher torque. For this reason, less permanent magnet material is usually needed for the surface magnet machine than for the interior magnet machine [13].

The magnets can be also buried in the rotor. By burying magnets it is possible to employ flux concentration and to drive a motor over a wider speed range through the use of field weakening control. There are several types of rotors of interior permanent magnet machine and each type has its own advantages and specific applications. A common geometry is presented in Figure 1, where the magnets are in V-shape. This kind of construction is typically used in industry. A drawback of this kind of construction is that it requires usually more magnet material than the surface mounted magnets. The V-shaped interior permanent magnet construction is

also less robust mechanically, since there are only small iron bridges to hold the magnets. On the other hand, it is possible to use rectangular magnets which are easier to produce than the curved ones.

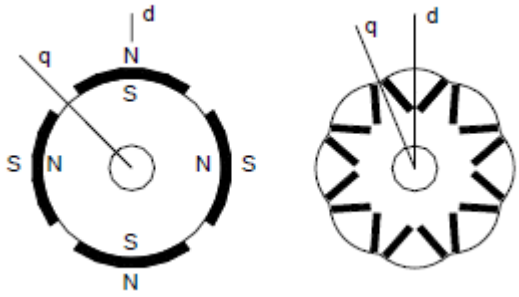

Figure 1. Two different permanent magnet rotor structures: surface rotor structure (left) and interior magnets (right)

In order to be able to produce efficient and compact PMSMs, the design criteria have to be known. There are certain properties that are interesting from the energy conservation point of view, for example efficiency, power density and power factor. These properties can be affected by changing several different design parameters which include pole pair number, the size of permanent magnets, the type of winding, etc. From an economical point of view, also the material costs have to be taken into account. For example the permanent magnet materials are usually rather expensive: compared to the price of copper, the price of NdFeB-magnet material is about eleven times higher [13], thus may be convenient reducing as much as possible the amount of magnets. It is evident that one of the key issues in the PMSMs design is the definition of the rotor geometry which has to satisfied the design specifications such as the rated torque and at the same time has to minimize the costs.

In the last years, in particular for IPMMs, different rotor geometries have been proposed and studied in the literature, based on analytical models, lumped parameter models, finite element analysis. Furthermore several design approaches and optimization techniques have been used in order to find the best solution inside a well-defined solution space. Due to many degrees of freedom, there is no unique approach to the rotor design of a PMSM.

Analytical models and lumped parameter models are really effective when the rotor structure is simple; when the rotor structure is complicated these kind of approaches are enough for orienting the designer in the right direction but it is not sufficiently precise for forecasting the exact machine performance. Another serious disadvantage of these methods is that they are not easy to be managed and require some finite analysis in order to take into account the saturation; otherwise disregarding the saturation leads to imprecise results. During the rotor design, it is

important to evaluate the torque ripple at both no-load and under load conditions, because in case of poor design choices, it could reach high values compromising the motor performances. Approaches like the analytical models and the lumped parameter models can not be used to quantify the torque ripple, for this reason the finite element analysis (FEA) needs to be adopted at least as last stage of refinement.

According to what it has been said until now, it is evident that the design of an electrical machine is is a multi-objective optimization problem. Because there are several parameters that have to be optimized, the final solution is always a compromise between different criteria.

ABSTRACT

This Master Thesis deals with the electromagnetic and thermal design of a permanent magnet synchronous motor, carrying out a comparison between a preliminary sizing and a finite element analysis aiming to validate the obtained results chasing a specific goal: the minimization of the cogging torque, i.e. the torque oscillations at nulls currents.

In the first chapter, the mathematical model and the main features of a PMSM are presented. The capability curves and the circle diagram are introduced to better describe the PMSM performances; at the end the concept of the design space applied to the design of a PMSM is exposed.

In the second chapter, a standard preliminary sizing based on analytical modelling of electrical machines is presented. The synthesis process is restricted to surface mounted permanent magnet synchronous machines because of their simple geometry. The described design procedure starts from the selection of free parameters not related to specific applications and leads to compute the main dimensions of the machine by calculating the magnetic voltages in all parts of the PMSM.

In the third chapter, the steps followed in order to validate the preliminary sizing by means of FEM analysis are explained. After a brief introduction to FEM, two design test cases are taken into account. In this thesis, the design refinement by FEM has a specific aim that is the cogging torque minimization by finding the best combination between magnet width and slot opening. Then, inserting the new obtained values of magnet span and slot opening, the analytical and FEM results are compared.

In the fourth chapter, the thermal problem for electrical machines is introduced and the main heat removal equations are presented. Then, an equivalent lumped-parameters thermal circuit is drawn with the purpose of keeping the temperatures under a certain level by choosing the most suitable convection-heat-transfer coefficient and thus the most efficient cooling system for both analyzed design test cases.

1 PERMANENT MAGNET SYNCHRONOUS MOTORS: MODELLING AND PERFORMANCE

1.1 Introduction

The theory of the vector control applied to induction motors has proved that the current is composed by two orthogonal components: the first one generates the rotor flux and the second one generates the torque. The permanent magnet synchronous motors do not need the current component that generates the rotor flux and so, with the same load condition, these motors allow to work with a higher power factor and higher efficiency respect with the induction motor. As it has already said above, using permanent magnets instead of the classic excitation system allows eliminating the drawbacks of this system like the mechanic problems related with rings and brushes and allows reducing the Joule losses. With respect to how permanent magnets are placed in the machine, the permanent magnet synchronous motors can be divided in two main classes: with the magnets positioned on the surface of the rotor, these are called surface permanent magnet synchronous motors (SPMSM), while with the magnets place inside the rotor, these are called interior permanent magnet synchronous motors (IPMSM).

From the functional point of view, the main difference between the SPMSM and the IPMSM lies in the mechanism of the torque production. The torque produced by SPMSM is only due to the interaction between the magnetic field generated by the stator winding and the magnetic field generated by the magnets. This torque term is usually known as permanent magnet torque. Differently, the torque produced by IPMSM has an additional component because the inductances of the q and d axis are different from each other and this is due to the rotor structure. From a magnetic point of view it may be noted that the rotor structure is isotropic because the relative permeability of the magnets is near to the unit. For this reason, the reluctances along the d- and q-axis are really similar if the motor is not saturated and thus the d- and q-axis inductances are basically the same. Yet, the rotor of IPMSM is an anisotropic structure from the magnetic point of view, because the d-axis flux meets more air than q-axis flux due to the fact that, along its path, it crosses the magnets. Hence the reluctance along the d- is greater than the q-axis one and consequently the d-axis inductance is less than the q-axis inductance. In Figures 1 and 2 the comments just explained are shown.

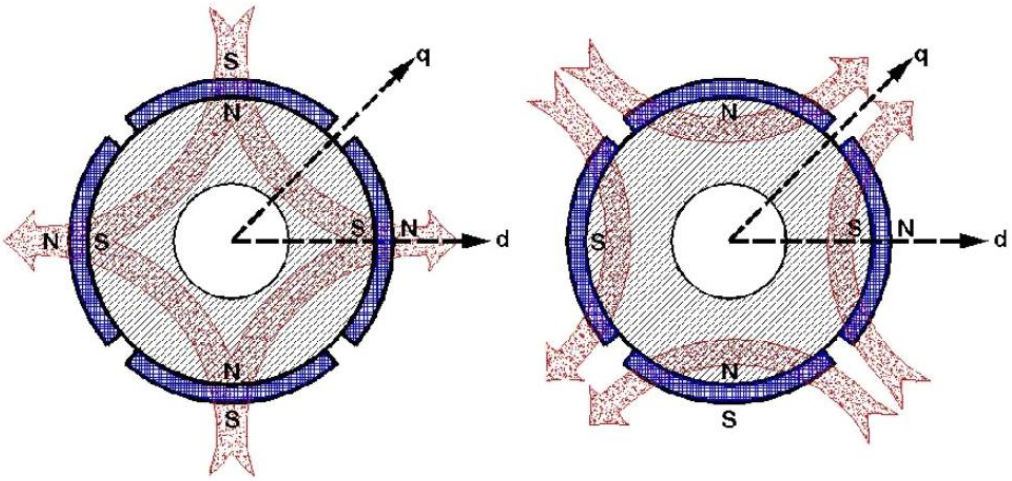

Figure 2.Possible flux paths in SPMSM

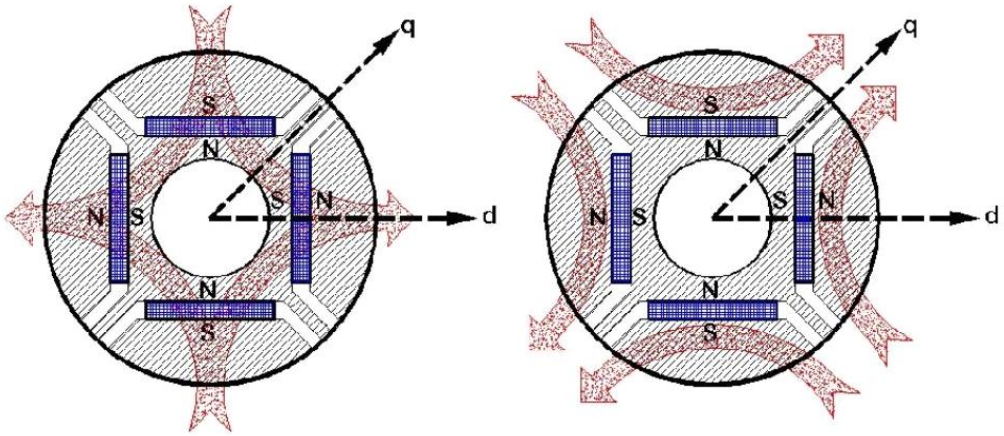

Figure 3.Possible flux paths in IPMSM

The high energy permanent magnets, such as rare earth or samarium cobalt, used for exciting the magnetic field of a PMSM, enable the PMSM to be significantly smaller than the induction motor and this aspect leads to the advantage of high torque/power density.

All PMSMs have a stator of conventional type used for three phase motors and as a consequence these kind of motors can be classified according to the rotor structure namely to the permanent magnets arrangement. With the permanent magnets on the external surface of the rotor, the air gap flux density is auto-limited by the permanent magnets properties. In order to increase the air gap flux density, the flux tube area should be reduced moving from the permanent magnet to the air gap and this is achieved by arranging permanent magnets in different ways inside the rotor structure.

Considering the rotor lamination, the IPMSM can be classified in radial or axial laminated motors. In the first case, the rotor is composed by a stack of laminations, isolated from each other and placed transversely along the shaft. In case of axially laminated rotor, the iron laminations are placed axially, properly bended to form a pack of laminations that constitute the rotor. SPMSM have radially laminated rotors and permanent magnets are not laminated because of their low electric conductivity. We will focus the modelling, sizing and design on these last motors.

1.2 The phase coordinate model

The phase coordinate model is based on the stator equations. One may introduce it under the hypotheses that the airgap flux density is sinusoidal, the iron losses are disregarded, the non-linear behaviour of the magnetic materials and the effect of the slots on the inductances are neglected. Assuming a star connection stator winding and with the usual symbols, the voltage-current equations and the flux-current relations in phase coordinate are:

$$\begin{bmatrix} V_a \\ V_b \\ V_c \end{bmatrix} = \begin{bmatrix} R & 0 & 0 \\ 0 & R & 0 \\ 0 & 0 & R \end{bmatrix} \begin{bmatrix} I_a \\ I_b \\ I_c \end{bmatrix} + \frac{d}{dt} \begin{bmatrix} \varphi_a \\ \varphi_b \\ \varphi_c \end{bmatrix}; \tag{1}$$

$$\begin{bmatrix} \varphi_a \\ \varphi_b \\ \varphi_c \end{bmatrix} = \begin{bmatrix} L_{aa} & L_{ab} & L_{ac} \\ L_{ba} & L_{bb} & L_{cc} \\ L_{ca} & L_{cb} & L_{cc} \end{bmatrix} \begin{bmatrix} I_a \\ I_b \\ I_c \end{bmatrix} + \begin{bmatrix} \varphi_{aPM} \\ \varphi_{bPM} \\ \varphi_{cPM} \end{bmatrix} \tag{2}$$

In a more compact form:

$$[V] = [R]\,[I] + \frac{d}{dt}[\varphi]; \tag{3}$$

$$[\varphi] = [L]\,[I] + [\varphi_{PM}] \tag{4}$$

Assuming that the machine under exam is isotropic and symmetric, the self and mutual inductances are:

$$\begin{aligned} L_{aa} &= L_l + L_{av} + \Delta L \cos 2\theta_m \\ L_{bb} &= L_l + L_{av} + \Delta L \cos(2\theta_m - 120) \\ L_{cc} &= L_l + L_{av} + \Delta L \cos(2\theta_m - 240) \end{aligned} \tag{5}$$

$$
\begin{aligned}
L_{ab} &= -\frac{1}{2}L_{av} + \Delta L\cos(2\theta_m - 120)\\
L_{bc} &= -\frac{1}{2}L_{av} + \Delta L\cos 2\theta_m\\
L_{ac} &= -\frac{1}{2}L_{av} + \Delta L\cos(2\theta_m - 240)
\end{aligned}
\tag{6}
$$

The flux linkage due to the effect of the permanent magnets is:

$$
\begin{aligned}
\varphi_{aPM} &= \varphi_{pm}\cos\theta_m\\
\varphi_{bPM} &= \varphi_{pm}\cos(\theta_m - 120)\\
\varphi_{cPM} &= \varphi_{pm}\cos(\theta_m - 240)
\end{aligned}
\tag{7}
$$

If (4) is replaced in (3), it may be obtained the following:

$$
[V] = [R]\,[I] + \frac{d[L]}{dt}[I] + [L]\frac{d\,[I]}{dt} + \frac{d}{dt}[\varphi_{PM}] \tag{8}
$$

From (8), one may get the torque expression by applying the power balance:

$$
[I]^T[V] = [I]^T\,[R]\,[I] + [I]^T\frac{d[L]}{dt}[I] + [I]^T[L]\frac{d\,[I]}{dt} + [I]^T\frac{d}{dt}[\varphi_{PM}]
$$

It is simple to demonstrate that $\frac{d([I]^T\,[L]\,[I])}{dt} = 2[I]^T[L]\frac{d[I]}{dt} + [I]^T\frac{d[L]}{dt}[I]$, so that (8) become:

$$
[I]^T[V] = [I]^T\,[R]\,[I] + \frac{1}{2}\frac{d([I]^T\,[L]\,[I])}{dt} + \frac{1}{2}[I]^T\frac{d[L]}{dt}[I] + [I]^T\frac{d}{dt}[\varphi_{PM}] \tag{9}
$$

where the first member is the total electric power, the first element of the second member represents the Joule losses, the second one is the stored electromagnetic energy and the last two terms represent the mechanical power.
From the mechanical power, the torque expression may be determined as a function of currents, inductances and thus the position of the rotor:

$$
Te = p\frac{P_{mecc}}{\omega_m} = \frac{1}{2}p[I]^T\frac{d[L]}{d\theta_m}[I] + p[I]^T\frac{d}{d\theta_m}[\varphi_{PM}] \tag{10}
$$

where p is the number of pole pairs and ω_m is the electric rotational speed and θ_m is the electric angle between the permanent magnet axis (d-axis) and the phase A winding axis.

$$
\theta_m(t) = \int_0^t \omega_m(\tau)d\tau + \theta_m(0)
$$

The equation (10) shows that the electromagnetic torque is composed by two terms: the first one is due to the anisotropy of the rotor structure, while the second one is due to the mutual interaction between the two electromagnetic fields generated by the stator winding and by the magnets placed on the rotor. Adding the equation that describes the mechanical balance on the shaft, it may be obtained the complete mathematical model in phase coordinate of an permanent magnet motor, which is a non-linear model of the fifth order:

$$
\begin{aligned}
&[V] = [R]\,[I] + \frac{d[L]}{dt}[I] + [L]\frac{d\,[I]}{dt} + \frac{d}{dt}[\varphi_{PM}] \\
&Te = p\frac{P_{mecc}}{\omega_m} = \frac{1}{2}p[I]^T\frac{d[L]}{d\theta_m}[I] + p[I]^T\frac{d}{d\theta_m}[\varphi_{PM}] \\
&T_e - T_l - B\frac{\omega_m}{p} = \frac{J}{p}\frac{d\omega_m}{dt} \\
&\frac{d\theta_m}{dt} = \omega_m
\end{aligned}
\tag{11}
$$

1.3 The d-q coordinate model

The most convenient and best known way of modelling and/or control a sinusoidal permanent magnet synchronous machine refers to instantaneous current, voltage, and flux linkage phasors in a synchronous reference frame locked to the rotor. Using a synchronous reference frame locked to the rotor means that the angle of the Park transformation must be equal to the electric distance between the axis of the magnet (d-axis) and the axis of the phase A of the stator, as shown in the Figure 4.

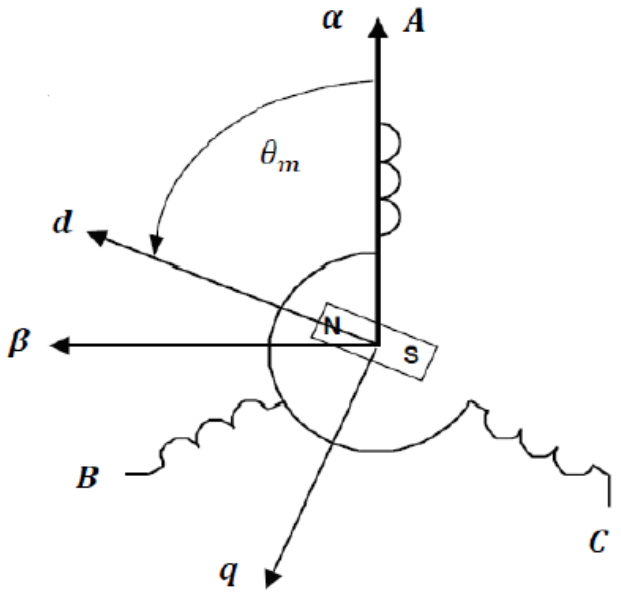

Figure 4.Synchronous rotating d-q reference frame

By using the Park transformation it is possible to describe any three phase system with sinusoidal quantities with only one vector in a plane, if the three phase system does not contain a homopolar component. If the reference frame is locked to the rotor the above mentioned vector is constant and the matrix of the inductances becomes diagonal and independent from the rotor position.
The Park transformation is based on the following matrix:

$$T(\theta) = \frac{2}{3}\begin{bmatrix} \cos(\theta) & \cos(\theta - \frac{2}{3}\pi) & \cos(\theta - \frac{4}{3}\pi) \\ -\sin(\theta) & -\sin\theta - \frac{2}{3}\pi & -\sin\theta - \frac{4}{3}\pi \\ 1/2 & 1/2 & 1/2 \end{bmatrix}.$$

If $[V_{dq0}] = [T][V]$, $[I_{dq0}] = [T][I]$, $[\varphi_{dq0}] = [T][\varphi]$, $[V_{PMdq0}] = [T][\varphi_{PM}]$, from (3), (4) and (10) one may obtain:

$$\begin{aligned} &[V_{dq0}] = [R][I_{dq0}] + [T]\frac{d[T^{-1}]}{dt}[\varphi_{dq0}] + \frac{d}{dt}[\varphi_{dq0}] \\ &[\varphi_{dq0}] = [L_{dq0}][I_{dq0}] + [\varphi_{PMdq0}] \\ &Te = \frac{1}{2}p[T^{-1}\, I_{dq0}]^T \frac{d[T^{-1}\, L_{dq0}\, T]}{d\theta_m}[T^{-1}\, I_{dq0}] + p[T^{-1}\, I_{dq0}]^T \frac{d[T^{-1}\, \varphi_{PMdq0}]}{d\theta_m} \end{aligned} \quad (12)$$

Then, it may be easily proved that:

$$[L_{dq0}] = \begin{bmatrix} L_d & 0 & 0 \\ 0 & L_q & 0 \\ 0 & 0 & L_0 \end{bmatrix}$$

$$\begin{aligned} &L_d = L_l + \frac{3}{2}(L_{av} + \Delta L) = L_l + L_{md} \\ &L_q = L_l + \frac{3}{2}(L_{av} + \Delta L) = L_l + L_{mq} \\ &L_0 = L_l\,. \end{aligned} \quad (13)$$

Moreover, $[T]\frac{d[T^{-1}]}{dt} = \begin{bmatrix} 0 & -1 & 0 \\ 1 & 0 & 0 \\ 0 & 0 & 0 \end{bmatrix} * \omega_m$ and $[\varphi_{PMdq0}] = [T][\varphi_{PM}] = \begin{bmatrix} \varphi_{pm} \\ 0 \\ 0 \end{bmatrix}$ and the voltage-current and flux-current equations in a scalar form can be written as:

$$v_d = Ri_d - \omega_m\varphi_q + \frac{d\varphi_d}{dt} \quad (14)$$

$$v_q = Ri_q + \omega_m\varphi_d + \frac{d\varphi_q}{dt} \quad (15)$$

$$v_0 = Ri_0 + \frac{d\varphi_0}{dt} \quad (16)$$

$$\varphi_d = L_d i_d + \varphi_{pm} \quad (17)$$

$$\varphi_q = L_q i_q \quad (18)$$

$$\varphi_0 = L_0 i_0 \tag{19}$$

while the torque expression is:

$$T_e = \frac{3}{2} p \varphi_{pm} i_q + \frac{3}{2} p (L_d - L_q) i_d i_q \tag{20}$$

From equation (20) it is evident the hybrid nature of permanent magnet synchronous motors, that is the possibility to produce the permanent magnet torque (the first term on the rightmost side) and the reluctance torque (the second term on the rightmost side). Note that the homopolar component of all quantities can be disregarded because the stator winding has usually a star connection.

The equations above related to the d-q model allow drawing the equivalent circuits of a PMSM (Figure 5). It is worth noting that the equivalent circuits just allow a visualization of what the equations represent and ignore the presence of any hysteresis or eddy current losses in either the machine lamination steel or the magnets themselves. The only machine losses that are explicitly modelled are the stator winding losses reflected in the stator resistance R; since the efficiency of a PMSM is typically quite high, disregarding the iron losses is often acceptable for the purpose of machine performance prediction. However in some cases, where higher accuracy is desired, the presence of these losses can be modelled by adding resistors in parallel with both L_d and L_q.

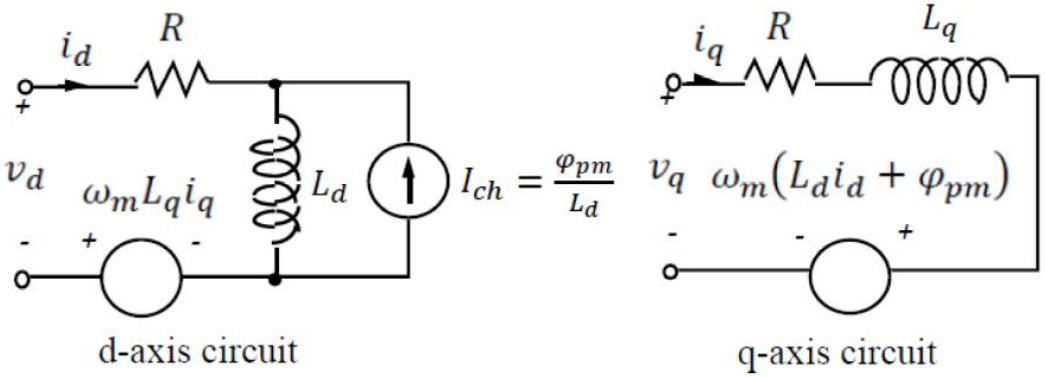

Figure 5.d-q frame equivalent circuits

As we can see in the d-axis circuit, a characteristic current I_{ch} is defined as the ratio between the flux linkage due to permanent magnets and the d-axis inductance.

$$v_d = R i_d - \omega_m \varphi_q + \frac{d\varphi_d}{dt} = R i_d - \omega_m L_q i_q + \frac{d}{dt}(L_d i_d + \varphi_{pm}) =$$
$$= R i_d - \omega_m L_q i_q + \frac{d}{dt}(L_d \left(i_d + \frac{\varphi_{pm}}{L_d}\right) = R i_d - \omega_m L_q i_q + \frac{d}{dt}(L_d (i_d + I_{ch})$$

The characteristic current is an important parameter that influences several aspect of the performances of a PMSM, including extended high speed operation and fault mode performance.

1.4 Torque generation in d-q current plane

After the definition of the characteristic current, demonstrating that the torque expression can be written as the following is easy:

$$T_e = \frac{3}{2} p \varphi_{pm} i_q + \frac{3}{2} p \left(L_d - L_q\right) i_d i_q = \frac{3}{2} p L_d (I_{ch} i_q - (1 - \xi) i_d i_q)$$

.

In the last equation $\xi = \frac{L_q}{L_d}$ is the saliency ratio, another important parameter that influences the performance of the PMSM. It is relevant remembering that the values of the inductances along the two orthogonal axes are equal (or nearly equal) in a non-salient PMSM (i.e. SPMSM) and therefore the second term on the rightmost expression disappears, as said at the beginning of this chapter, namely this kind of motor is not able to produce reluctance torque. In an IPMSM L_d is typically smaller than L_q because the total magnet thickness appears as an incremental airgap length in the d-axis magnetic circuit, thus i_d and i_q must have opposite sign in order to produce a reluctance torque that has the same sign of the permanent magnet torque, otherwise its effect will be a torque reduction. Each of the two terms in the torque expression has a useful physical interpretation: the first is the permanent magnet component of the torque and it is not a function of i_d but is directly proportional to the stator current component i_q which is in phase with the back-emf; instead, the second term is proportional to the product $i_d i_q$ and to the difference of the inductances $L_d - L_q$, that is related to the saliency ratio. This interpretation emphasizes the hybrid nature of the interior permanent magnet motor. Note that the torque is not linearly proportional to the stator current amplitude in the presence of the reluctance torque component, namely if there is any saliency in the magnetic circuit the torque is a non-linear function of the current amplitude. The relative amplitude of the permanent magnet and reluctance torque components are set during the machine design process by choosing the rotor topology and adjusting the amount of permanent magnet. At one design extreme, the reluctance torque disappears in a SPMSM, since L_d is equal to L_q; at the other extreme, the machine becomes a pure synchronous reluctance motor if the magnets are removed. The effect of this design choices are particularly evident in the high speed regime as will be discussed later in this chapter.

From figure 6 and from equation (20) we can observe that the torque can be written as $T_e = \frac{3}{2} p (\varphi_{pm} I \sin\beta + \frac{L_d - L_q}{2} I^2 \sin 2\beta)$ and thus in figure 7 both components of the torque are shown.

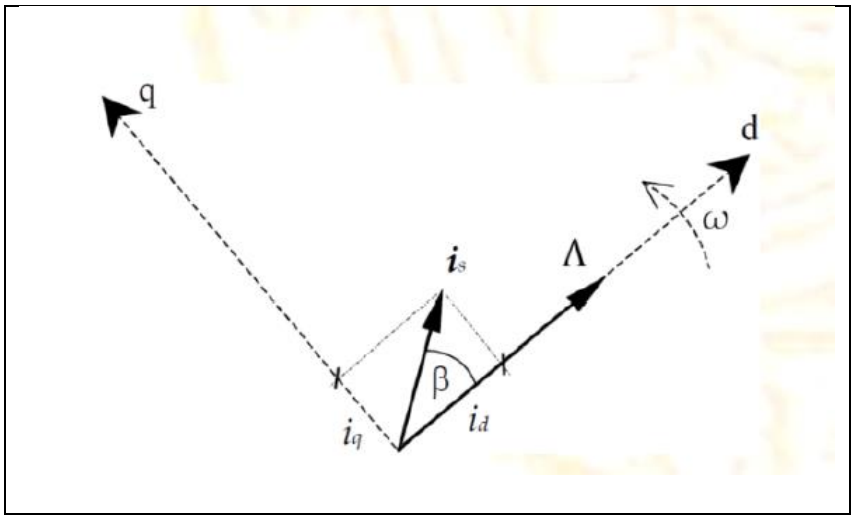

Figure 6.d-q frame stator current i_s and load angle β.

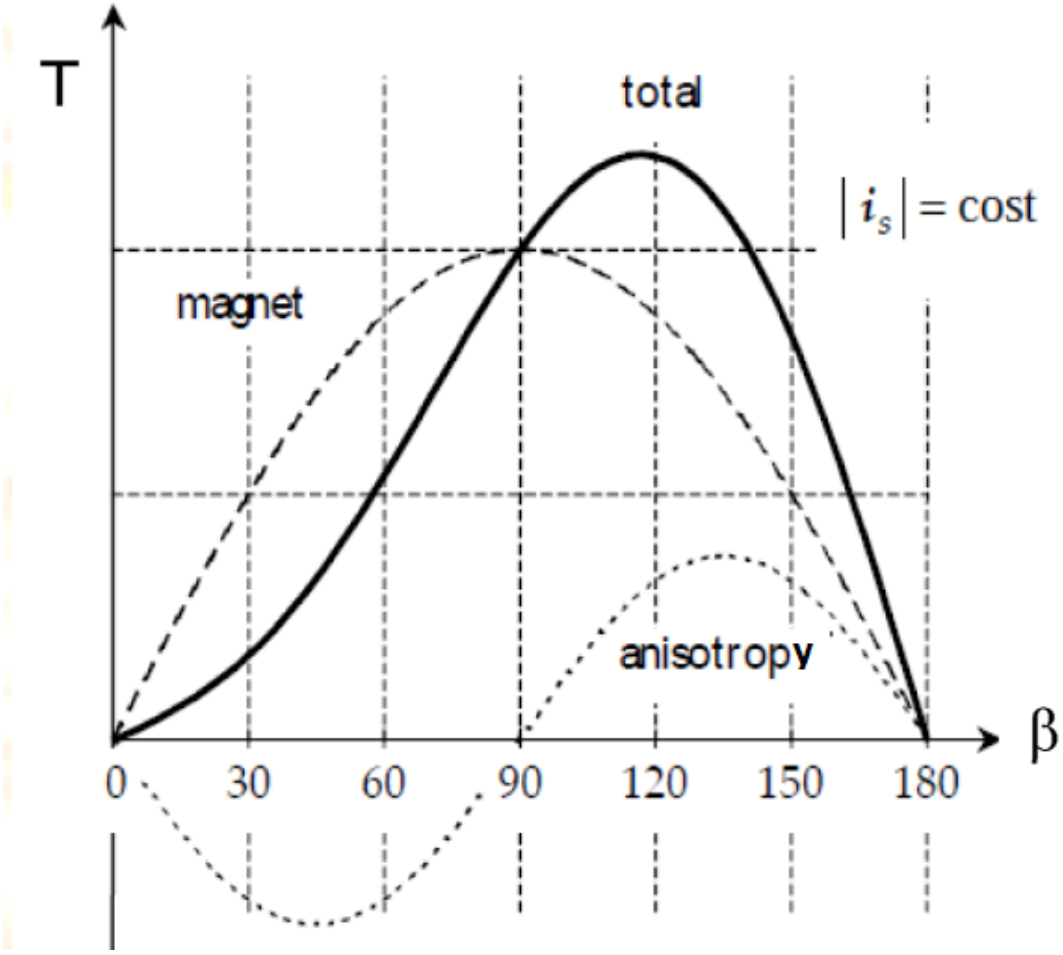

Figure 7.Magnet, anisotropy and total torque in a PMSM

In order to understand better the torque production characteristics of PMSM, it is useful to use the d-q current plane because it will be used to investigate the performance limits of the machine at high speed. The behavior of IPMSM on this

plane will be analyzed because the instantaneous torque has both permanent magnet and reluctance torque, so the behavior of other PMSM (which have only one of the two terms) is simple to evaluate [4]. Figure 8 shows several constant torque lines for an IPMSM. These constant torque loci have hyperbolic shapes because of the $i_d i_q$ product term that appears in the torque equation and so the presence of the reluctance component is directly responsible for this feature.

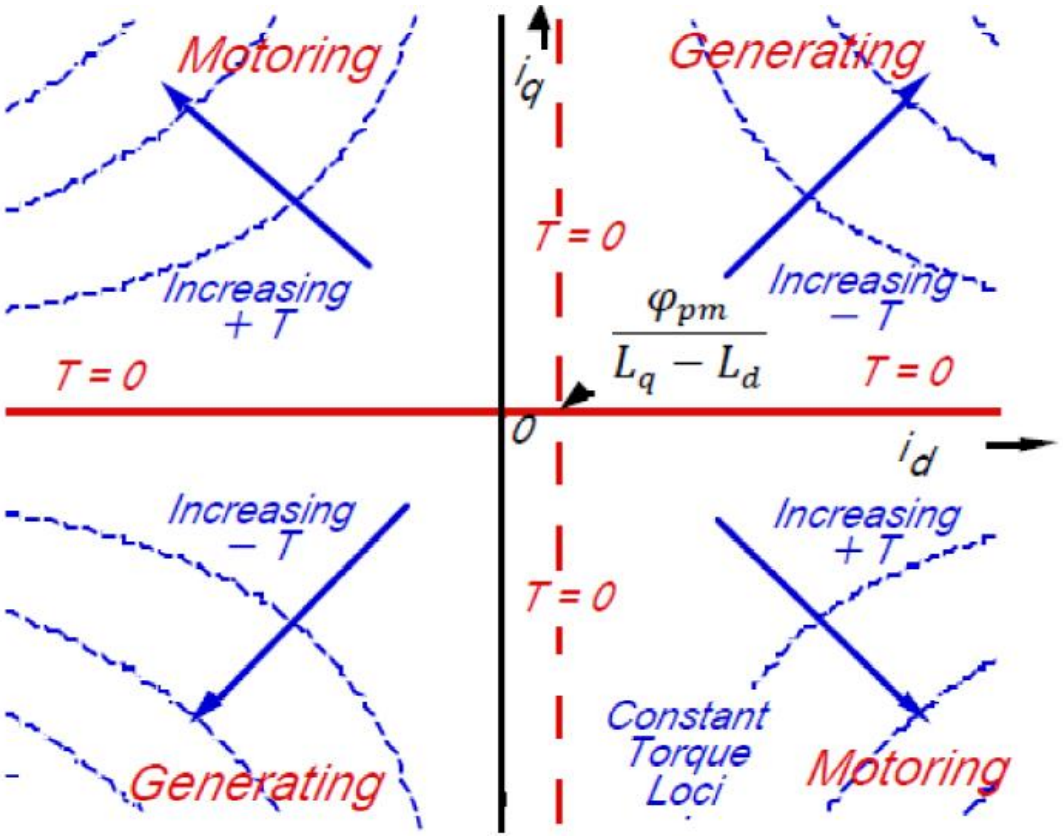

Figure 8.Constant torque loci for an IPMSM in the d-q current plane

This plot and the others that will be developed later are made with the assumption that L_d is constant, i.e. without take into account the magnetic saturation (L_d is less sensitive to the saturation). The entire d-q plane is divided into four quadrants with motoring torque in the second and fourth quadrants, and generating operation in the other quadrants. There are two orthogonal lines in this diagram that correspond to the loci for zero torque; the first one is the horizontal axis ($i_q = 0$), while the second one is the vertical asymptote defined by the current $i_d = \frac{\varphi_{pm}}{L_q - L_d}$. The second line corresponds to the locus of all the points where the permanent magnet torque is cancelled by the reluctance torque. Torque increases monotonically as one moves along any of the 45 degree trajectories (identified by the arrows in the figure 8) away from the intersection of the two zero-torque loci.

Since the value $i_d = \frac{\varphi_{pm}}{L_q - L_d}$ is usually positive, it can be shown that the achievable torque per Ampere will always be higher in the second and third quadrants, thus IPMSMs are designed to operate in these two quadrants in order to maximize the efficiency. Figure 9 shows the maximum torque per Ampere current trajectory that is the locus of all the points in the d-q current plane where the machine develops the maximum possible torque for each progressively higher value of stator current amplitude. Another important feature illustrated in the Figure 9 that will be useful later in the discussion of flux-weakening operation of the PMSM at high speeds is the current limit circle. Assuming that the current from the source supplying the motor is limited to $1\,p.u.$ (rated current), the above mentioned locus may be immediately obtained from the simple equation $1 = \sqrt{i_d^2 + i_q^2}$; in order to satisfy this limit, the machine current vector should be inside or on this circle otherwise the machine and the power source will be overloaded.

Figures 8 and 9 do not include the effect of the magnetic saturation but it has a significant effect on the performance characteristic of a PMSM.

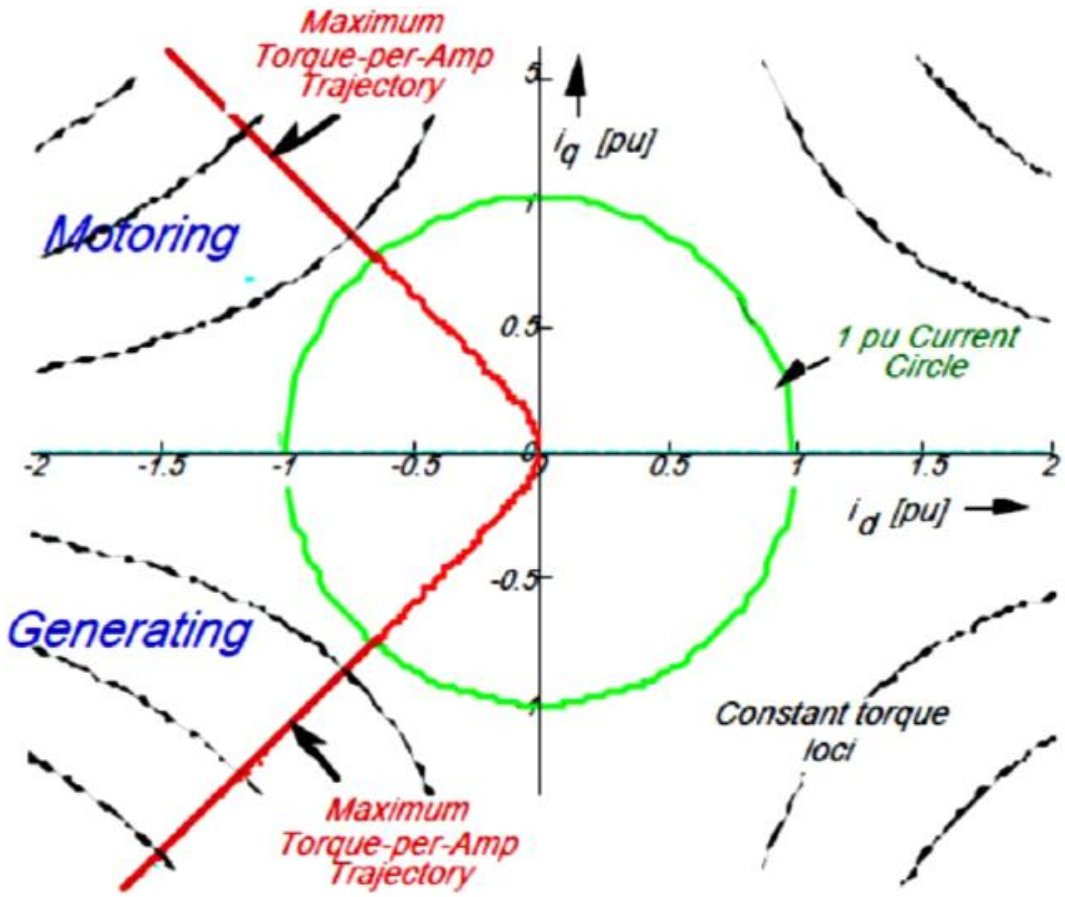

Figure 9.Maximum torque per Ampere trajectories in the d-q current plane

In particular, the q-axis inductance tends to be very sensitive to the magnetic saturation as the value of i_q increases because the magnetic path along the q-axis is

almost totally composed by iron. On the other hand, the d-axis inductance tends to be less sensitive to the magnetic saturation because the magnetic path along the d-axis is dominated by the thickness of the magnet that has the same behave of the air from the point of view of the magnetic permeability.
The constant torque curves become distorted from their simple hyperbolic shapes because the inductances are no longer constant, but instead it changes with the current. The maximum torque per Ampere trajectory in the motoring regime swings counterclockwise in the direction of the negative d-axis because of the saturation. As a consequence of the saturation, the motor needs more current with the purpose of produce the same torque.

1.5 Performances of a PMSM

1.5.1 Introduction

The available operating range of speed and torque that can be achieved by a permanent magnet synchronous motor is a very important feature in determining the suitability of the machine for the specific application. The torque and speed capability curves are determined by the machine type and by the limits on the voltage and on the current allowed by the electric drive that supply the machine. In many cases, the desired torque-speed characteristic has the typical shape as in Figure 10.

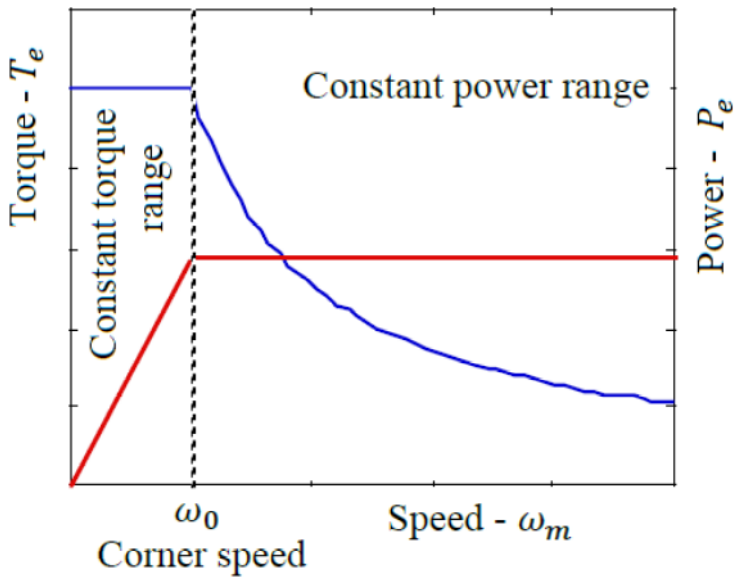

Figure 10.Typical torque and power versus speed curve

When the speed is lower than corner speed, the machine works at constant torque and it is limited by the maximum available stator current. This first zone is called

constant-torque range and the power increases from zero to the rated value; the second zone is the constant-power range and obviously in this zone the machine works at constant power. From the corner point to the maximum achievable speed the machine operates simultaneously at the current and voltage limits. In the constant power range, as the speed increases the torque decreases; since the stator flux is the ratio of the applied voltage to the excitation frequency, the fact that the voltage is constant in this range implies that in order to increase the speed the stator flux should decrease.

The ratio between the maximum speed at which the machine can deliver the rated power and the corner speed defines the constant power speed ratio $CPSR = {\omega_{max}}/{\omega_0}$. The achievable values of CPSR vary widely among different types of machines; PMSM are able to get high CPSR values (circa five).

Equation (17) suggests that the d-flux φ_d can be reduced despite the presence of permanent magnets which have a fixed value of the flux by adding a negative d-axis current. This method, known as flux weakening, uses the d-axis flux linkage $L_d i_d$ created by the d-axis current to counteract the magnetic flux linkage due to the permanent magnets, in order to reduce the total d-axis flux. Although the concept of the flux weakening is not new, its usefulness is limited in some PMSM because the machine parameter values. In particular the surface permanent magnet synchronous machines tends to be poor candidate for effective flux weakening because the magnets behave as a large airgap in the magnetic circuit, leading to low values of the d-axis inductance. A low value of L_d means that in order to decrease the total d-axis flux at high speed, the use of an unacceptable value of the d-axis current is necessary; as a result the values of CPSR that can be achieved with the SPMSM with conventional distributed winding is circa 2. It may be noted that the specific value of the current that deletes the magnet flux linkage can be computed from Equation (17): $i_d = -\frac{\varphi_{pm}}{L_d} = -I_{ch}$. The IPMSMs are better candidates for extended ranges of constant power operation because this kind of motor has an extra degree of freedom during the design that is the possibility of adjust the relative contributions of the magnet torque and the reluctance torque to the total torque. By reducing the magnet torque in favour of more reluctance torque, the value of the magnet flux linkage can be reduced in comparison to its value of a SPMSM designed for the same application.

Consequently, the value of the characteristic current of an IPMSM can be reduced, thus less d-axis current is needed to counteract the magnetic flux linkage due to the permanent magnets; this simple observation leads to the consideration that achieving a wide constant power speed range is easier with an IPMSM than with a SPMSM [4].

1.5.2 Current and voltage limits interaction

The torque-speed curves, as said above, are determined by the current and voltage limits imposed either by the power electronic source and the machine parameters;
The current limit, as described in the last paragraph, defines a circle in the d-q current plane with a radius of such that the instantaneous current vector must terminate inside or on the edge of this circle in order to satisfy the current constraint due to thermal considerations.
The impact of the voltage limit in the d-q current plane is easy to obtain from Equations (14) and (15) of the machine and from the voltage limit equation in per unit with the assumptions that the voltage drops due to the stator winding resistance are disregarded and the steady state condition is considered:

$$V_{max}^2 = v_d^2 + v_q^2 = 1$$
$$v_d = -\omega L_q i_q$$
$$v_q = \omega(L_d i_d - \varphi_{pm})$$

It is easy to obtain the following equation that defines an ellipse in the d-q current plane:

$$(i_d + \frac{\varphi_{pm}}{L_d})^2 + (\frac{L_q}{L_d})^2 i_q^2 = (\frac{V_{max}}{L_d})^2 \frac{1}{\omega^2} \text{ and thus } (i_d + I_{ch})^2 + \xi^2 i_q^2 = (\frac{V_{max}}{L_d})^2 \frac{1}{\omega^2}.$$

This ellipse is centered on the negative d-axis at $i_d = -I_{ch}$ with major and minor radii of $V_{max}/(L_d\omega)$ and $V_{max}/(L_q\omega)$ oriented in the d and q direction respectively.
The effect of the magnetic saturation is ignored as it has been done with the constant torque loci and the maximum torque per Ampere trajectory. Similar to the current constraint, in order to satisfy the voltage limit the current vector must lie inside or on the border of this ellipse.
As we can observe, both major and minor radii are inversely proportional to excitation frequency. As a consequence, as the rotor speed increases the ellipse shrinks while the centre does not change; this means that the available range of stator current is increasingly limited as the speed increases.
It is obvious that all PMSM must simultaneously satisfy the voltage and the current constraints and so the acceptable operating area is the intersection between the current circle and the voltage ellipse and this intersection shrinks as the speed increases; Figure 11 clearly illustrates this concept. When the speed is low, the radii of the ellipse are so large that the intersection area consists of the entire current

limit circle; this demonstrates that during the constant torque operation the current limit is the only active constraint. In this range, the maximum torque operating point is the intersection between the current limit circle and the maximum torque per

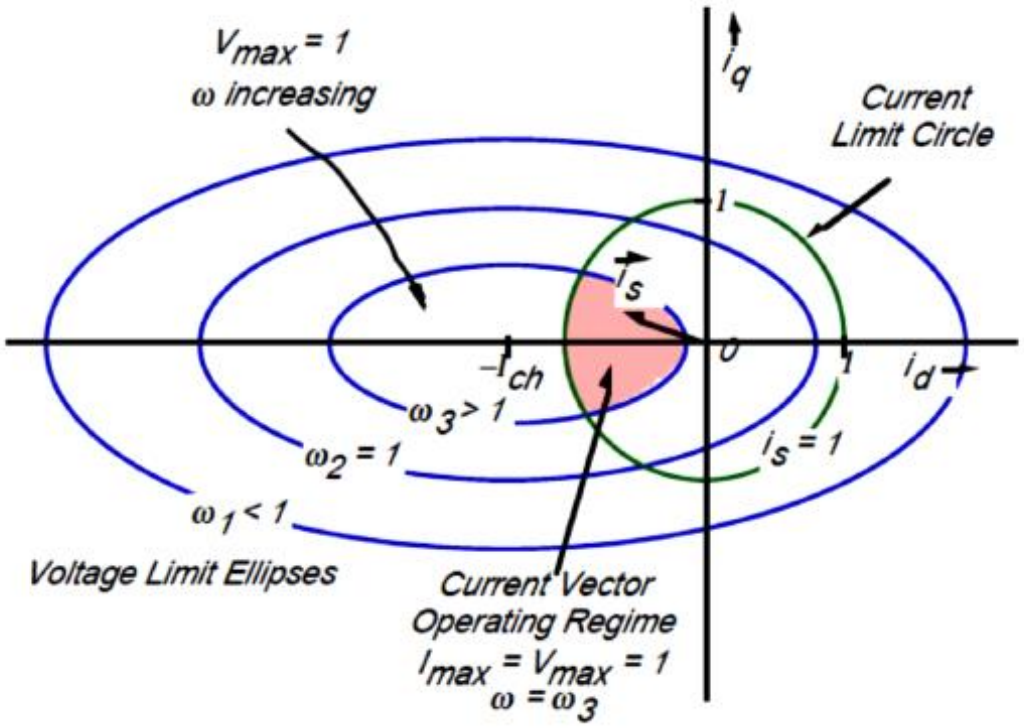

Figure 11.Interaction between current limit circle and voltage limit ellipse

torque per ampere trajectory; this condition persists until the voltage ellipse shrinks sufficiently in size so that the ellipse intersects the maximum torque operating point. This condition occurs at the corner speed at which there is the transition between the constant torque range and the constant power region; from this point the machine should develop the maximum power while simultaneously it is operating at its voltage and current limits. As the rotor speed increases above the corner speed, the PMSM can not continue to work at its maximum torque point because the shrinkage of the voltage ellipse moves this point outside of the intersection between the circle and the ellipse, making it inaccessible for steady state operation. Under this condition, the operating point should follow the intersection point between the current limit circle and the voltage ellipse with the purpose of developing the highest possible torque. As the speed increases, the operating point moves along the current limit circle, the amplitude of the negative d-axis current increases while the q-axis current component decreases; this gradual increase of the d-axis current correspond to higher level of flux weakening as previously explained.

1.5.3 Capability

There are three distinct cases of flux weakening operation differentiated on the basis of the characteristic current values. Based on the considerations mentioned in the previous subsection, we will describe these cases.

When $I_{ch} > I_{max}$ there is a finite maximum rotor speed above which a PMSM cannot produce any useful torque; the reason becomes evident by inspecting the migration of the operating point at high speed in d-q current plane as shown on the left in Figure 12: when the rotor speed reaches a sufficiently high value the intersection between the current limit circle and voltage limit ellipse becomes a point. In the same figure, on the right the resulting power-speed characteristic for this condition is shown and we can see that the power reaches a peak at a rotor speed that depends on the machine parameters and decreases sharply dropping to zero as the speed increases.

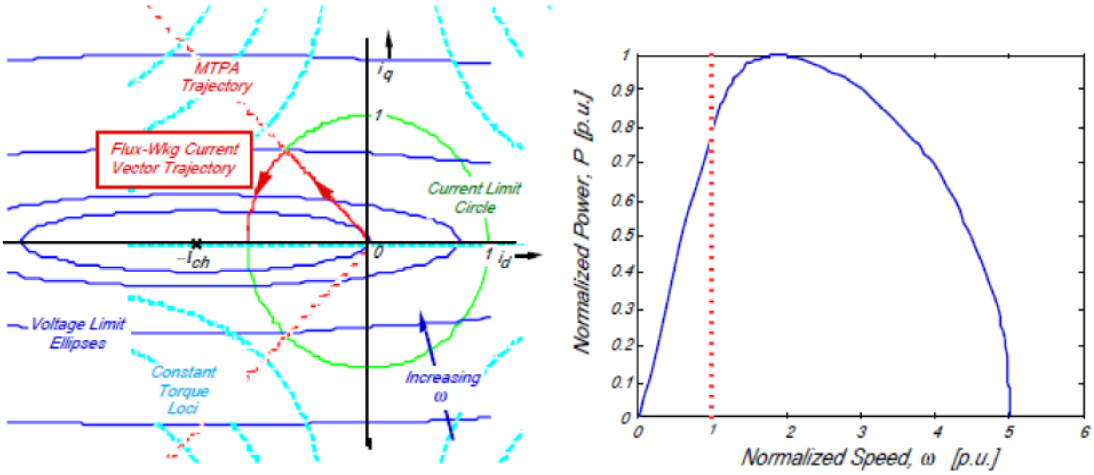

Figure 12.Flux weakening current vector trajectory (right) and power-speed characteristic (left) – case $I_{ch} > I_{max}$

If $V_{max} = I_{max} = 1$, one may obtain the maximum rotor speed at which the torque drops to zero by imposing $i_d = -1$ and $i_q = 0$ in the voltage limit equation, so that $\omega_{max} = 1/(L_d(I_{ch} - 1))$. This relationship shows that the maximum speed is inversely proportional to the characteristic current. SPMSMs obey at the same expression and now the reason why CPSR value for SPMSM with conventional winding is quite low is clear: the characteristic current of this kind of machine is greater than 1 pu.

When $I_{ch} = I_{max}$ the maximum speed becomes infinite and this is a very important condition that must be considered during the design of an IPMSM for wide speed range application. In this special case, the centre of the voltage limit ellipses lies on the leftmost point of the current limit circle as shown in the Figure 13, consequently

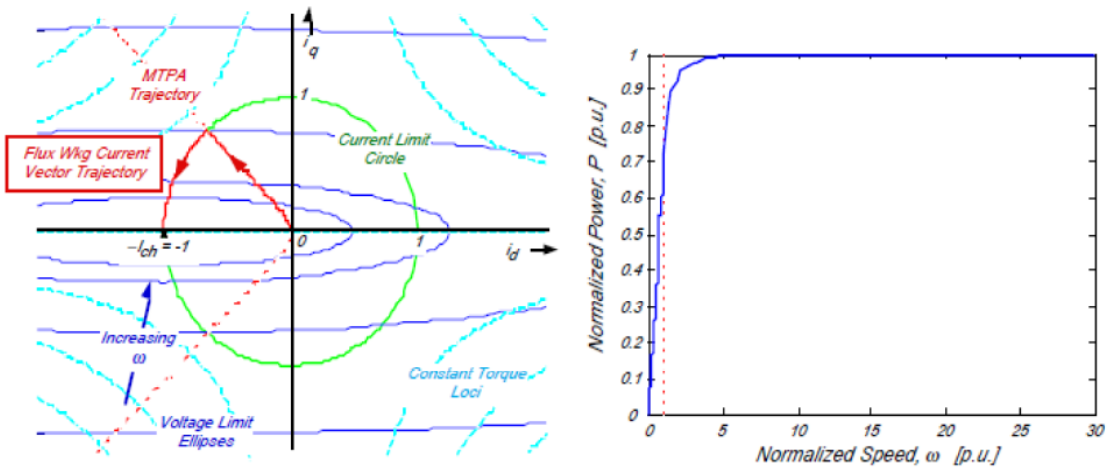

Figure 13.Flux weakening current vector trajectory (right) and power-speed characteristic (left) – case $I_{ch} = I_{max}$

the intersection between these two areas never drops to the null set as the speed increases. The power-speed capability curve shows the best behaviour possible because it becomes a constant value as the rotor speed increases, reflecting the fact that the drop in the torque is exactly compensated by the increase in the speed and so the output power is constant. Another important feature of this case is the fact that the power factor is near to the unity at high speed and this is desirable from the point of view of achieving the highest possible inverter utilization and highest efficiency. Obviously this reasoning does not take into account the losses and mechanical considerations, hence in the reality the CPSR is not infinite; nevertheless it is possible to design an IPMSM with a high value of this parameter by matching as close as possible the characteristic current to the rated current.

If $I_{ch} < I_{max}$ the intersection between the current limit circle and the voltage limit

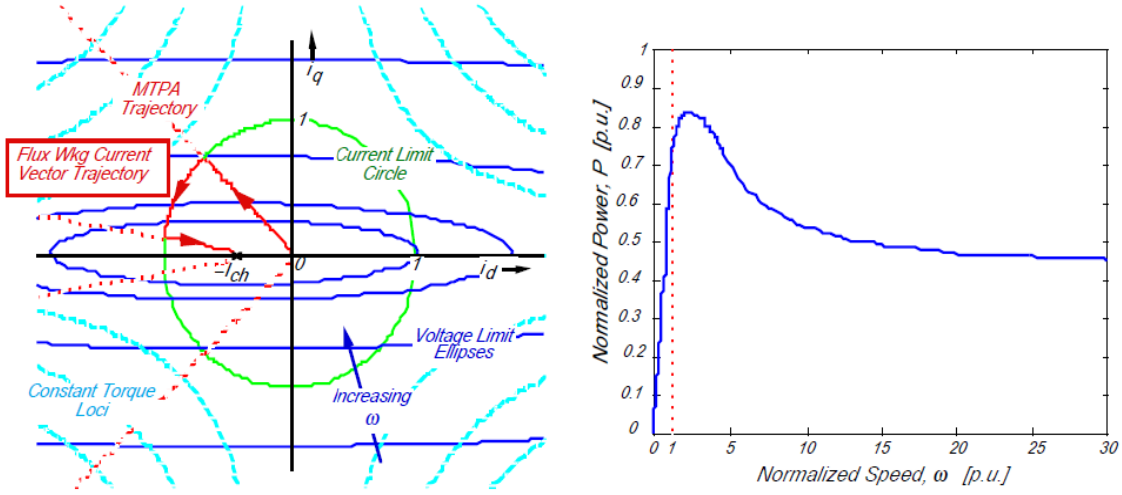

Figure 14.Flux weakening current vector trajectory (right) and power-speed characteristic (left) – case $I_{ch} < I_{max}$

ellipse never drops to the null set, thus the power never drops to zero as the rotor speed increases. Yet, the fact that the centre of the voltage ellipses lies inside the current circle means that there will be a certain value of the speed above which it is impossible to follow the optimum flux weakening trajectory for the current vector because the current circumference does not intersect the voltage ellipse. Under this condition, the best way to act is moving the stator current vector inside the current limit circle in order to extract the highest possible torque, in this high speed regime. The resulting power speed curve (Figure 14) for this case shows that the power reaches the peak at speed slightly above the corner speed and then falls as the speed increases, reaching an asymptote less than the rated power.

1.6 PMSM design space

In the previous section, the importance of the permanent magnet flux and the saliency ratio in determining the performance of PMSM have been highlighted; during the design, with the appropriate modelling, one may reduce the number of independent design parameters to these two normalized variables. For this reason, it may be convenient drawing a plot that shows all the possible designs with different combinations of magnet flux linkage and saliency ratio.

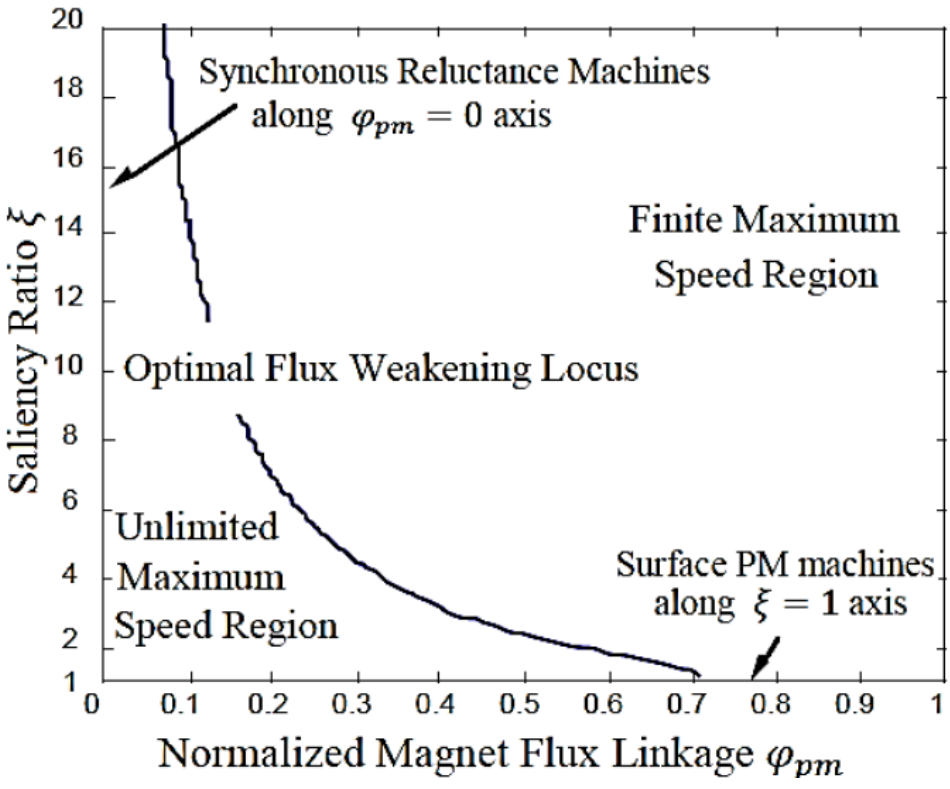

Figure 15.Design plane

This figure shows the locus of machine designs that exhibit the optimum flux weakening operation characteristic; any PMSM designed using a combination of φ_{pm} and ξ values that falls on this locus is capable of achieving a wide CPSR with a constant output power and equal to the rated value at high speed.
It can be proved that every designs on this locus correspond to an PMSM having a characteristic current equals to 1 pu.
The existence of this locus implies a considerable flexibility available to the machine designer in developing a PMSM that meets the conditions for optimum flux weakening. On the other side each specific application tends to limit the range of acceptable combination of the above mentioned parameters.
Moreover, we can observe in the figure 15 that machine designs falling to the right of the optimum flux weakening locus have finite speed ranges and the output power falling to zero over a specific maximum speed value. The farther one moves away on the right side from the locus, the lower is the maximum speed. Machine designs on the left of the optimum flux weakening locus have ideally infinite speed ranges although the power at high speed is less than its rated value. The farther one moves away on the left side from the locus, the lower is the output power.
Another important feature of this plane is that it shows a wide range of designs: machine designs that lie on the ordinate axis correspond to the family of synchronous reluctance machines, thus these machines have an infinite constant power speed range with an output power at high speed less than the rated value. Oppositely machine design falling on the abscissa axis corresponds to the family of non salient machine, like SPMSM, for which the optimum flux weakening locus intersects the $\xi = 1$ axis, hence a surface permanent magnet machine can be designed to achieve a wide CPSR; this can be achieved by adjusting the value of permanent magnets flux linkage to 0.71 pu. Unfortunately the value of the per unit inductance needed to achieve this condition is also 0.71 because I_{ch} should be equal to unity but this is very high value of per unit inductance for a standard SPMSM that typical cannot be achieved using conventional distributed windings (however it is possible to achieve this condition with special fractional slot windings and low slots per pole values).
As a result, almost all SPMSM fall to the right of the intersection of the optimum flux weakening locus and the abscissa axis and this means that they fall inside the design region with finite constant power speed ranges.

2 DESIGN PROCEDURE

2.1 Introduction

Usually an electrical machine is designed for given initial conditions. The system for which the machine is intended defines the requirements concerning certain basic characteristics, the most important of which are:

- Machine type (synchronous, asynchronous, DC, reluctance machine, etc.);
- Type of construction (external or internal pole, axial or radial flux machine, etc.);
- Rated power, including also the power factor;
- Rated rotational speed or rated angular speed;
- Number of pole pairs of the machine (related to frequency converter drives);
- Rated frequency of the machine (related to frequency converter drives);
- Rated voltage of the machine;
- Number of phases of the machine;
- Intended duty cycle (S1-S9);
- Enclosure class and structure of the machine;
- Additional information such as efficiency, peak torque, etc.;
- Manufacturability.

Besides the above ones, there are a considerable number of free parameters. When aiming for an optimal solution, the task becomes extremely complicated unless the number of these free parameters is somehow limited. Many free parameters vary only slightly and therefore, to simplify the task, these parameters can be assumed constant.

Actual machine design starts with the selection of the main dimensions of the machine. The term 'main dimensions' refers to the air-gap diameter measured at the stator bore and the equivalent core length. The equivalent length of the core takes into account the influence of the flux fringing at possible cooling ducts of the machine and also at the ends of the machine.

In electrical machine design, there are certain empirically defined variation ranges of current and flux densities, which can be applied in the preliminary phase of the design. The permitted loading levels are defined for a machine on the basis of the design of the insulation and the cooling of the machine. In principle, machine design is a rather complicated iteration process, in which the initial values are first selected for the dimensions of the machine. Next, the machine is designed electrically, and

finally the cooling of the machine is computed. If the cooling of the machine is not efficient enough, the conductors will overheat, which may damage the insulations and the design has to be started from the beginning again by increasing the dimensions of the machine, by using better materials or by selecting a more efficient cooling method. The material selection has a significant influence on both the losses and the thermal resistances. If a low-loss iron material and high-thermal-class insulation materials are selected, the output power of the machine can be improved without increasing its size. Moreover, if the magnetic flux density is too low the iron core will not be utilized well; on the other hand, when the flux density is too large the iron will saturate.

According to [14] the current density in a stator winding of PMSM varies between $4 - 6.5\ A/mm$ and the air gap flux density of a non-salient pole synchronous machine varies between $0.8 - 1.05\ T$.

2.2 Mechanical dimensions

2.2.1 Radial and tangential stress based on Maxwell's stress tensor

Maxwell's stress tensor is probably the most generic idea of producing magnetic stresses, forces and torque. In numerical methods, it is often employed in the calculation of forces and torque. The idea is based on Faraday's statement according to which stress occurs in the flux lines.

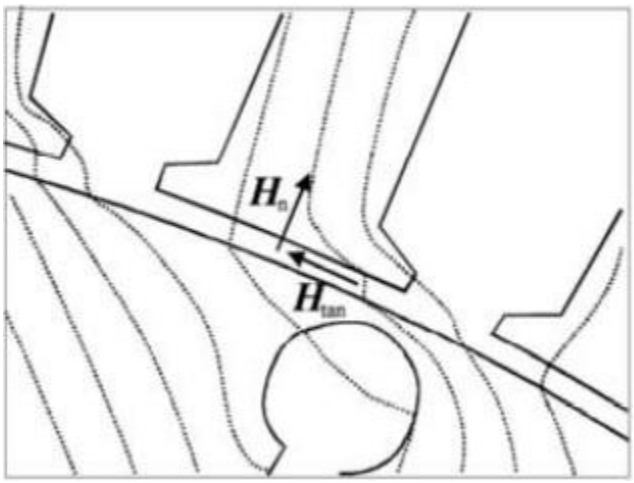

Figure 16.Flux solution of an induction motor; tangential and normal component of the field strength

Figure 16 depicts the flux solution for an air gap of an asynchronous machine, when the machine is operating under a heavy load selected in order to illustrate clearly the tangential routes of the flux lines. In the figure, the flux lines cross the air gap somewhat tangentially so that if we imagine the flux lines to be flexible, they cause a notable torque rotating the rotor counterclockwise. According to Maxwell's stress theory, the magnetic field strength between objects in a vacuum creates a stress σ_F on the object surfaces, given by:

$$\sigma_F = \frac{1}{2}\mu_0 H^2 \tag{21}$$

The stress occurs in the direction of lines of force and creates an equal pressure perpendicularly to the lines. When the stress term is divided into its normal and tangential components, from the point of view of the torque production, tangential term σ_{Ftan} is of the greatest interest. The total torque exerted on the rotor can be obtained by integrating the stress tensor for instance over a cylinder that confines the rotor. The torque is obtained by multiplying the result by the radius of the rotor. Furthermore it is proved that linear current density A on a metal surface creates tangential field strength components on the metal surfaces, so that we can write:

$$\sigma_{Ftan} = \mu_0 H_n H_{tan} = B_n A \tag{22}$$

This expression allows to directly determine the torque of the machine when the rotor dimensions are selected.
Typically, the tangential stress in the air gap of a PMSM may vary between $21\ kPa$ and $48\ kPa$ [14].

2.2.2 Rotor size and equivalent length

The equation (22) defines the tangential stress in the air gap and its local value may be evaluated considering the local values of the linear current density and the flux density $\sigma_{Ftan}(x) = B_n(x)A(x)$. If a sinusoidal air-gap flux density with peak value $\widehat{B_\delta}$ is assumed and a sinusoidal linear current density with peak value $\hat{A}$ and RMS value A is applied, it may be obtained for the average tangential stress:

$$\sigma_{Ftan} = \frac{\widehat{B_\delta}\hat{A}\cos\varphi}{2} = \frac{\widehat{B_\delta}A\cos\varphi}{\sqrt{2}} \tag{23}$$

This tangential stress produces the torque of the machine when acting upon the rotor surface.
Typical tangential stress values give us a starting point for the design of an electrical machine: one may define the size of the rotor first by using a suitable tangential

stress value on the rotor surface. If the rotor radius is r_r, the rotor equivalent length is l', the rotor surface facing the air gap is S_r and the average tangential stress on the surface is σ_{Ftan}, the torque T of the rotor may be written simply as

$$T = \sigma_{Ftan} r_r S_r = \sigma_{Ftan} r_r (2\pi r_r l') = \sigma_{Ftan} 2\pi r_r^2 l' = \sigma_{Ftan} \pi \frac{D_r^2}{2} l' = 2\sigma_{Ftan} V_r \quad (24)$$

and thus one may estimate the rotor volume. Obviously, the weight of the rotor is proportional to its volume and it is easy to demonstrate that the higher the tangential stress and the supply frequency, the lower the weight.

By selecting a small number of pole pairs p and a high supply frequency f, we obtain, in principle, a light machine for a certain output power. Since the output power of a machine may be written as $T = P\Omega$, the torque of a high-speed machine is small when compared with a low-speed machine of equal output power. At high speeds, however, the motor power density increases together with the loss density, and hence effective methods to reduce the losses and to improve the cooling of the machine have to be applied. With high frequencies, suitable means to reduce the stator winding skin effect have to be adopted so that there is no need to reduce greatly the linear current density. As the frequency rises, in order to maintain the air-gap flux density, better stator steel materials and more effective cooling methods have to be selected.

With respect to the length of the rotor, it is chiefly restricted by the critical angular speeds of the rotor. At a critical speed, the rotor has one of its mechanical resonances. There are several bending modes for the mechanics of each rotor: at the lowest critical speed, the rotor bends like an arc having two nodal points; at the second critical speed, the rotor bends into an S-shape with three nodal points and so on. Usually, the ratio of the length of the machine to the air-gap diameter

$$\chi = l'/D_r \quad (25)$$

is selected for operation of the rotor below the first critical rotation speed.

For synchronous machines we may use an empirical expression that gives χ as a funtion of the number of pole pairs (Pyrhonen, Tapani, & Hrabovcovà, 2008):

$$\chi \approx \frac{\pi}{4p}\sqrt{p}$$

It has talked about ‘equivalent length’: at the end of the machine and at possible radial ventilating ducts, the edge effects have to be taken into account. The flux density of the machine changes in the direction of the shaft; it remains approximately constant over a distance of the sheet core and decreases gradually to

zero along the shaft of the machine as an effect of the edge field. The lengthening of the machine caused by the edge field can be approximated by the equation

$$l' \approx l + 2\delta \tag{26}$$

However, this correction is of no great significance and thus, usually, the real length l is accurate enough in the calculations. In large machines, however, there are ventilating ducts that reduce the equivalent length of the machine and we should also take into account them in the calculation of the equivalent core length.

2.2.3 Air gap

With respect to the length of the air gap, in machines in which the magnetizing current is taken from the supply network, the air gap is dimensioned to produce a minimum magnetizing current and, on the other hand, an optimal efficiency. In principle, a small air gap gives a low magnetizing current, while the eddy current losses of the rotor and stator surface increase because of permeance harmonics created by the open or semi-closed slots. A small air gap also increases the surface losses in the rotor caused by the current linkage harmonics of the stator. Although the air gap is of great significance, no theoretical optimum has been solved for its length, but usually empirical equations are employed instead in the definition of the length of the air gap as a function of the rated power P [14].

$$\delta = \frac{0.2 + 0.01P^{0.4}}{1000}[m] \qquad p = 1 \tag{27}$$

$$\delta = \frac{0.18 + 0.006P^{0.4}}{1000}[m] \qquad p > 1 \tag{28}$$

In PMSMs, the air-gap length is determined by mechanical constraints. It can be calculated from Equations (27) and (28). The synchronous inductance depends on the air-gap length: since the magnet length itself and the possible sleeve thickness have a significant influence on the magnetic air gap of the machine, the synchronous inductance easily becomes low and the machine maximum torque high. However, in some cases, the thickness of the magnet and even the length of the physical air gap must be increased to get a smaller synchronous inductance. Generally, the physical air gap is made as small as possible to save the amount of material in the permanent magnet. This holds especially for low-speed, high-torque permanent magnet machines. In higher-speed machines, the air-gap harmonic content may cause very high losses in the permanent magnet material or in the ferromagnetic material under

the permanent magnets, and in such cases the air gap must be increased to keep the magnet temperature low enough. In a PMSM, the determination of the air gap is thus a demanding optimization task, so one may start from an initial value of the air gap thickness (a typical value is $1\ mm$) and then it will be optimized, for example using a FEM-based software, after a first preliminary analytical sizing.

2.3 Winding

With the mechanical dimensions obtained in the previous section, one may be able now to get the real length l of the machine (note that the same lengths for the stator and rotor have been assumed) and the inner stator diameter D_s. The next task is to design a suitable stator winding for the machine.

The main simplifying assumptions are related to the fact of starting by selecting the winding type and the number of slots per pole per phase q. In this preliminary sizing, one may start by considering a distributed winding, that can be a single-layer or a double-layer winding, and by assuming q as an integer number (this number may be also a fractional number and this situation is very common in permanent magnet synchronous motors: this kind of configuration is called fractional-slot winding).

With these assumptions we are now able to calculate the number of stator slots Q as

$$Q = 2pmq \tag{29}$$

in which m is the number of phases in the machine, the stator slot pitch and the stator pole pitch as

$$\tau_u = \frac{\pi D_s}{Q} \tag{30}$$

$$\tau_p = \frac{\pi D_s}{2p} \tag{31}$$

This is a decisive phase with respect to the final characteristics of the machine: the winding type and the more suitable permanent magnets dimensions are connected to each other via the back-induced-EMF:

$$E_{PM} = \frac{2\pi f k_{w1} N_{ph} \widehat{\Phi_m}}{\sqrt{2}} \tag{32}$$

It may be observed from Equation (29) that the back-EMF depends on the number of coil turns in a phase N_{ph}, the maximum magnetic flux in the air-gap $\widehat{\Phi_{PM}}$, the winding factor k_{w1} and the supply frequency f (note that we are assuming a sinusoidal air gap flux and Equation (32) refers to the RMS value of the back-EMF). As

previously said, the value of E_{PM} has a significant influence on the machine performance. Depending on the desired performance, this value may vary from slightly under to slightly over the supply voltage. If the motor performance after the design is not desired the designer may consider changing E_{PM}.
The flux linking the air gap is calculated by integrating the flux density over the pole pitch (x-coordinate) and the equivalent length (y-coordinate) of the machine (figure 17). In practice, this value may be calculated by defining the average value of the air-gap flux density:

$$\widehat{\Phi_m} = \int_0^{l'} \int_0^{\tau_p} (B_\delta)\ dx\, dy = \alpha_{PM} \widehat{B_\delta} \tau_p l' \tag{33}$$

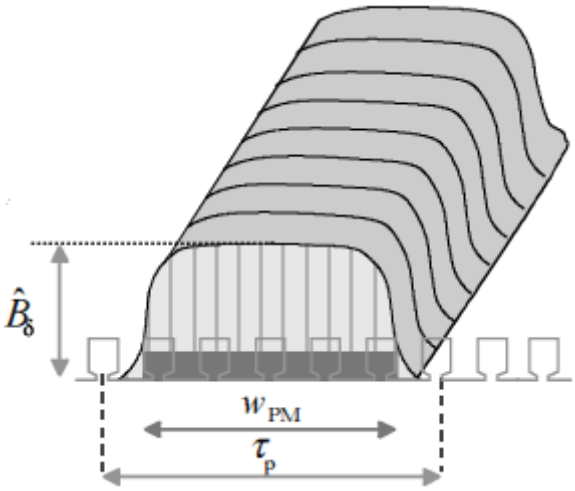

Figure 17.The air gap behaviour with a rectangular permanent magnet

In SPMSM, if the magnets have an equal thickness over the pole pitch, the air gap flux density is more or less rectangular and the average flux may defined by the relative magnet width $\alpha_{PM} = w_{PM}/\tau_p$. Rotor surface magnets may, of course, be given a form that produces a sinusoidal flux density. Embedded magnets and a suitable pole shoe shape may also give a sinusoidal flux density in the air gap.

The saturation of the teeth and thus the losses has a great influence on the choose of the value of α_{PM}: in principle, it is possible to start with an initial value of the magnet width and then, with the help of a FEM-based software, it may be optimized in order to obtain a specific objective that in this work will be the reduction of the oscillations of the torque at no-load condition (cogging torque).
Since the tangential stress has already been selected, the amplitude of the fundamental of the air gap flux density has to be correlated with the selected stress and we may choose a value from $0.85\,T$ and $1.05\,T$. The maximum value of the rectangular flux density is needed and it is calculated by the first term of the air gap flux density Fourier series (see Equations (32) and (33)):

$$B_1 = \frac{4 \sin(\alpha_{PM} \frac{\pi}{2})}{\pi} \widehat{B_\delta} \tag{34}$$

Since the winding is spatially distributed in the slots on the stator surface, the flux penetrating the winding does not intersect all windings simultaneously, but with a certain phase shift. Therefore the E_{PM}, as one can see in the equation (32), is not calculated directly with the number of turns N_{ph}, but the winding factors $k_{w\nu}$ corresponding to the harmonics ν are required. It is easily proved that the winding factor is the product between the pitch factor $k_{p\nu}$ and the distribution factor $k_{w\nu}$.

$$k_{w\nu} = k_{p\nu}\, k_{d\nu}$$

$$k_{p\nu} = \sin(\nu \frac{W}{\tau_p} \frac{\pi}{2}) \qquad k_{d\nu} = \frac{2\sin(\nu \frac{\pi}{2m})}{\frac{Q}{mp}\sin(\nu \frac{\pi p}{Q})}$$

The pitch factor is not equal to unity only in the case of a double layer winding, in which usually a short pitch winding may be realized in order to reduce some specific harmonics and to reduce the end winding length. Obviously it depends on the winding pitch W/τ_p. The distribution factor depends on the number of stator slots, the number of pole pairs and the number of phases.

We may now calculate the number of coil turns N in a phase winding from the Equation (32). Almost always, this value is not integer, so next we have to find a suitable integer closest to the previously calculated number of turns. Note that a single coil turn is composed of two conductors in slots, connected by the coil ends. In a single-phase winding, there are thus $2N$ conductors in series. With m phases in a machine, the number of conductors becomes $2mN$. There may be a number of a parallel paths in a winding, in which case the number of conductors is $2amN$. The number of conductors per slot becomes

$$z_q = \frac{2amN}{Q} \tag{35}$$

One may choose an initial value of $a = 1$; the result of Equation (35) has to be rounded because z_q has to be an integer number; moreover, z_q has to be an even number in a double-layer winding (in a single-layer may be both an even or odd number). The rounding to an even number may make a large difference to z_q calculated above and changing the number of parallel paths may help.

After rounding-off, a new number of turns N is calculated from (35). In order to keep the induced voltage unchanged, we will iterate a value for E_{PM} such that the new

calculated value of $\widehat{B_\delta} = z_{q\_nonrounded}/z_{q\_selected}$ is very close to the above calculated value from the Equation (34).

2.4 Stator slots and teeth dimensions

When the air gap flux density is definitely known, the stator tooth dimensions are dimensioned next. Firstly, in this work, the tooth width is chosen to be constant, thus the slot has a trapezoidal shape and assume that the slots are semi-closed slots (see Figure 18). Another assumption is related to the flux densities value in the ferromagnetic materials: by selecting a value between $1.5\ T$ and $2\ T$ [14], one may be able to determine the tooth width. When a tooth occurs at a peak value of the air-gap flux density, an apparent tooth flux passes the slot pitch

$$\widehat{\Phi_d'} = l'\ \tau_u\ \widehat{B_\delta}$$

If the teeth of the machine are not saturated, almost the complete flux of the slot pitch flows along the teeth, and there is no flux in the slots and the slot insulations. Neglecting the slot opening and taking into account the space factor k_{Fe} of iron, we obtain for a tooth with uniform diameter and cross-sectional area S_d

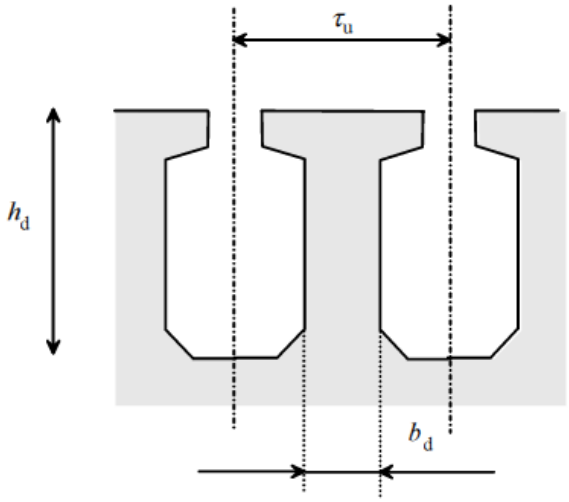

Figure 18.The dimension of a tooth and of a slot

$$S_d = k_{Fe}\ l\ b_d$$

The space factor of iron k_{Fe} depends on the relative thickness of the insulation of the electric sheet and on the press fit of the stack. The insulators are relatively thin, their typical thickness being about $0.002\ mm$, and consequently the space factor of iron can in practice be as high as 98%.

Assuming that the complete flux $l'\tau_u\widehat{B_\delta}$ is flowing in the tooth, we obtain its apparent flux density $\widehat{B_d'}$

$$\widehat{B_d'} = \frac{\widehat{\Phi_d'}}{S_d} = \frac{l'\ \tau_u}{k_{Fe}\ l\ b_d}\ \widehat{B_\delta} \qquad (36)$$

From Equation (36), the tooth width b_d may be computed.

To determine the stator slot dimensions, we have first to estimate the stator current; in PMSMs is obtained with the shaft power P, the stator phase voltage U_{ph}, the efficiency ε and power factor $\cos\varphi$ (note that these quantities are assumed as input required variables and one should evaluate them with the real values obtained at posteriori, at the end of design):

$$I_s = \frac{P}{m\ \varepsilon\ U_{ph} \cos\varphi} \tag{37}$$

When the stator current have been resolved, we have to determine the areas of the conductors S_{cs}. The resistive losses of the windings are chiefly determined by the stator current density J_s. The number a of the parallel paths has also to be borne in mind:

$$S_{cs} = \frac{I_s}{a\ J_s} \tag{38}$$

The wound area S_{Cus} of the stator slot is obtained by

$$S_{Cus} = \frac{z_q\ S_{cs}}{k_{Cus}} \tag{39}$$

where k_{Cus} is the space factor of the slot. The space factor depends principally on the winding material, the voltage level and the winding type of the machine. The windings of small electrical machines are usually made of round wire. In that case, the space factor of an insulated wire in a free slot (with the area reserved for the slot insulation subtracted) varies, depending on the quality of winding assembly, from 60 to 66%.

The space factor value is, however, defined for noninsulated slots. Values of $k_{Cus}\ \epsilon\ (0.5,\ 0.6)$ are typical for low-voltage machines. The lower limit is for round enamelled wires and the upper limit for ideal prefabricated rectangular windings in low-voltage machines. In high-voltage machines, the insulation takes more space and the slot space factor varies, $k_{Cus}\ \epsilon\ (0.3,\ 0.45)$, the lower value being for round wires and the upper for rectangular wires [14].

With respect to the slot shape, in order to simplify the calculation of some dimensions, we choose the slot shape of Figure 19. Note that one may assume that the dimensions related to the insulations (between winding and tooth and between

layers) are included in the space factor of the slot; hence, a space factor circa equal to 0.5 is chosen as initial value and then it may automatically be changed in the sizing loop in order to adjust the slot area and thus the current density.

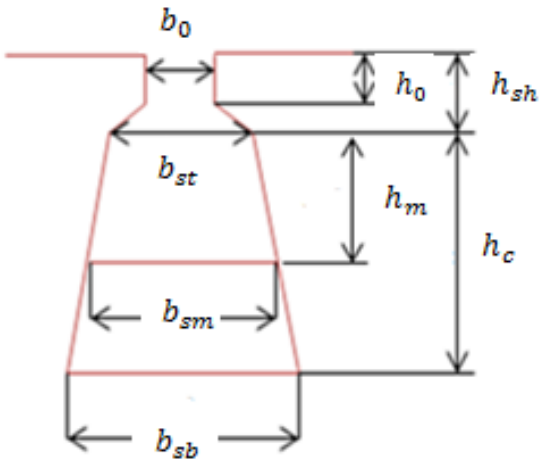

Figure 19.Slot dimensions

One may start the slot design by assuming an initial value of the slot opening b_0. It will be chosen, as in next chapters will explained, with the purpose to reduce the cogging torque by simulating the behaviour of the machine with a FEM-based software (as it has said in the previous section, in this thesis also the magnet span α_{PM} will be optimized in order to get the minimum oscillation of the torque at no-load condition).

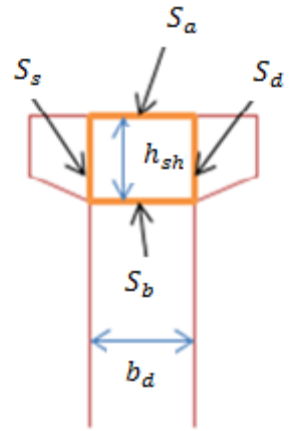

Figure 20.Calculation of the tooth shoe height

In order to calculate h_{sh}, one may observe that the flux flowing in S_b is the sum of three terms, which are the three fluxes flowing in the areas S_a , S_d and S_s (note that $S_d = S_s$):

$$l' b_d \widehat{B_\delta} = 2h_{sh} \widehat{B_d'} k_{Fe} l + \\ + b_d \widehat{B_d'} k_{Fe} l \qquad (40)$$

From the equation above one is able to find the value of h_{sh}, then an initial choice of $h_0 = h_{sh}/3$ is made; this value could be optimized in a second step in order to avoid the saturation of the tooth shoe.

Other dimensions are determined as follows:

$$b_{st} = \frac{\pi\,(D_s + 2h_{sh})}{Q} - b_d$$

The slot height h_c and the bottom slot width b_{sb} are found by putting the two unknowns in a system of two equations and by assuming that the area of the slot is equal to the value calculated in the Equation (39):

$$\begin{cases} S_{Cus} = \dfrac{b_{st} + b_{sb}}{2} h_c \\ b_{sb} = b_{st} + \dfrac{2\,\pi\,h_c}{Q} \end{cases}$$

By putting the second equation of the system in the first one, we can solve an equation of second degree in which h_c is found. Then we can determine the value of b_{sb}.

In the case of a double-layer winding, we have a little insulation layer between two layers of copper. In this section, in which the aim is being able to do a starting sizing of a permanent magnet synchronous motor, we do not estimate the thickness of the insulation layer. Hence we can estimate the height h_m and the width b_m by using the same system of equations above and by assuming that the two areas related to the two layers are equal, so that:

$$\begin{cases} \dfrac{S_{Cus}}{2} = \dfrac{b_{st} + b_m}{2} h_m \\ b_m = b_{st} + \dfrac{2\,\pi\,h_m}{Q} \end{cases}$$

2.5 Magnetic voltages over the machine

2.5.1 Introduction

When the air-gap diameter, the air gap length, the peak value of the air-gap flux density and the dimensions of the stator slots of the machine are known, we may start to calculate the magnetic voltages over the air gap and the teeth. An exact definition of the magnetic voltages in these areas requires an analysis of the flux diagram in the respective areas. The manual solution of a flux diagram is a difficult task; however, with sufficient accuracy, the calculations can be made to estimate the line integral of the field strength H in this area:

$$F_m = \int H\,dl$$

The apparent peak value $\widehat{\Phi_d'}$ of the stator tooth flux is obtained by calculating the flux at the distance of a tooth pitch at the peak value of the flux density (see section 2.4). As the teeth saturate, one may observe that a part of the flux flows along the air space of the slot. However, inn the middle of the tooth, the field strength H and the differential section dl of the integration path are parallel, and therefore the integration is easy.

Obviously, the total magnetic voltage has to be calculated and thus we need the heights of stator and rotor yokes with the purpose to determine the magnetic voltage drop over them; finally, we need to know the magnetic voltage over the permanent magnets and in this way we will able to find the thickness of the magnets.

2.5.2 Magnetic voltage over a tooth

The hypothesis that we have used in the section 2.4 with the purpose of determining the tooth width b_d (Equation (36)) is that all the flux is passing through the tooth. In practice, a part of flux (that we call$\widehat{\Phi_u}$) passes through the slot along an area S_u, so that

$$\widehat{\Phi_d} = \widehat{\Phi_d'} - \widehat{\Phi_d} = \widehat{\Phi_d'} - S_u\widehat{\mathrm{B}_u}$$

By dividing the result by the area of the tooth iron S_d we obtain the real flux density of the tooth iron

$$\widehat{\mathrm{B}_d} = \widehat{\mathrm{B}_d'} - \frac{S_u}{S_d}\widehat{\mathrm{B}_u} \qquad \frac{S_u}{S_d} = \frac{l'\tau_u}{k_{Fe}\, l\, b_d} - 1$$

To calculate the flux density in the slot, the magnetic field strength in the tooth is required. Since the tangential component of the field strength is continuous at the interface of the iron and the air, that is $H_d = H_u$, the flux density of the slot is $\widehat{\mathrm{B}_u} = \mu_0\widehat{H_d}$, so we have

$$\widehat{\mathrm{B}_d} = -\frac{S_u}{S_d}\mu_0\widehat{H_d} \tag{41}$$

The flux density on the tooth is now obtained by solving the intersection of the BH curve of the specific electric sheet and the line given by Equation (41). In Figure 22, it may be seen an example of a graphic solution of the problem. However, almost always, the apparent flux density $\widehat{\mathrm{B}_d'}$ is not so different by the value $\widehat{\mathrm{B}_d}$ that takes into account the part of the flux not flowing in the tooth.

The magnetic voltage over the tooth is approximately

$$F_{m,d} = \widehat{H_d}\, h_d$$

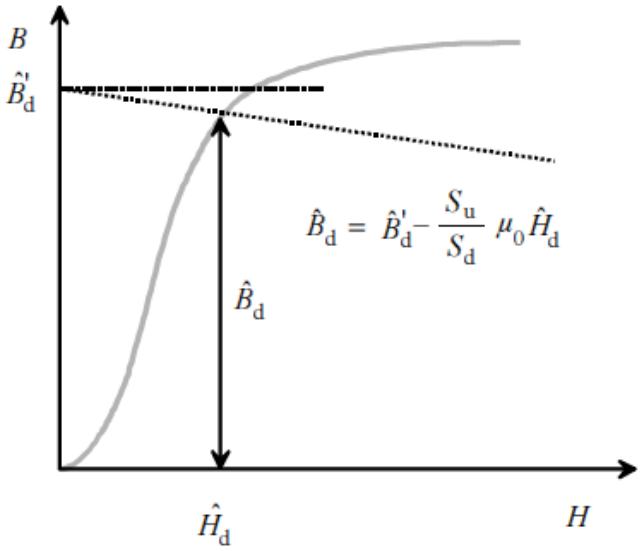

Figure 21.Definition of the flux density of the tooth by the intersection with the BH curve of the electrical sheet

2.5.3 Magnetic voltage of stator and rotor yokes

The flux-per-pole penetrating the air gap and the teeth section is divided into two equal parts at the stator and rotor yokes, as we can see in the Figure 22.

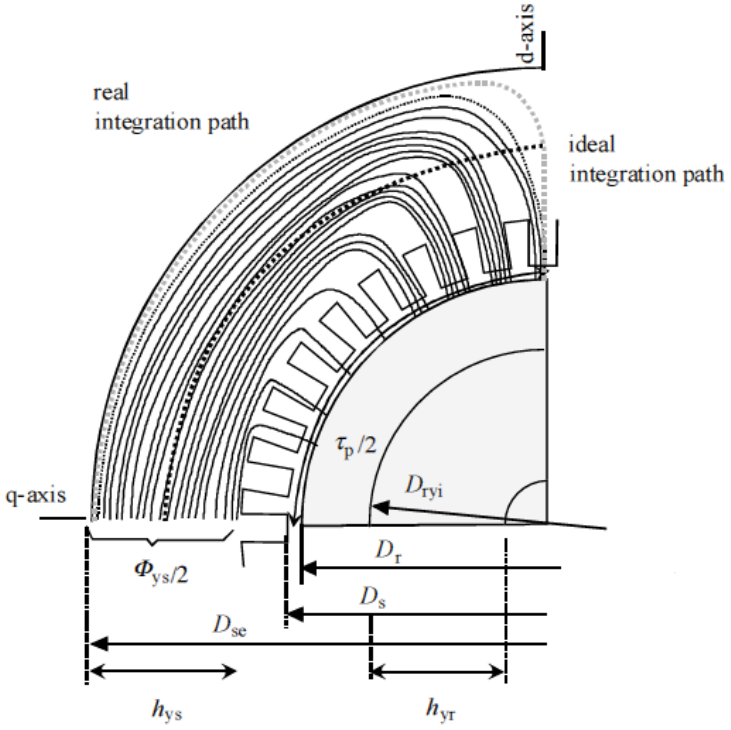

Figure 22.Flux in the stator yoke and integration path of the magnetic voltage

At the peak of the air-gap flux density on the d-axis, the flux densities in the yokes are zero. The maximum flux densities for the yokes occur on the q-axis, on which the air-gap flux density is zero. By choosing the maximum flux densities $\widehat{B_{ys}}$ and $\widehat{B_{yr}}$ in both yokes on the basis of the properties of the ferromagnetic materials, we have that

$$\widehat{B_{ys}} = \frac{\widehat{\Phi_{PM}}}{2\,S_{ys}} = \frac{\alpha_{PM}\,\widehat{B_\delta}\,\tau_p\,l'}{2\,k_{Fe}\,l\,h_{ys}} \tag{42}$$

$$\widehat{B_{yr}} = \frac{\widehat{\Phi_{PM}}}{2\,S_{yr}} = \frac{\alpha_{PM}\,\widehat{B_\delta}\,\tau_p\,l'}{2\,k_{Fe}\,l\,h_{yr}} \tag{43}$$

Equations (41) and (42) allow finding the height h_{ys} of the stator yoke and the height h_{yr} of the rotor yoke. Note that S_{ys} and S_{yr} are the cross-sectional areas respectively of the stator and rotor yokes. The calculation of the magnetic voltage of the yoke is complicated, since the flux density at the yoke changes constantly over the pole pitch, and the behaviour of the field strength is highly non-linear. However, in manual calculation, the magnetic voltages of the stator and rotor yokes may be calculated as the following:

$$F_{m,ys} = \widehat{H_{ys}}\tau_{ys}$$
$$F_{m,yr} = \widehat{H_{yr}}\tau_{yr}$$

Here $\widehat{H_{ys}}$ and $\widehat{H_{yr}}$ are the field strengths corresponding to the highest flux density, and τ_{ys} and τ_{ys} are the lengths of the pole pitch in the middle of the yoke (Figure 21):

$$\tau_{ys} = \frac{\pi\,(D_{se} - h_{ys})}{2p}$$
$$\tau_{yr} = \frac{\pi\,(D_{ryi} - h_{yr})}{2p}$$

in which D_{se} is easy to determine from the dimensions that we have calculated in the previous sections, while D_{ryi} is a function of the permanent magnet thickness and thus, as we will see later in this chapter, this value will be calculated a posteriori.

$$D_{se} = D_s + 2(h_{sh} + h_c + h_{ys})$$

$$D_{ryi} = D_r - 2h_{PM}$$

2.5.4 Magnetic voltage of the air gap

The air gap of an electrical machine has a great influence on the magneto-motive-force (m.m.f.) and it is simple to observe that its related magnetic voltage has a value much bigger than other magnetic voltages because of the great value that the reluctance of the air has. For this reason, very often in the analysis and design of an electrical machine, we may apply the Ampère law only over the air gap and disregard the magnetic voltages over the other parts of the machine.

To be able to calculate the magnetic voltage manually over an air gap, the geometry of the air gap has to be simplified. Often in an electrical machine, the surfaces of both the stator and the rotor are split with slots. The flux density always decreases at the slot opening, and therefore it is not easy to define the average flux density of the slot pitch between the stator and the rotor. However, in 1901 F.W. Carter provided a solution to the problem of manual calculation (Carter, 1901). On average, according to Carter's principle, the air gap seems to be longer than its physical measure. The length of the physical air gap δ increases with the Carter factor. The first correction is carried out by assuming the rotor to be smooth. We obtain

$$\delta_{es} = k_{Cs}\,\delta \tag{44}$$

The Carter factor k_{Cs} is based on the dimensions in Figure 23. When determining the Carter factor, the real flux density curve is replaced with a rectangular function so that the flux remains constant under the teeth and is zero at the slot opening.

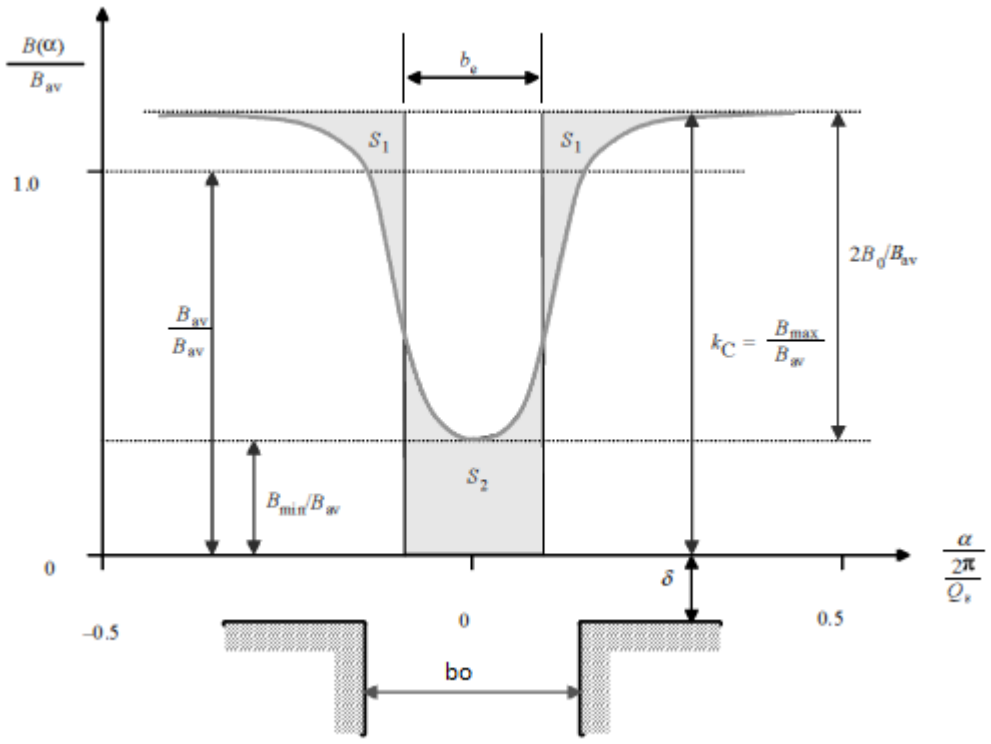

Figure 23.Air gap flux density in a distance of 1 slot pitch

In this figure, we can observe that the shaded area $S_1 + S_1$ is equal to S_2. The equivalent slot opening b_e, in which the flux density is zero, is

$$b_e = \kappa\, b_0$$

where

$$\kappa = \frac{2}{\pi}\left[\arctan\frac{b_0}{2\delta} - \frac{2\delta}{b_0}\ln\sqrt{1+\left(\frac{b_0}{2\delta}\right)^2}\right]$$

and the Carter factor is

$$k_{Cs} = \frac{\tau_u}{\tau_u - b_e}$$

In a SPMSM, one may approximately assume the rotor to be smooth, so that it may possible to consider the equivalent gap given by the Equation (44) for determining the magnetic voltage of the air gap:

$$F_{m,\delta_{es}} = \frac{\widehat{B_\delta}}{\mu_0}\,\delta_e$$

2.5.5 Total magnetic voltage and height of permanent magnets

Now all the main dimensions of the machine and the magnetic voltages required by different parts of the machine have been determined. The sum of the magnetic voltages has to be covered by the current linkage produced by permanent magnets. Note that half of the magnetic circuit is calculated in this work (half of the stator and rotor yokes, one stator tooth and one air gap): the magnetic voltage sum of half of the magnetic circuit has to be covered by one permanent magnet:

$$F_{m,tot} = F_{m,\delta_e} + F_{m,d} + F_{m,PM} + \frac{F_{m,ys}}{2} + \frac{F_{m,yr}}{2} = H_c h_{PM}$$

We may assume that the permanent magnet flux density B_{PM} is equal to the air gap flux density $\widehat{B_\delta}$. The magnetic voltage over the permanent magnet is

$$F_{m,PM} = \frac{H_c}{B_r}\,B_{PM} h_{PM}$$

As it has said in the subsection 2.5.3, the magnetic voltage over the rotor yoke is a function of our unknown h_{PM} so that we can finally the height of the magnet:

$$h_{PM} = \frac{U_{m,\delta_e} + U_{m,d} + \frac{U_{m,ys}}{2} + \frac{\pi\widehat{H_{yr}}(D_r - h_{yr})}{4p}}{H_c - \frac{H_c}{B_r}B_{PM} + \frac{\pi\widehat{H_{yr}}}{2p}} \quad (45)$$

Finally, one may determine the magnetic voltage over the rotor yoke $F_{m,yr}$.

2.6 Inductances and resistances

Since the dimensions have been defined and the winding has been selected, the resistances and inductances of the machine are now calculated.
The most important inductance of the machine is called magnetizing inductance. Next, a magnetizing inductance of a poly-phase winding is calculated for an unsaturated machine. As we said previously, by assuming a sinusoidal flux density distribution over the pole pitch and the length of the machine, we may integrate the flux of the machine and the result of the integration gives $\widehat{\Phi_m} = \alpha_{PM}\tau_p l'\widehat{B_\delta}$.
The is namely 'the peak value of the air-gap flux' and describes the maximal flux that penetrates a diagonal coil and hence produces the maximum flux linkage of a phase winding $\widehat{\Psi_m}$. By multiplying the effective number of turns we get

$$\widehat{\Psi_m} = \widehat{\Phi_m}\, k_{w1} N_{ph}$$

On the other hand, the magnetic flux density of an air gap can be determined by applying the current linkage of the phase; in other words, the current linkage $\widehat{\Theta}$ of the stator creates a flux in a direct-axis air gap

$$\widehat{B_m} = \frac{\mu_0 \widehat{\Theta}}{\delta_{ef}}$$

where δ_{ef} the effective air gap met by the current linkage of the stator winding.
By substituting in the equation above we obtain that

$$\widehat{\Psi_m} = k_{w1} N_{ph} \alpha_{PM} \frac{\mu_0 \widehat{\Theta}}{\delta_{ef}} \tau_p l'$$

and

$$\widehat{\Theta} = \frac{4\, k_{w1} N_{ph}}{2\,\pi\, p} \sqrt{2}\, I_s$$

By substituting the last equation in the expression of $\widehat{\Psi_m}$ and by dividing the result by the peak value of the current, we obtain the main inductance L_{mph} of a single-phase winding:

$$L_{mph} = \frac{2}{\pi}\,\mu_0 l'\,\frac{2}{\pi p}\alpha_{PM}\frac{\tau_p}{\delta_{ef}}\left(k_{w1}N_{ph}\right)^2$$

The magnetizing inductance of an m-phase machine can be calculated by multiplying the main inductance by m/2. In most applications, $m = 3$, thus

$$L_m = \frac{3}{2}\frac{2}{\pi}\,\mu_0 l'\,\frac{2}{\pi p}\alpha_{PM}\frac{\tau_p}{\delta_{ef}}\left(k_{w1}N_{ph}\right)^2 \tag{46}$$

Hence, the magnetizing inductance depends on the phase number m, the effective turns of winding and the length of the machine, the number of pole pairs and the effective air gap.

An effective air gap includes an air gap lengthened with the Carter factor and the effect of iron, which also increases the apparent air gap. In such a case, the iron circuit is strongly saturated. In permanent magnet synchronous machines, in which the equivalent air gap includes in the d-direction the length of the permanent magnets, the proportion of iron remains very low. In this work, δ_{ef} is calculated as the following:

$$\delta_{ef} = \frac{F_{m,\delta_e} + F_{m,d} + F_{m,PM} + \frac{F_{m,ys}}{2} + \frac{F_{m,yr}}{2}}{F_{m,\delta_e}}\delta_e$$

Magnetizing inductance is not constant but changes as a function of voltage and torque. The voltage dependence can be easily explained. Increasing the voltage increases the flux density, which may saturate the iron parts. The torque dependence can be explained by Faraday's principles. When the torque increases, the tension of the flux lines increases. The lines travel along more saturated paths, and the machine requires more magnetizing current than before.

Together with the inductances, the resistances define the characteristics of an electrical machine.

The resistance of a winding can first be defined as a DC resistance:

$$R_{DC} = \frac{N_{ph} l_{av}}{\sigma_{Cu}\, a\, S_{cs}} \tag{47}$$

Resistance is highly dependent on the running temperature of the machine, and thereforea designer should be well aware of the warming-up characteristics of the machine before defining the resistances. Usually, we may first investigate the resistances of the machine at the design temperature or at the highest allowable temperature for the selected winding type Θ.

Windings are usually made of copper. The conductivity of commercial copper wire is $\sigma_{Cu20} = 57 * 10^6\ S/m$ (at room temperature) and the temperature coefficient of resistivity is $\alpha_{Cu} = 3.81 * 10^{-3}\ 1/K$, so that we may estimate that

$$\sigma_{Cu} = \frac{\sigma_{Cu20}}{1 + \Theta\, \alpha_{Cu}}$$

An accurate definition of the winding length in an electrical machine is a fairly difficult task. SPMSMs are a simple case:

$$l_{av} = 2\, l + \left(2\, \frac{\pi\, (D_s + h_d)}{W}\right)$$

in which W is the winding pitch, D_s the inner stator diameter, h_d is the tooth length and l is the stator stack length. The second term of the addition is related to the average length of the end winding.

Using the length of the winding, the DC resistance may be calculated according to Equation (47) by taking all the turns and parallel paths into account.

One should consider the influence of the skin effect on the phase resistance: alternating current creates an alternating flux in the conductor material. In electrical machines, the skin effect occurs chiefly in the area of the slots, but it is also present in end windings. However, in this work, the skin effect is disregarded.

2.7 Power losses, efficiency and power factor

With respect to the losses, now all the iron parts of the machine can be analysed. In permanent magnet synchronous machines the base frequency of the armature core usually stator) is the frequency of the network (50 Hz in Europe) or the frequency of the supplying frequency converter, and the frequency of the rotor is zero in the stationary state. However, the rotor surface experiences high-frequency alternating flux components because a changing permeance caused by the stator slots. For instance, in the rotor of a permanent magnet synchronous machine, the base frequency is zero, but other pulsation losses occur on the rotor surface because of stator slotting. Further, the power losses given by the manufacturer are presented for AC magnetizing, not for rotating magnetizing, which is the dominant form of

motion of the field in the stator yoke. These facts have led to the utilization of the empirical factors k_{Fe}. These factors are used to correct the iron loss calculations.
Losses in an iron circuit are of two different types, namely hysteresis losses and eddy current losses. To calculate the core losses, we need the masses of different iron parts: with the main dimensions, we are able to calculate the volumes of the stator and rotor yokes, the total volume of the stator slots and teeth and thus all the masses m_{Fe}. Now we may calculate the power losses for the n sections of the machine:

$$P_{Fe} = \sum_n k_{Fe,n}\, P_{10} \left(\frac{\widehat{B_n}}{1}\right)^2 m_{Fe,n}{}^{\frac{3}{2}} \quad \text{or} \quad P_{Fe} = \sum_n k_{Fe,n}\, P_{15} \left(\frac{\widehat{B_n}}{1{,}5}\right)^2 m_{Fe,n}{}^{\frac{3}{2}}$$

Here P_{10} and P_{15} are the specific power losses respectively at $1\,T$ and $1.5\,T$, given by the manufacturer and corresponding to the supply frequency.
In this work, resistive losses in the three-phase winding are calculated as

$$P_{Cu} = m\, R_{DC}\, I_s$$

Following the definition of the iron and resistive losses, the windage and friction losses and the additional losses of the machine can be defined according to [11]. These are empirical methods to calculate these kinds of losses and the results may be very different from the practice. This is the reason why, in this work, the losses (also the iron and Joule losses) will be calculated by FEM-based software in order to estimate, as it will see in the chapter 4, the temperatures in the main parts of the machine.
The sum of losses P_{loss} in the machine allow to determine the input power of the machine as

$$P_{in} = P + P_{loss}$$

where P is the output power (remember that P is an input value in the design procedure described in this chapter).
Now the efficiency ε and the power factor $\cos\varphi$ of the machine may be resolved as

$$\varepsilon = \frac{P}{P_{in}} \qquad \cos\varphi = \frac{P_{in}}{\sqrt{3}\, V\, I_s}$$

Here V is the line to line voltage (V star connected). These last obtained values have to be compared with the required values for the efficiency and power factor used in this thesis work as input parameters at the beginning of the described general sizing. If the above calculated values are lower than the required ones, we should iterate the design tool in order to get the desired performances.
As a matter of fact, accurate management of heat and fluid transfer in an electrical machine is a more difficult and complicated issue than the conventional electromagnetic design of an electrical machine. However, as shown previously in this material, problems related to heat transfer can to some degree be avoided by utilizing empirical knowledge of the machine constants available. When creating completely new constructions, empirical knowledge is not enough, and thorough modelling of the heat transfer is required. Finally, prototyping and measurements verify the successfulness of the design.

2.8 Matlab implementation

A dimensioning loop for surface mounted permanent magnet synchronous machines has been implemented using the MATLAB software. In brief, all the implemented design process is presented in Figure 24.
The initial parameters are chosen during steps 1-4. These parameters are quite free to choose: they depend on the specific application and the reasons that lead to choose a specific value rather than another one have been explained in the previous sections (see section 2.1). However, the aim of this work is to realize a general and starting sizing of a PMSM and an optimization of these free parameters is always possible in a successive step, for instance by means of finite element analysis (as it will be seen in the next chapter).
At step 5 some of the main mechanical dimensions are defined. These are the machine length (see Equations 23-26), air gap thickness (one may choose an initial value of $1\ mm$ or see equations 27-28) and thus the stator inner diameter and the effective machine length. Also in step 6 an assumption related to the number of slots-per-pole-per-phase and to the number of layers in the slot are done (section 2.3).
From step 7 to step 10: one may assume that the Back-EMF is close to the supply voltage. In particular, in this work it has computed the most suitable coefficient k so that the new calculated value (after the rounding of the number of conductors in a slot) of the air gap flux density is as close as possible to the desired value chosen at step 2.
The dimensions of the stator slots and teeth (section 2.4), the dimensions of yokes and all diameters are calculated at step 11 (see subsection 2.5.3). By defining the total magnetic voltage of the magnetic circuit at step 12 (subsection 2.5.5), one may

calculate the permanent magnet length in the radial direction according to Equation (45). The rest of the machine properties are calculated during steps 14 and 15 (according to section 2.6 and 2.7).

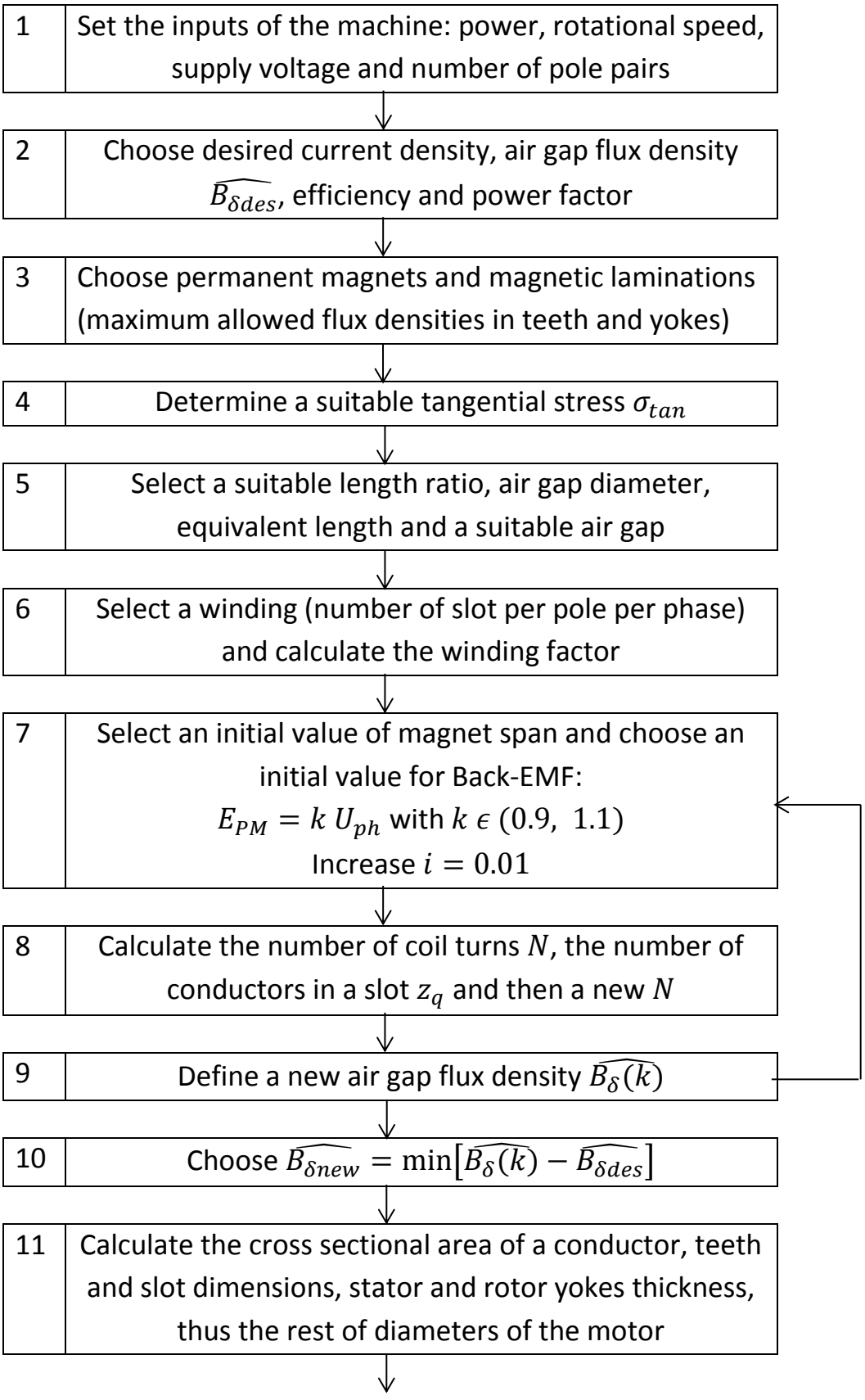

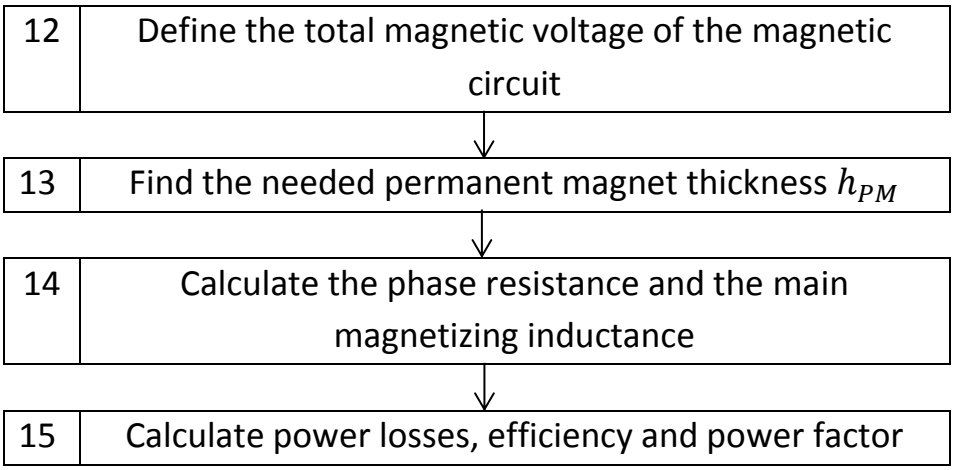

Figure 24.Implemented design process of a permanent magnet synchronous motor in brief

3 VALIDATION OF PRELIMINARY DESIGN BY MEANS OF FEM ANALYSIS

3.1 Introduction to FEM

The spreading of numerical models appropriate for computing electric and magnetic fields is due to the requirement of more accuracy during the design and the analysis of electro-magnetic devises, that in our case are electrical machines; it is also due to the growing of the complexity of the structures under study. These numerical methods are based on the determination of the magnetic field distribution inside the motor under study, solving Maxwell's equations.

An analytical solution of the field problem is rarely possible to determinate, because usually the structure under study is geometrically complex and the materials are non-linear and therefore only a numerical solution is possible.

The finite element method is a numerical technique that allows achieving a field solution, even with time variable fields and with materials that are anisotropic and non-linear. Using the finite element method, the whole analysis domain is divided into elementary subdomains, which are called finite elements, and the field equations are applied to each of them. The study of the electromagnetic field distributions allows a precise analysis, highlighting dangerous field gradient, saturation, etc. [3].

Furthermore it provides a complete estimation of the machine performances, which would be hardly achievable adopting analytical methods. Moreover, classical methods may be adopted for simple devises, as for instance a surface mounted permanent magnet motor; as the structure grows in complexity, the analytical design become almost impossible or lacking in accuracy.

At last but not the least important advantage of this technique is the possibility to reduce the number of prototypes. However, the finite element method has some disadvantages: being a numerical technic, the solution is necessarily approximate.

If the method is not correctly applied, it might generate inaccurate or wrong results. Moreover the computation time is generally high and it grows proportionally to the required accuracy: it is influenced by the dimension of the finite elements; obviously a fine subdivision increases the accuracy but at the same time increases the computation time.

In order to reduce it, each periodicity and symmetry (geometric and electromagnetic) of the structure are exploited. Furthermore simulating just one part of the structure allows to improve the accuracy of the solution considering the same computation time.
Usually the size of the finite elements is smaller near the part of the machine where the most of energy is stored, while the size is bigger where the structure doesn't present any field criticality.

The finite element analysis is organized in the following steps [3]:

1. partition of the domain; in two dimensional problems usually each element is a triangle while in three dimensional problem each element is a tetrahedron;
2. choice the interpolating function: these functions are necessary to the resolution of the field problem inside each element and they can be really simple since the small dimension of the finite elements;
3. formulation of the system to solve the field problem: the system of equations could be developed by means a variational or a residual method;
4. solution of the problem by means common numerical algorithms because the finite element method transforms a system of partial differential equations in a system equations;
5. post-processing: once the field problem is solved, from the values of the field in each node is possible to determinate the others electromagnetic quantities.

Although the electrical machines are three dimensional structures, a 3D analysis requires heavy processing and long computation time. The field problem can be carried out by a two-dimensional analysis, using the machine symmetry, and this allows an appreciable reduction in the computation time.
In rotating machine the planar symmetry is adopted: it is assumed that the magnetic field is identical in each plane normal to the rotational axis. The omitted phenomena due to the 2D analysis (such as the effect of the ending edge of the machine) could be taken into account, correcting the obtained solution, if they are not negligible.
In 2D analysis, starting from the well-known Maxwell's equations, it is easy demonstrate that the current density vector $\boldsymbol{J}$ has only the component normal to the plane x-y and consequently the potential vector $\boldsymbol{A}$ has only the z-component. In this condition the magnet flux density vector **B** has components only on the plane x-y because $\nabla \times \boldsymbol{A} = \boldsymbol{B} = \left[\frac{\delta A_z}{\delta y}, -\frac{\delta A_z}{\delta x}, 0\right]$.
When an electrical machine is analysed by finite element method, usually only the magnetic field problem is investigated; such a problem is the most common in the analysis of electrical machine. In any case, the study of the magnetic field distribution is not sufficient for a complete analysis of the machine.

Boundary conditions assignment assumes a fundamental importance in the solution the field problem; the choice of the boundary conditions not only influences the final solution, but also can reduce the domain under study. Imposing the boundary conditions means to assign the value of the magnetic vector potential A on a given part of the boundary, that in a 2D problem is a line.

All the boundary conditions can be classified into 3 classes: Direchlet boundary, Neumann boundary and periodic boundary conditions. Using Direchlet boundary condition, the value of magnetic vector potential $\boldsymbol{A}$ is assigned to each point of the boundary. The homogeneous Direchlet boundary condition ($\boldsymbol{A} = 0$) is usually adopted during the study of electrical machine. Under this assumption, the flux lines are tangential to the boundary and no flux line crosses that boundary; such a condition is equivalent to considering an external material with null magnetic permeability. In the reality some flux lines can go out from the stator back iron and a realistic finite element analysis requires imposing a homogeneous Direchlet's boundary condition not on the external circumference of the machine but to an external and virtual circumference draws outside the stator.

When a PMSM motor operates at no-load, the flux lines are tangential to the d-axis, as shown in the figure 25 (an IPM motor is shown but we may so the same considerations for a SPM motor). The structure appears symmetric with respect to each d-axis, both geometrically and magnetically.

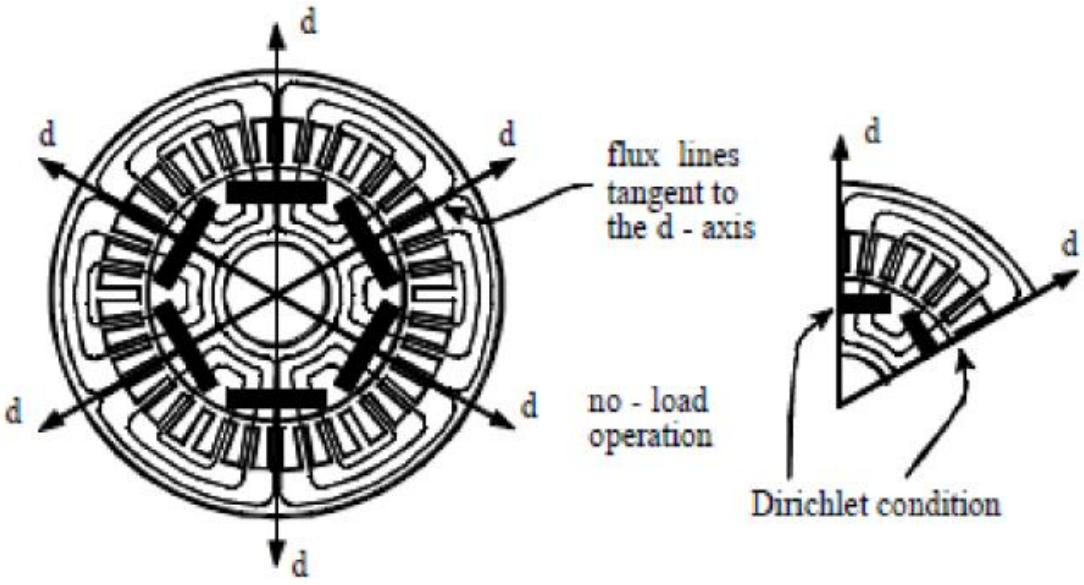

Figure 25.Dirichlet's boundary condition

The Neumann's boundary condition corresponds to imposing a given value to the derivative of the magnetic vector potential A, so that the flux lines have a given incidence angle with the boundary.

In the case of homogeneous Neumann's condition $\frac{dA}{dn} = 0$ (where n is the unit vector normal to the boundary line) the flux lines are forced to be normal to the boundary line. As an example, let us consider again the IPM motor at no-load operation, in Figure 26: the motor appears symmetric with respect to each q-axis, both magnetically and geometrically, and each part is exactly the mirrored image of the other part, with respect to the q-axis. Since the flux density components cannot be discontinuous, the flux lines must be perpendicular to the q-axis, and the structure can be simplified as shown figure by imposing the homogeneous Neumann's condition along the boundary defined by the q-axes.

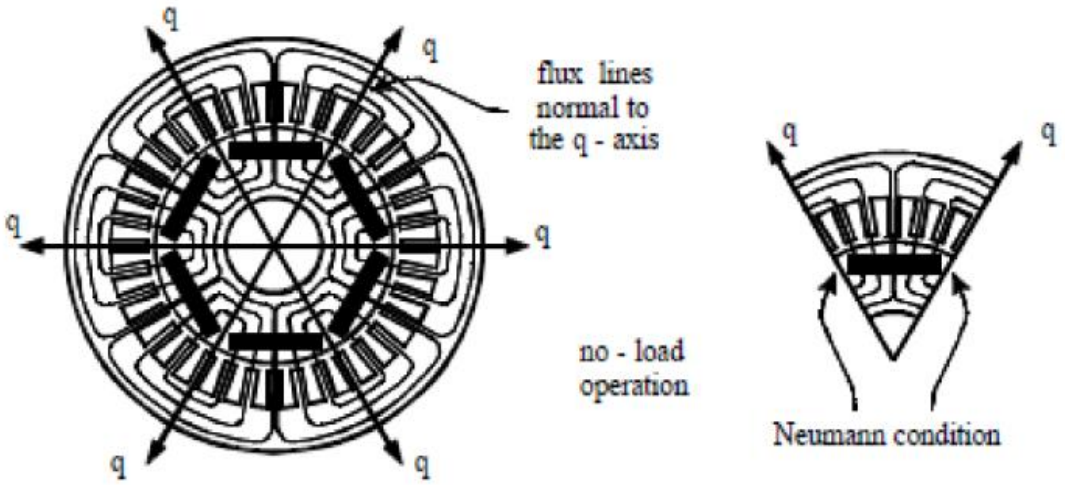

Figure 26.Neumann's boundary condition

A periodic boundary condition assigns a correspondence between the values of the magnetic vector potential along two or more boundary lines. In general terms, two boundary lines are chosen and between them a principal line is selected, and then the magnetic vector potential of the other line is expressed as a function of the magnetic vector potential of the principal line. These kinds of boundary conditions are really useful in structures that exhibit a repetition of the electromagnetic fields and the Direchlet's and Neumann's boundary conditions are not enough to reduce as much as possible the analysis domain. As an example, the section of an IPM motor is shown in figure 27; the machine has 3 pole pairs and therefore there is a recurrence of the magnetic field with respect to the angle θ equals to 3. It may be possible to study only a third of the machine, as shown in Figure 27a , by imposing on the boundary that $A_z(r,\theta) = A_z\left(r, \theta + 2k\frac{\pi}{p}\right)$, namely an even periodic condition.

It also may be considered only one sixth of the machine by imposing on the boundary an odd periodic condition: $A_z(r,\theta) = A_z\left(r, \theta + (2k-1)\frac{\pi}{p}\right)$, as shown in Figure 27b.

In this example, it is evident that the process of locating the symmetry lines and the periodic lines, together with the corresponding boundary conditions, may reduce the study of a complex structure to only one part of it. This implies the advantages of shorter computation time considering the same accuracy, or a greater accuracy if the same computation time is considered.

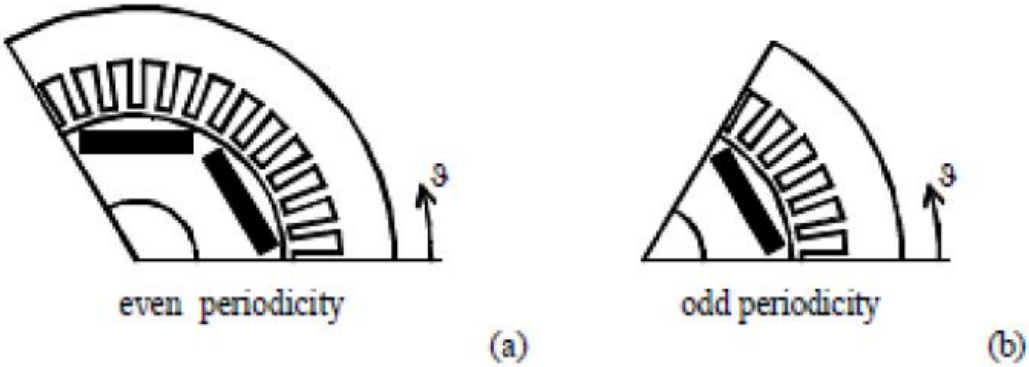

Figure 27.Periodic boundary conditions

3.2 Comparison between FEM and analytical results

After completing the dimensioning tool, the results had to be validated for ensuring that the tool is working correctly. To be able to make conclusions, it is essential that the results calculated with the dimensioning tool can be trusted.
The validation method consists in the following steps:

1. doing a preliminary sizing with the implemented analytical sizing (according to chapter 2) and drawing the motor with the imposed initial values and with the main dimensions obtained by analytical design;
2. choosing the best combination between the permanent magnet span and the slot opening that minimizes the cogging torque by means of finite element method (FEM).
3. comparing the FEM results with the analytical ones

The Magnet 2D software of Infolytica have been used for the FEM modelling and calculation. In this way it is possible to study more accurately how the obtained solution behaves. The results calculated with FEM are compared with the ones obtained using the dimensioning tool. The results should be at least close to those obtained by the dimensioning tool. Some small differences might appear since the dimensioning tool is based only on analytical equations which include a lot of

approximations. With FEM some of the machine properties, for example magnetic flux densities and losses can be modelled more accurately. Therefore it is enough if the results are close to each other.

3.2.1 Design test cases

Two designs have been tested, different from each other by the number of slots-per-pole-per-phase q: in the first case, $q = 1$ and the winding has a single-layer; the second analyzed case is a double-layer winding with short pitching and $q = 2$. The number of pole pairs is the same for both cases ($p = 4$).
In the table below, we can see the initial data of the motor that are the inputs of the dimensioning script:

Table 1.Initial data of the motor

Shaft Power [W]	$\boldsymbol{P = 160000}$
Speed [rpm]	$\boldsymbol{n = 2500}$
Line to line voltage [V]	$\boldsymbol{V = 690}$
Number of pole pairs	$\boldsymbol{p = 4}$
Desired efficiency	$\boldsymbol{\varepsilon = 0.95}$
Power factor	$\boldsymbol{cos\,\varphi = 0.91}$
Permanent magnets	**Neodymium Iron Boron**
Coercivity [A/m]	$\boldsymbol{H_c = 813242}$
Remanence flux density [T]	$\boldsymbol{B_r = 1.06}$
Temperature rise in winding [K]	$\boldsymbol{\Theta = 80}$
Lamination material	**M800-50A**

The main dimensions obtained with the dimensioning tool are required in order to run the script that draws the machines below (all dimensions and parameters are presented in Appendix 1):

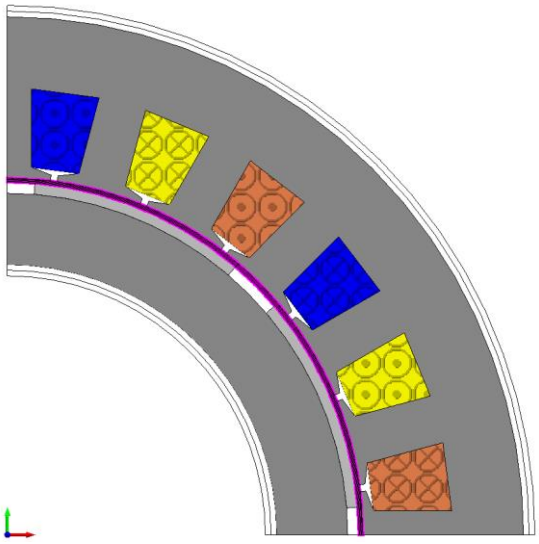

Figure 28.SPMSM after preliminary sizing: $q = 1$, single-layer winding

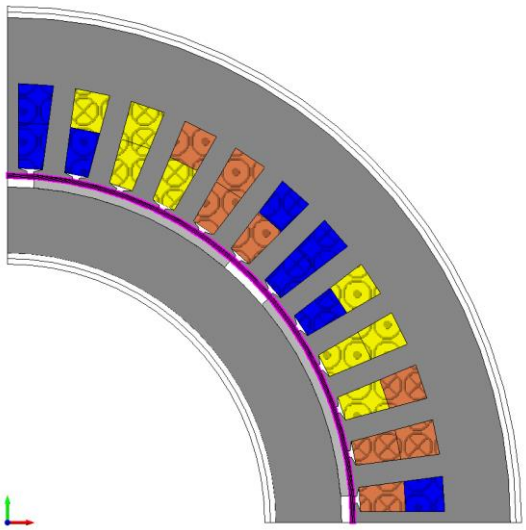

Figure 29.SPMSM after preliminary sizing: $q = 2$, double-layer with short pitching winding

The only dimensions that we mention in this section are the relative magnet width α_{PM} (in p.u. of the pole pitch) and the slot opening b_0 (in mm): as it has already said in the chapter 2, the chosen initial values are

$$\alpha_{PM} = 0.8 \qquad b_0 = 3\ mm$$

3.2.2 Cogging torque minimization

3.2.2.1 Description of the phenomenon

Cogging torque describes the interaction of the rotor magnets acting on the stator teeth or poles independent of any current. While this torque is often considered beneficial in step motors, it is considered detrimental in brushless permanent magnet motors.

This dissatisfaction with cogging torque often lacks quantitative support. One of the first things engineers invariably do when they pick up a small motor is to spin the shaft with their fingers (Hanselman, 2006). The pulsations felt during this process are caused by cogging torque. In comparing several motors based on this qualitative examination, engineers will judge the one with the least cogging torque the best, even if it performs the worst in the actual motor application.

In reality, cogging torque is often very small relative to the beneficial mutual torque produced by a motor. Furthermore, even a slight mismatch between the back EMF of the motor and the motor current often produces greater ripple torque than the

cogging torque itself. In this situation, cogging torque is masked by the larger torque variation in the mutual torque. As a result, the qualitative shaft spin test is often misleading.

Despite the insignificance of cogging torque in many applications and in the presence of mutual torque ripple due to back EMF-current mismatch, cogging torque is a motor characteristic worth understanding. Simply put, cogging torque is the torque created when the rotor permanent magnets attempt to align themselves with a maximum amount of ferromagnetic material.

To understand cogging torque, consider the cogging torque term in equation below:

$$T_{cog} = -\frac{1}{2}\Phi^2 \frac{dR}{d\theta} \tag{48}$$

where Φ is the magnet flux crossing the air gap and R is the total reluctance through which the flux passes. Clearly, if the reluctance R does not vary as the rotor rotates, the derivative in (48) is zero and the cogging torque is zero. In addition, cogging torque is independent of flux direction because the magnet flux is squared.

To illustrate how (48) applies to a common motor structures, consider the motors shown in figures 28 and 29. As each magnet in the motor rotates past the stator teeth, the reluctance experienced by the magnet under the slot openings changes because of the longer flux path length into the slots terminating on the shoes. Therefore, the slot openings create a varying reluctance for the magnet flux, thereby creating cogging torque. If the stator teeth did not have shoes the reluctance variation and resulting cogging torque would be much greater. Thus, the primary purpose for shoes is cogging torque reduction.

3.2.2.2 Cogging torque minimization methods

Shoe design represents a fundamental tradeoff. The narrower the slot opening b_0, the smaller the cogging torque becomes. In the limiting case, if there was no slot openings, cogging torque would be zero. On the other hand, the slot opening must be wide enough to insert coils, with the cost of inserting coils being directly proportional to the slot opening width. A side effect of making the slot opening narrow to minimize cogging torque is that doing so increases the slot leakage inductance component of the winding.

The radial dimension of the shoes also plays a role in cogging torque production. If the radial shoe dimension becomes too small, the ferromagnetic shoe tips become saturated by the magnet flux, thereby adding another varying component to the reluctance that produces cogging torque.

In addition, increasing the air gap length δ relative to the slot opening decreases the flux path variation and decreases cogging torque. If the air gap length is increased, the magnet length must be increased by the same percentage to keep the air gap

flux constant. If the air gap flux decreases, the cogging torque will decrease due to the drop in flux as well, but the desired mutual torque will diminish as well, leading to lower motor performance.

Since each magnet produces cogging torque as it passes by stator slots, the relationship between the number of magnet poles and the number of stator slots influences cogging torque. In integral slot motors, each magnet appears in the same position relative to the stator slots. As a result, the cogging torque created by all magnets are in phase with each other, and the net cogging torque is equal to the product of the number of magnet poles and the cogging torque created by one magnet. That is, the cogging torque from each magnet simply adds to create the net result. On the other hand, in fractional slot motors, each magnet appears in a different position relative to the stator slots. As a result, the cogging torques created by all magnets are out of phase with each other, and the net cogging torque is reduced since the cogging torque from each magnet adds together and at least partially cancels the cogging torque from other magnets. This fact is one of the primary reasons for choosing a fractional slot motor.

The final fundamental way to decrease cogging torque is also based on the $dR/d\theta$ term in (48). The reluctance R describes reluctance that extends along the axial direction of the motor as well. From this point of view, the net change in reluctance can be minimized if the slot openings are spread out over the surface area of the magnet. Here, the slots are skewed so that each magnet sees a net reluctance that stays the same or nearly the same as slots pass by. In this way, changes along the axial dimension are used to diminish the effect of changes along the circumferential dimension. As a result, the $dR/d\theta$ experienced by the entire magnet decreases and the cogging torque decreases.

Recently, a lot of authors have studied the problem of the cogging torque minimization by means of the FEM: in [1] and [15] new techniques are used in order to reduce the cogging torque consisting in pole width modulation, also by using magnets with different widths in the same machine; another method has been presented and it consists in the determination of harmonics in an analytical way in PM machines [7].

3.2.2.3 Slot opening and magnet width modulations

This method has been used with the purpose to find the best combination of the slot opening and the magnet span that minimizes the cogging torque in the machines of Figures 28 and 29. This third step of the validation tool represents the specific optimization objective of the machine design for this thesis work.

As it may be seen in Figures 28 and 29, only a quarter of the machine has been modelled. As already said in the section 3.1, this is possible by applying the suitable boundary conditions to specific surfaces. In this case both even periodic condition

and Dirichlet's condition have been applied in both design test cases, as shown in Figure 30. In this way, one may reduce the computation time and keep the same accuracy or increase the accuracy and keep the same computation time.

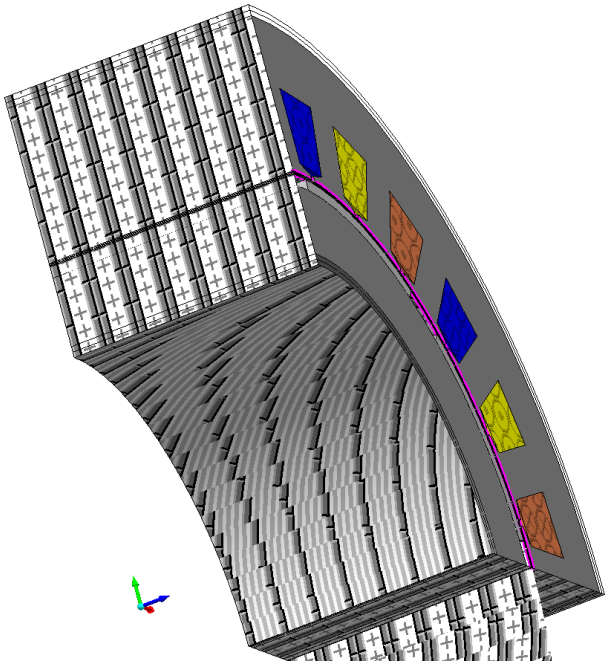

Figure 30.Boundary conditions

In Figure 31 the mesh used to model the machine is shown together with a zoom in the air gap area.

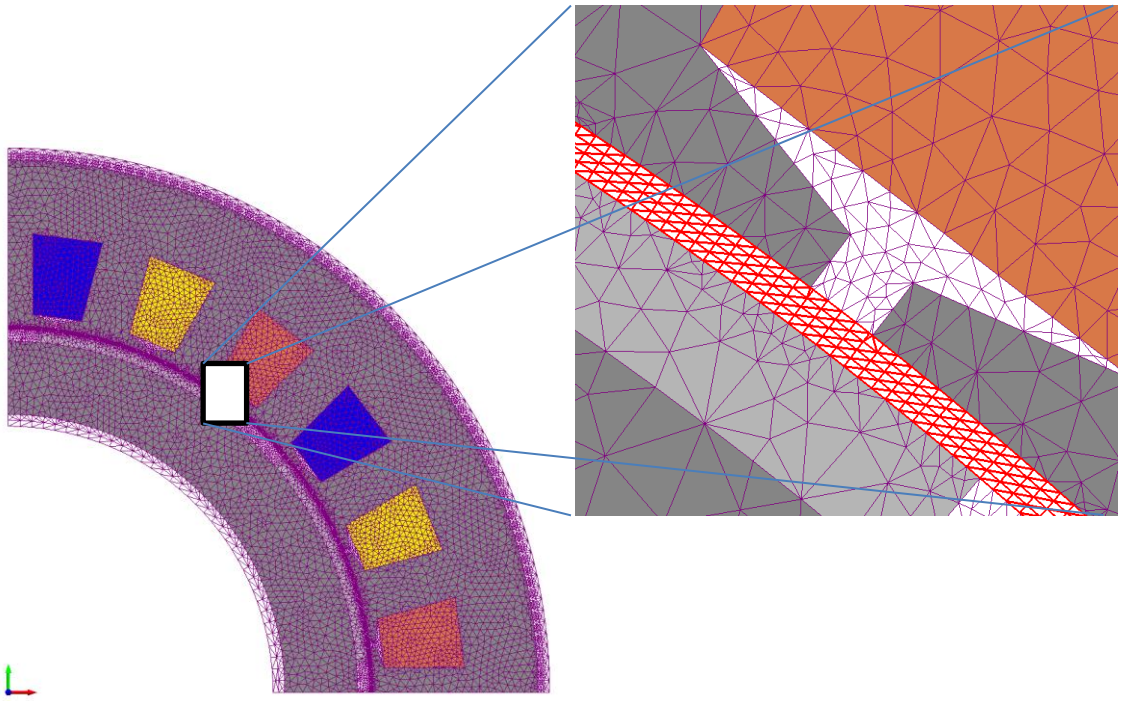

Figure 31.Mesh size used for the simulation tests

In the Figures below (32-33), the results of combined simulations are shown for both cases $q = 1$ and $q = 2$.

With respect to the dependence that the cogging torque has with the slot opening, it may be observed for both cases that this dependence is quite linear and this means that the narrower the slot opening b_0, the smaller the cogging torque becomes. The slot opening range of simulation varies between the minimum acceptable from a manufacturing point of view ($b_0 = 2\,mm$) and the value after which the slot becomes an open slot.

More interesting is the dependence with the magnet width: in the first case ($q = 1$), the minimum is visible and its value is $\alpha_{PM} = 0.7$; in the second case ($q = 2$), the slot opening that minimizes the cogging torque is again $b_0 = 2\,mm$ but we need one plot more in order to find the exact value of the magnet span: fixing the value of b_0, we can see that zooming for $0.63 < \alpha_{PM} < 0.73$ the minimum of cogging torque is at $\alpha_{PM} = 0.68$ (see Figure 34).

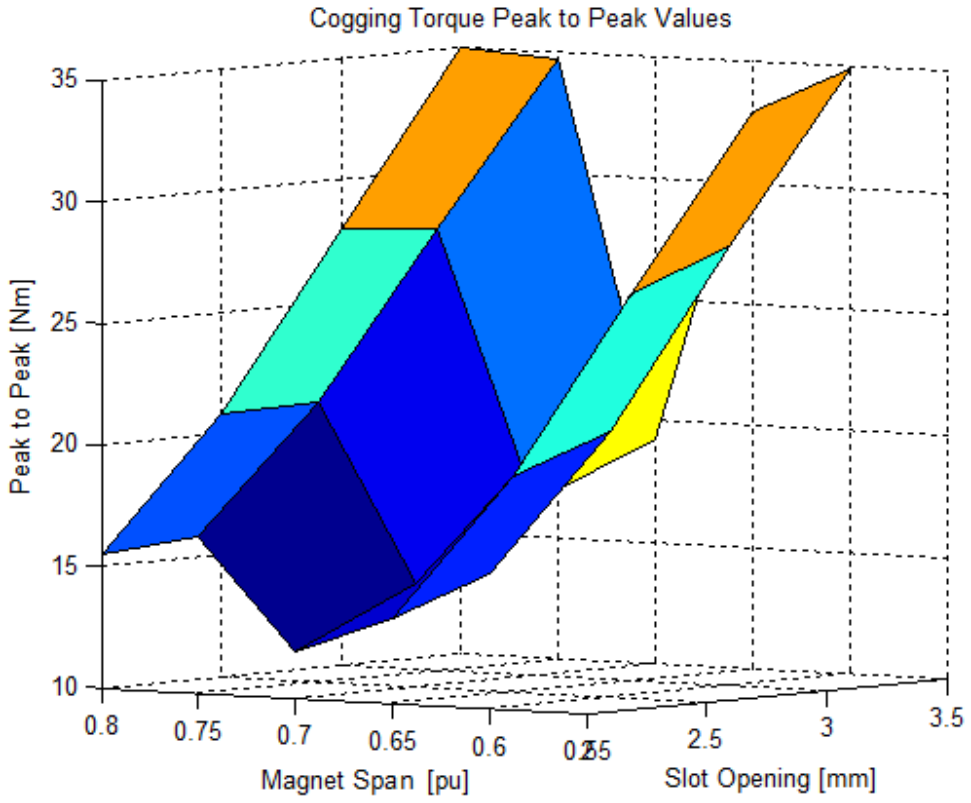

Figure 32.Cogging torque minimization through combined simulations by changing the slot opening and the magnet width ($q = 1$, single-layer)

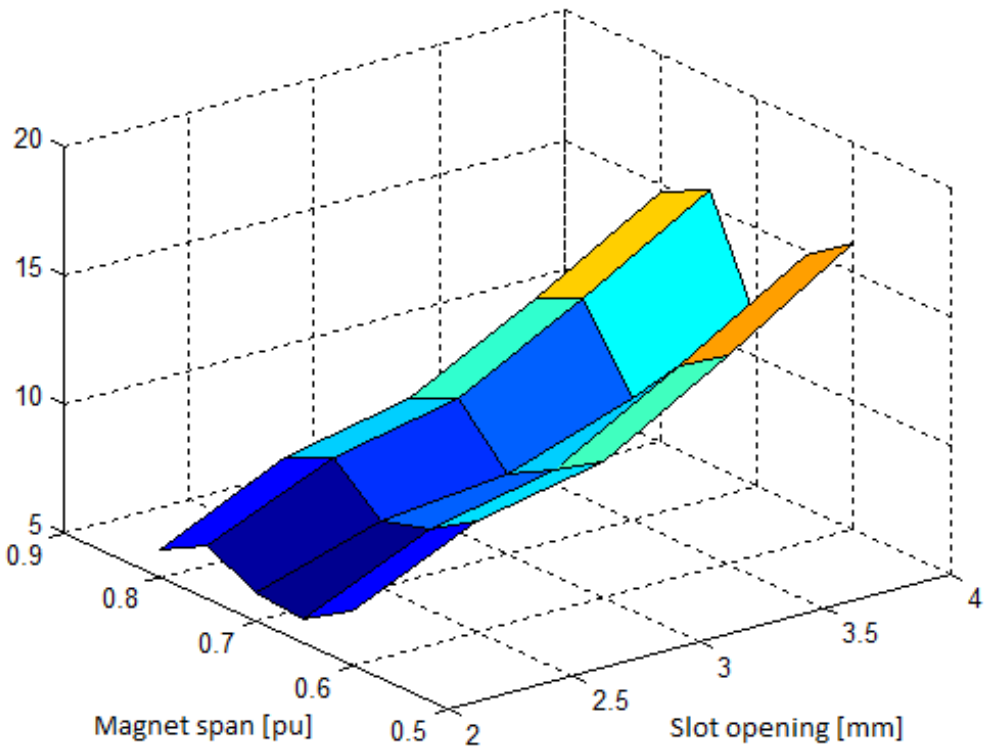

Figure 33.Cogging torque minimization through combined simulations by changing the slot opening and the magnet width ($q = 2$, double-layer)

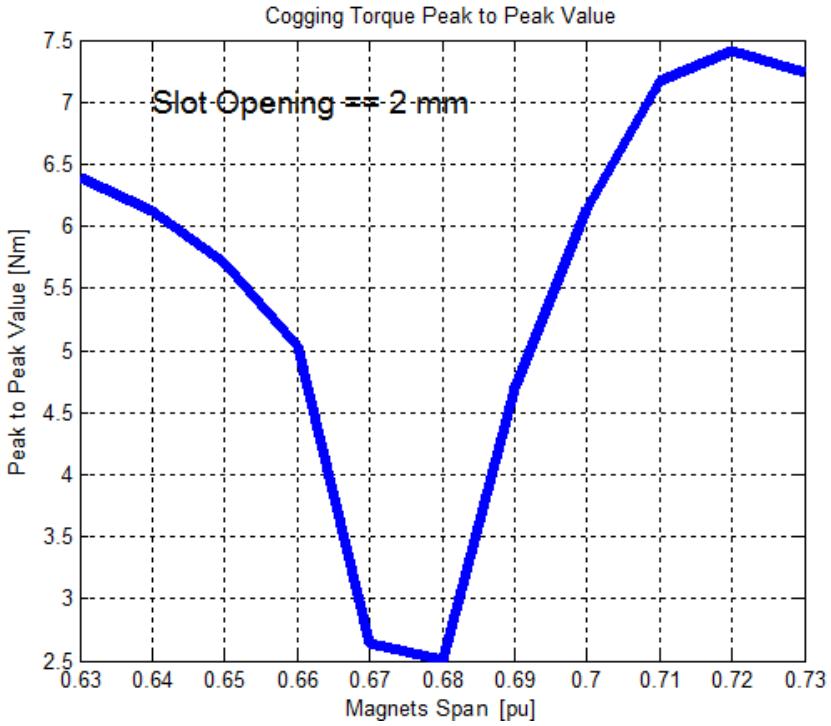

Figure 34.Cogging torque vs magnet width ($q = 2$)

In the next figures, the cogging torques and their Fourier spectrums with the new values of the magnet span and the slot opening are plotted: Figures 35 and 36 are related to the first case, 1-slot-per-pole-per-phase motor, and Figures 37 and 38 refer to the 2-slots-per-pole-per-phase machine.

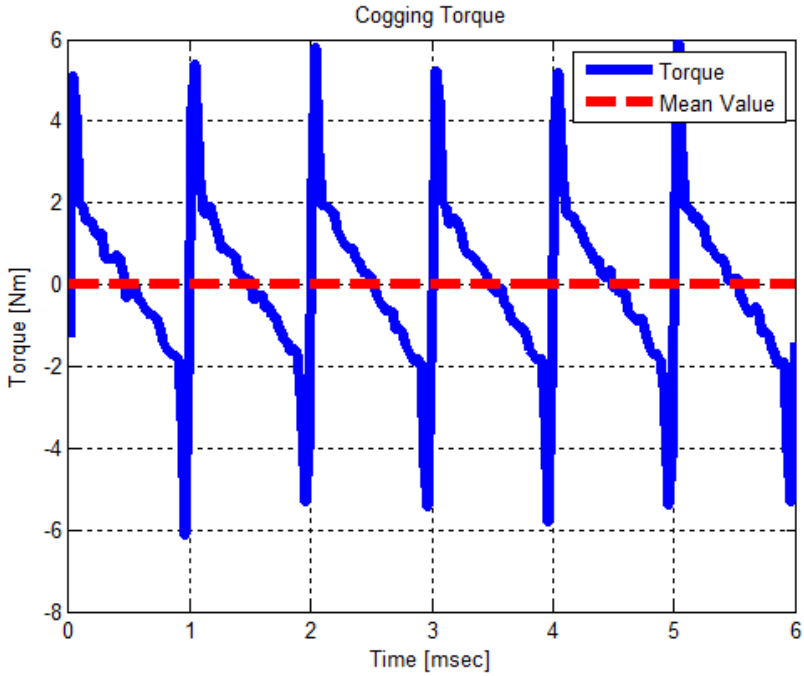

Figure 35.Cogging torque in the 1-slot-per-pole-per-phase PMSM

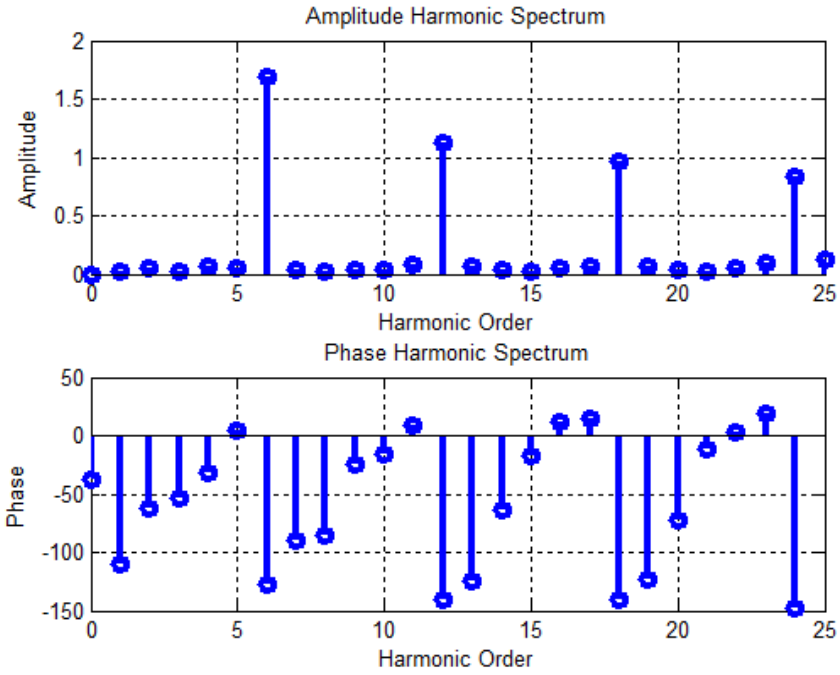

Figure 36.Amplitude and phase spectrums of cogging torque in the 1-slot-per-pole-per-phase PMSM

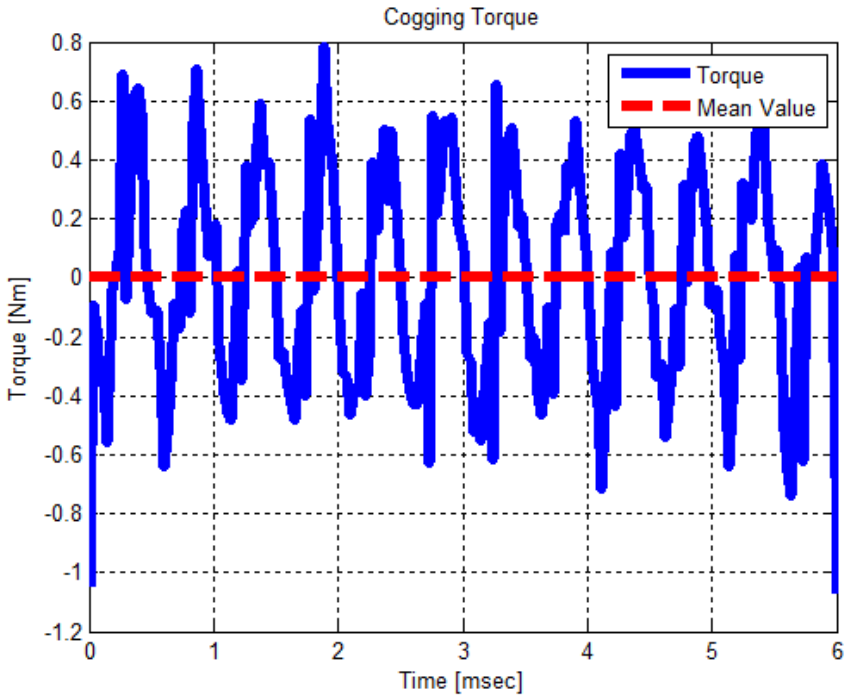

Figure 37.Cogging torque in the 2-slots-per-pole-per-phase PMSM

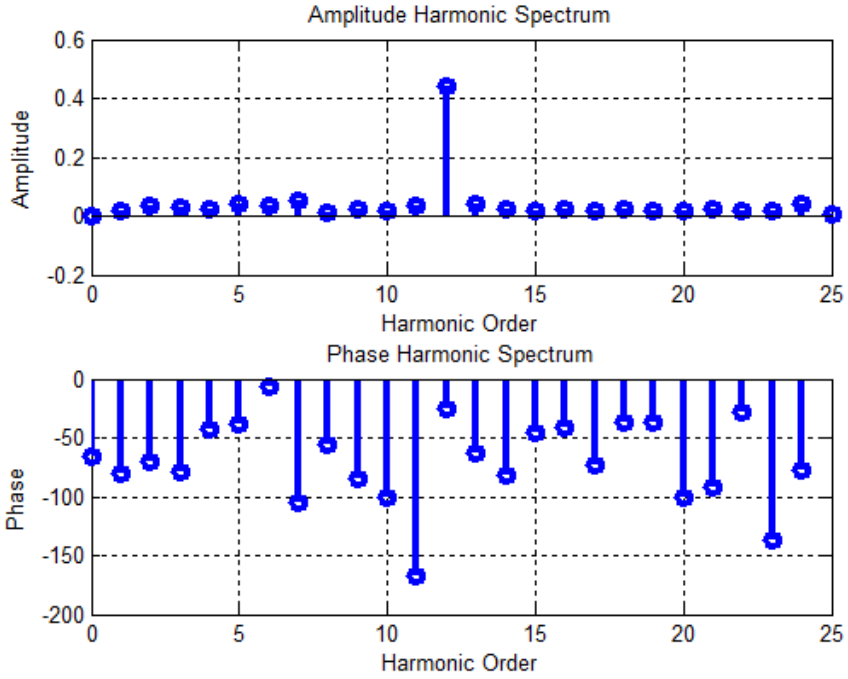

Figure 38.Amplitude and phase spectrums of cogging torque in the 2-slots-per-pole-per-phase PMSM

As it can be observes in the figure above, it is proved that the number of oscillations of the torque at no-load condition under a pole pairs is equal to $\boldsymbol{2mq}$, where $\boldsymbol{m}$ is the number of phases and $\boldsymbol{q}$ the number of slots per pole per phase; if this number is

multiplied by the number of pole pairs $\boldsymbol{p}$ of the machine, one may obtain the total number of oscillations along the whole machine circumference.

3.2.3 Fem results and comparison

In the previous step of validation tool, for both cases under study, they have been obtained magnet width values that minimize the cogging torque smaller than the initial value $\alpha_{PM} = 0.8$. Hence, in order to keep the air gap flux constant, the magnet thickness should be increased. In fact, putting the new values obtained with Magnet 2D in the dimensioning tool, it can be noted that the magnet length passes from $h_{PM} = 5\,mm$ to $h_{PM} = 5.8\,mm$ in the case $q = 1$; the same thing happens in the second analysed case ($q = 2$): with $\alpha_{PM} = 0.8$ the magnet height is $h_{PM} = 4.3\,mm$, while when $\alpha_{PM} = 0.68$, the height becomes $h_{PM} = 7.1\,mm$. All main dimensions obtained with the new values of the magnet span and the slot opening are described in the Appendix 2.

In the figures below, both machines with the new dimensions found by the analytical sizing are shown.

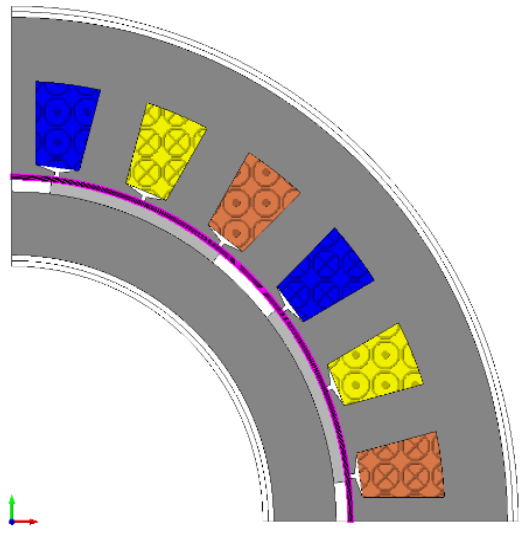

Figure 39.SPMSM after cogging torque minimization: $q = 1$, single-layer winding and $\alpha_{PM} = 0.7$

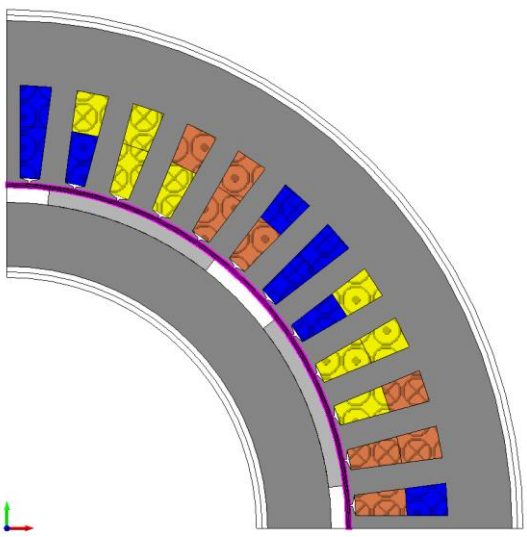

Figure 40. SPMSM after cogging torque minimization: $q = 2$, double-layer winding and $\alpha_{PM} = 0.68$

In this subsection, some important plots of both test cases are shown with the purpose of validating the implemented preliminary design. Considering the motors in Figures 39 and 40, simulations at no-load and load conditions have been done. No-

load results represent a very important validation step because one may compare most of the imposed and calculated quantities during the analytical design, like back-EMF and flux densities in the air gap, in yokes and in teeth. Load results are important mostly for comparing the rated torque, but also to observe the current density, the flux densities in the ferromagnetic materials and the power losses. These last will be the inputs of the thermal model described in the next chapter.

3.2.3.1 No-load results for the 1-slot-per-pole-per-phase PMSM

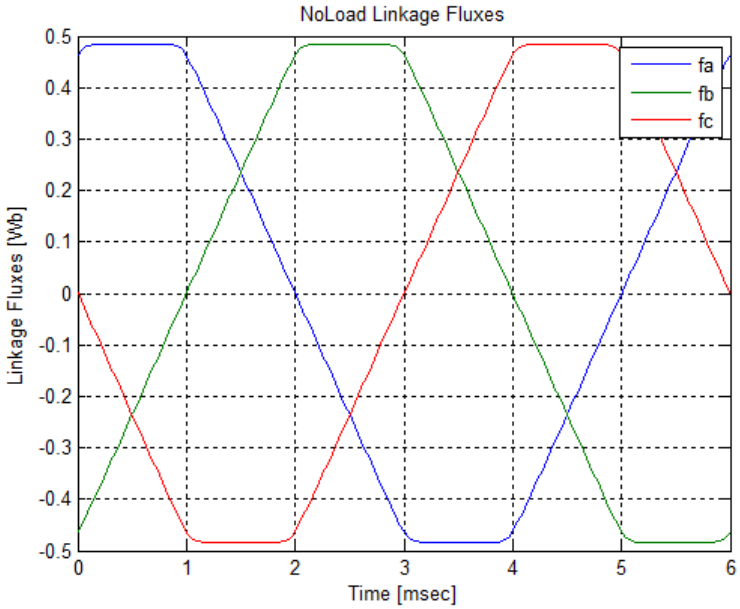

Figure 41.Linked fluxes for the three phases

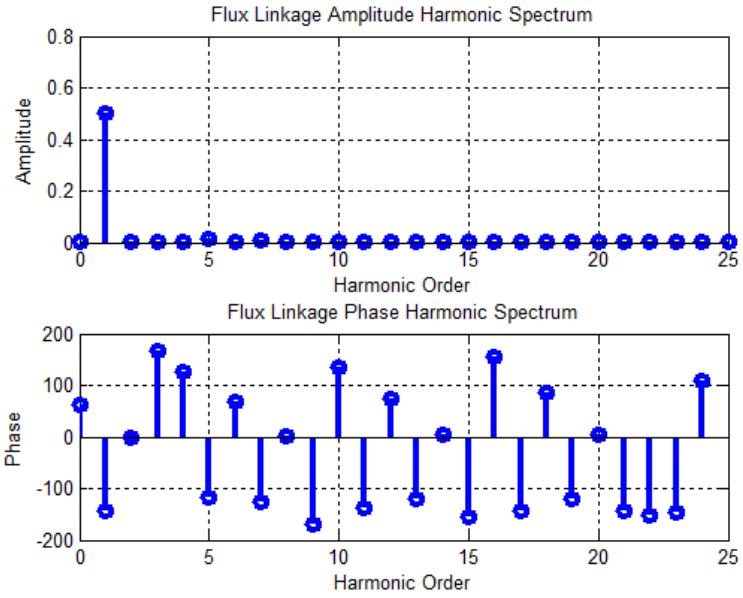

Figure 42.Linked fluxes amplitude and phase spectrum

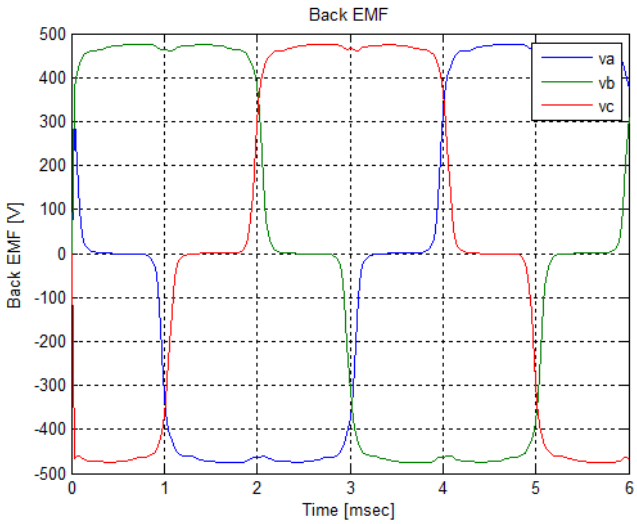

Figure 43.Back-EMFs in the three phases

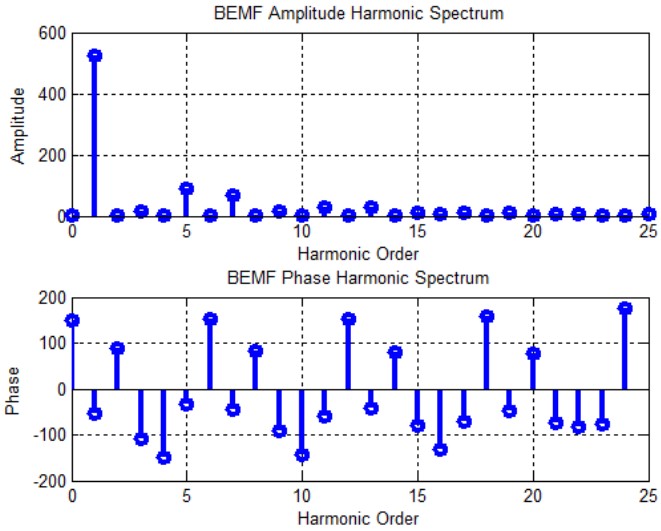

Figure 44.Back-EMFs amplitude and phase spectrum

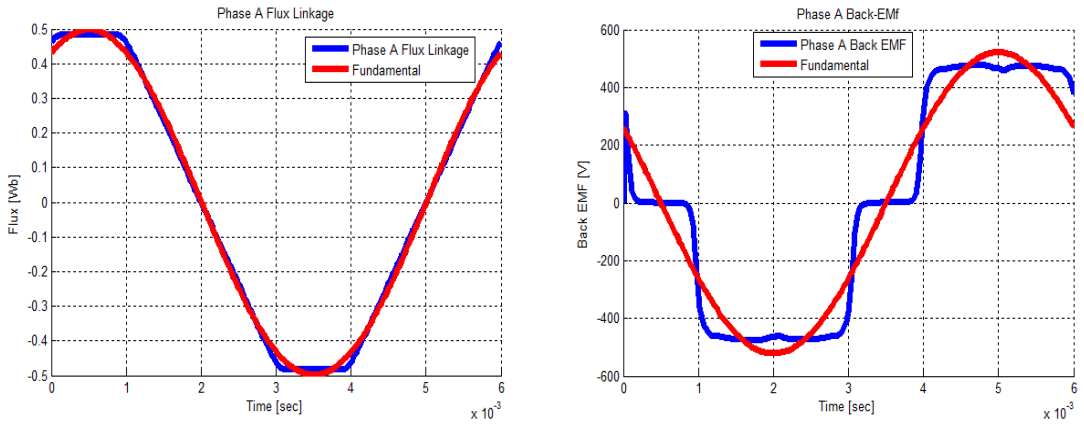

Figure 45.Fundamental harmonics of back-EMF and linked flux (phase A)

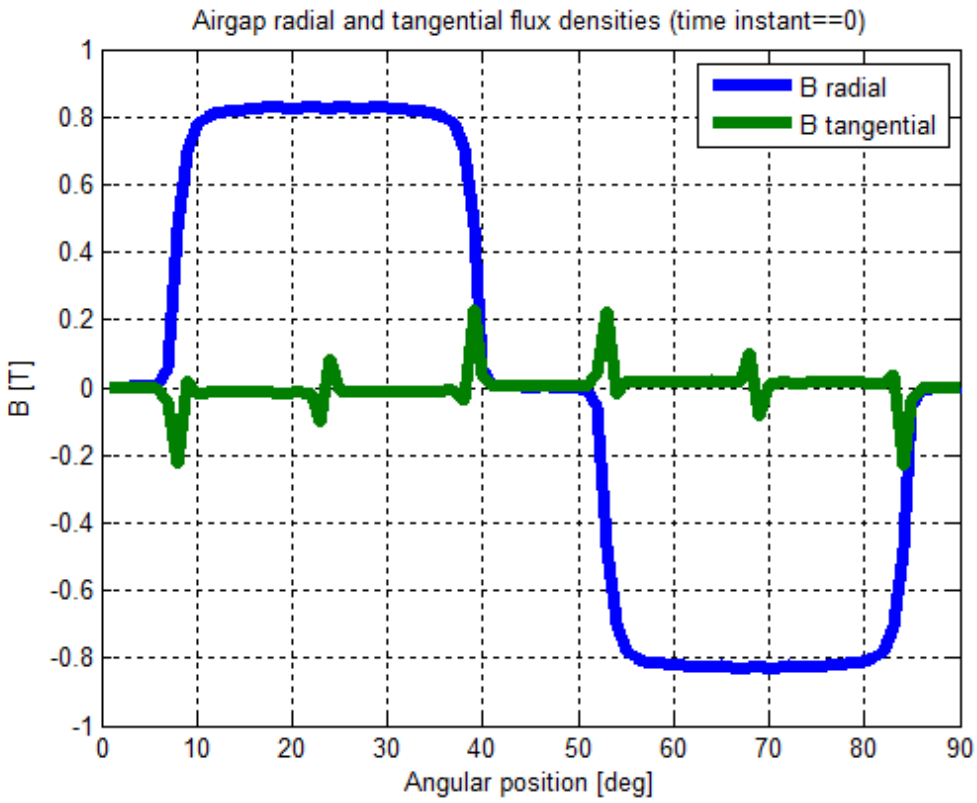

Figure 46.Radial and tangential air gap flux density

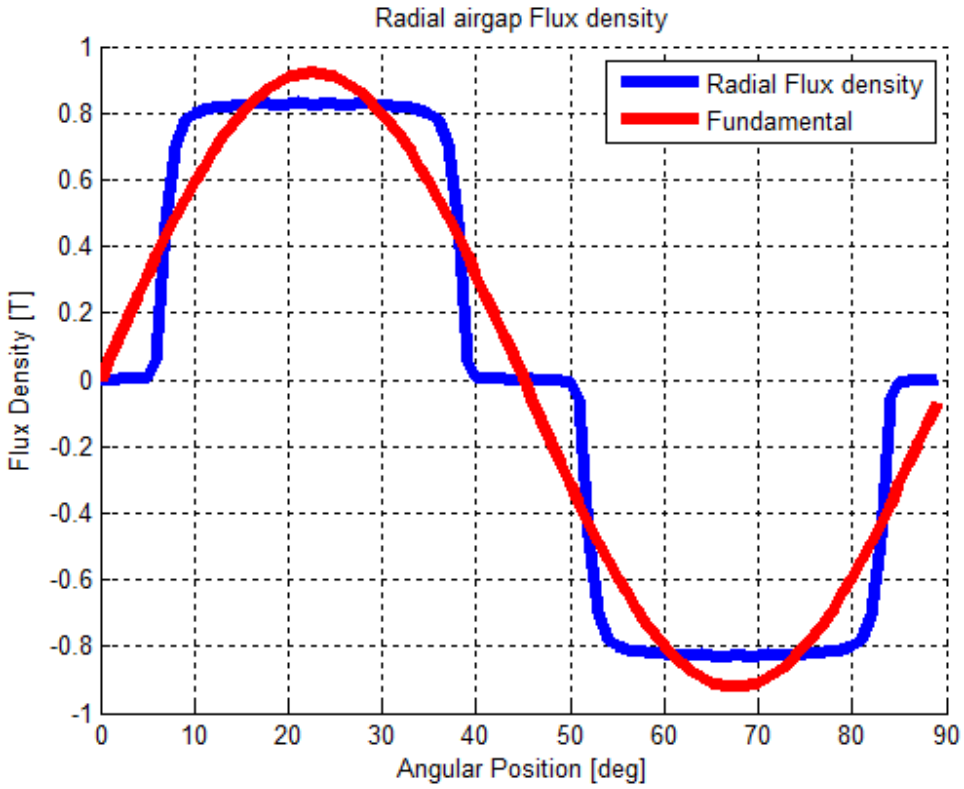

Figure 47.Fundamental harmonic of the air gap flux density

In the figures below it may be observed the trend of the flux density during the whole rotation of the rotor taken in a specific point at the middle of the tooth (Figure 48) and the trend of the flux density taken in a specific point at the middle of the stator yoke thickness in correspondence of the q-axis (Figure 49).

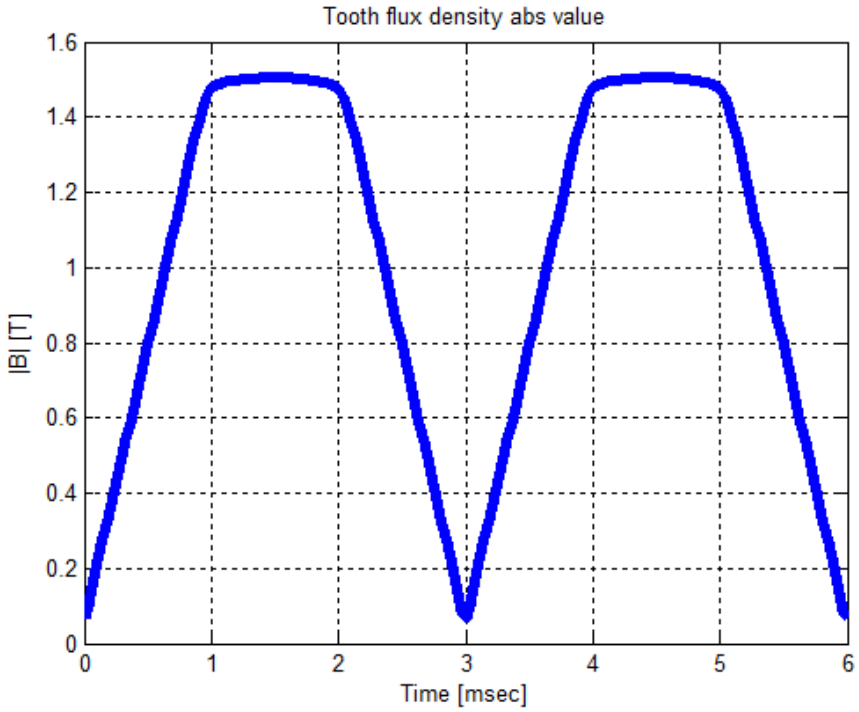

Figure 48.Flux density in the middle of a tooth

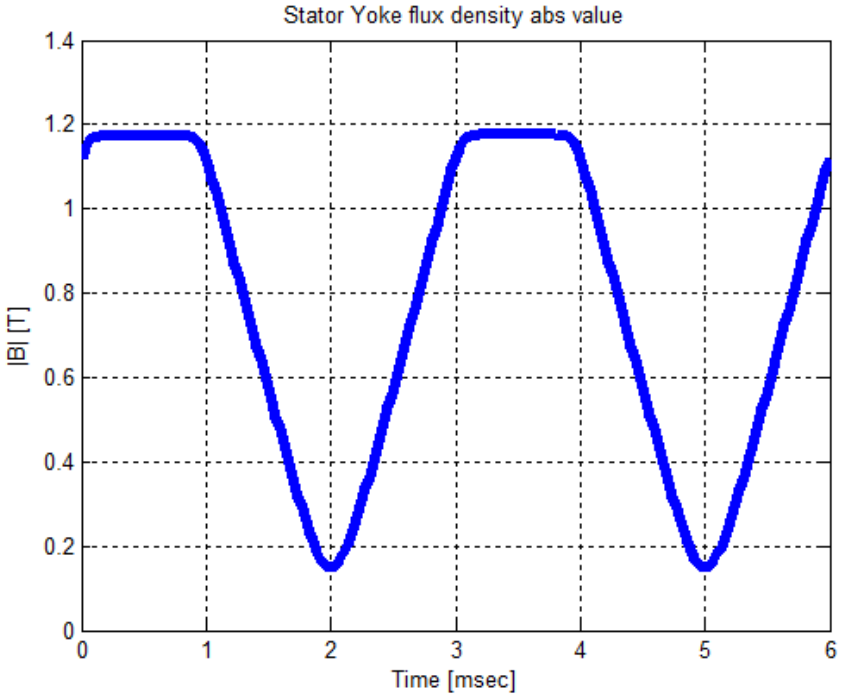

Figure 49.Flux density in the stator yoke

3.2.3.2 Load results for the one slot per pole per phase PMSM

In the first chapter (section 1.3), the torque expression has been obtained in d-q coordinate model for a PMSM (Equation 20). Then the fact that a surface mounted permanent magnet synchronous motor has not the reluctance component of the torque was pointed out. This is due to the common value that inductances have on the two axes: $L_d = L_q$. Hence, the torque expression for a SPMSM become

$$T_e = \frac{3}{2} p \varphi_{pm} I_q$$

In order to get the maximum torque, only the q-axis current should supply the machines under study at load condition. This is achieved simply by putting each current that supplies the winding in phase with each back-EMF obtained at no-load condition (see Figure 43).

In the Figure 50, torque ripples obtained by subtracting the mean values are plotted at different values of q-axis current I_q; then, in Figure 51, the characteristic curve torque vs q-axis current is shown. The current range in both figures varies between $I_q = 0$ to $I_q = 2I_n$, in which I_n is the rated current calculated in the preliminary sizing (see Equation 37).

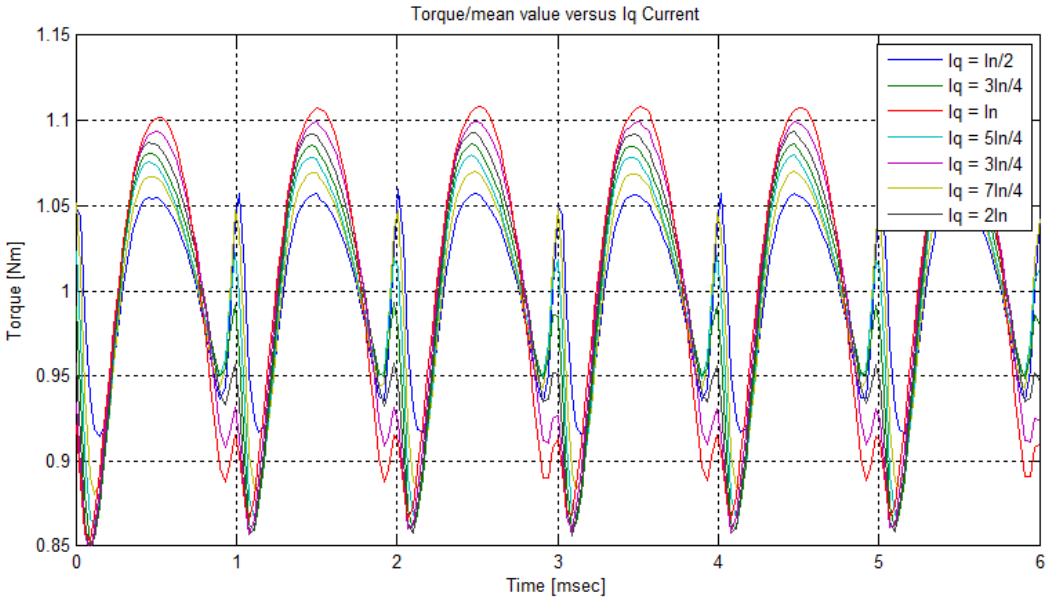

Figure 50.p.u torque profile vs mean value, for different values of I_q

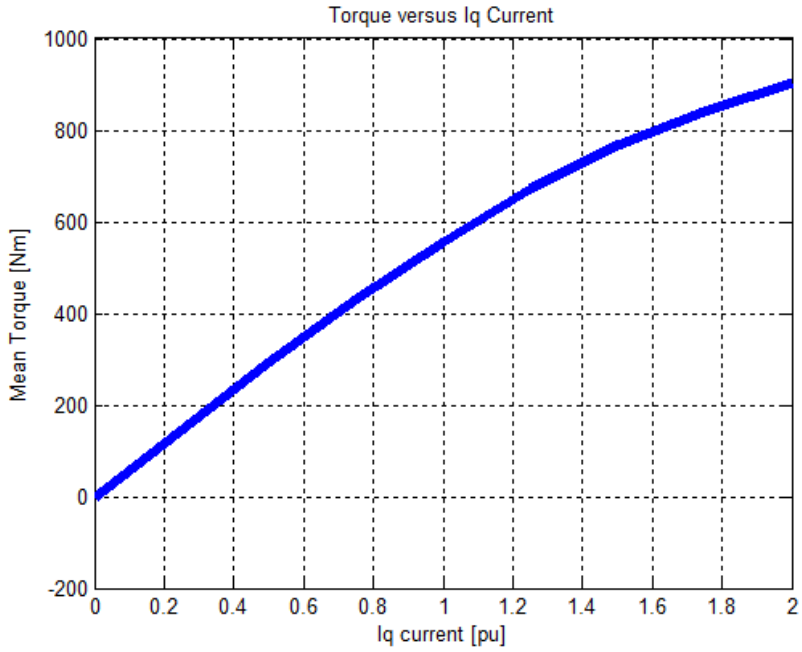

Figure 51.Mean torque vs. I_q

The rated torque T_n, as one may observe in the figure below, is in correspondence of $I_q = I_n$ and is equal to $576{,}81\ Nm$, that is lower than the required value calculated in the dimensioning tool $T_n = 611.15\ Nm$.
In next figures, some other quantities at load condition are shown, like the current density trend in a slot after a whole rotation (Figure 52), the flux densities in the iron parts of the motor (Figures 53 and 54) and the losses in winding (referred to one slot), permanent magnets (referred only to the north pole magnet) and in the stator structure as a function of the q-axis current (Figures 55-57).

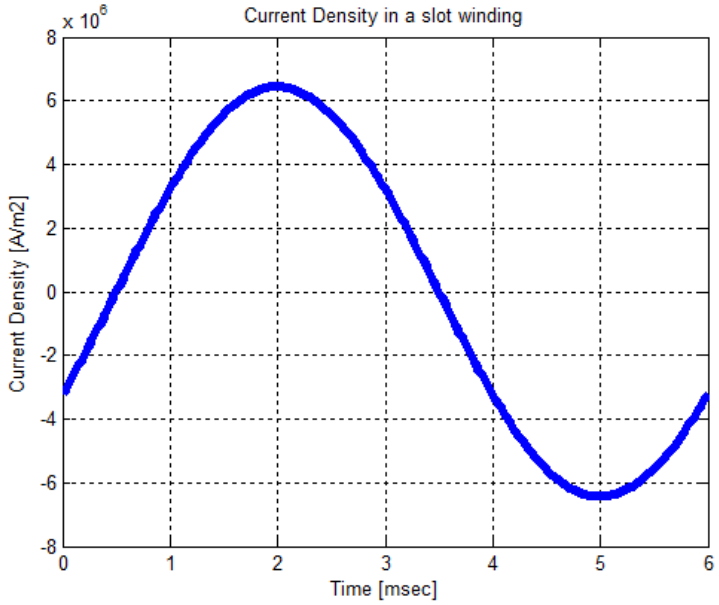

Figure 52.Current density in a slot winding

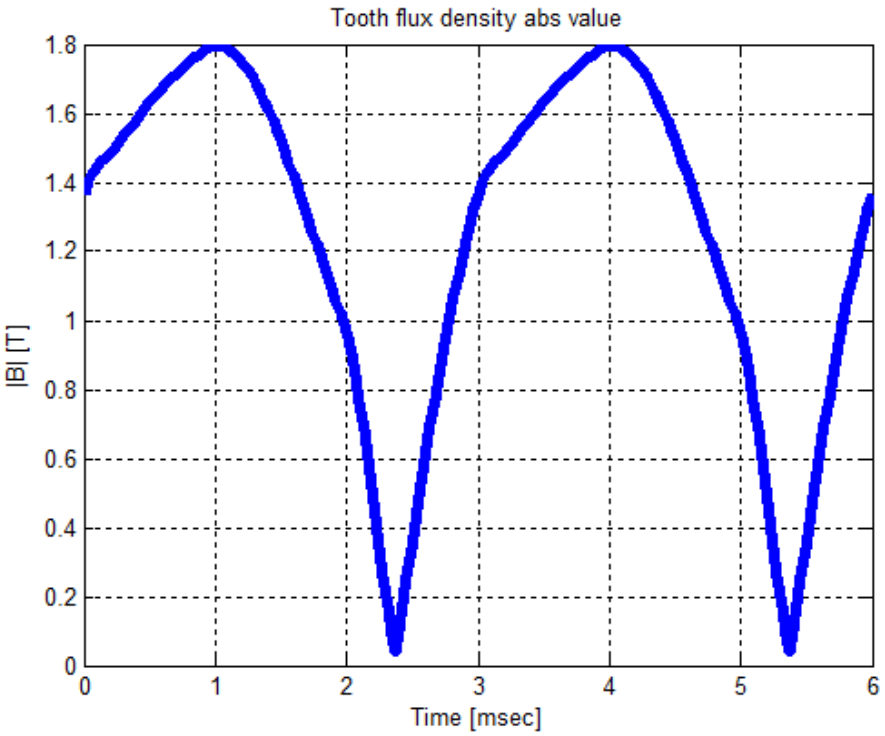

Figure 53.Flux density in the middle of a tooth

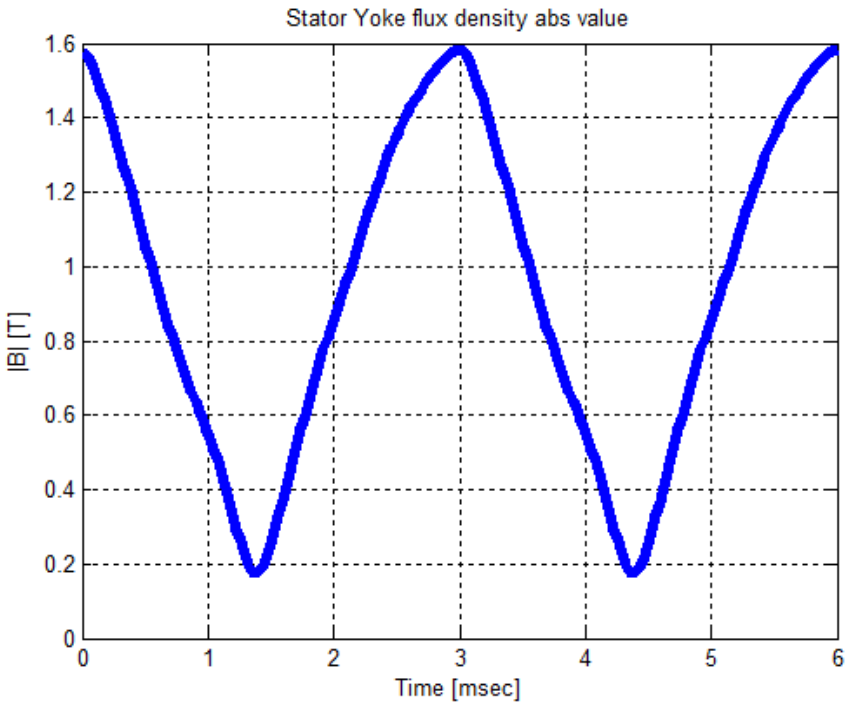

Figure 54.Flux density in the stator yoke

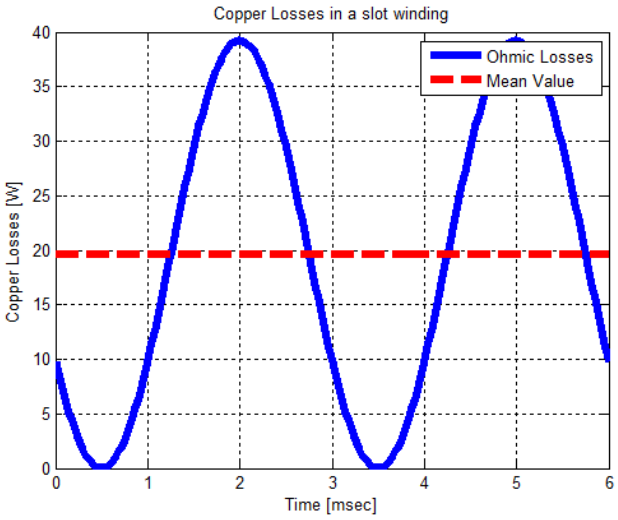

Figure 55.Joule losses in a slot winding

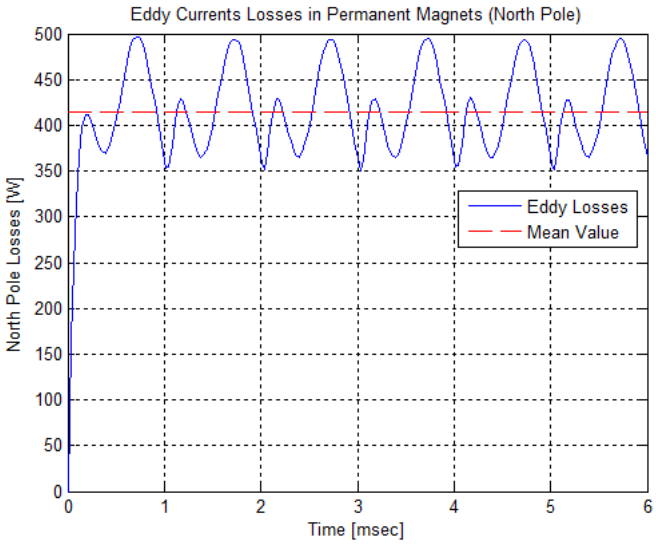

Figure 56.Eddy current losses in permanent magnets

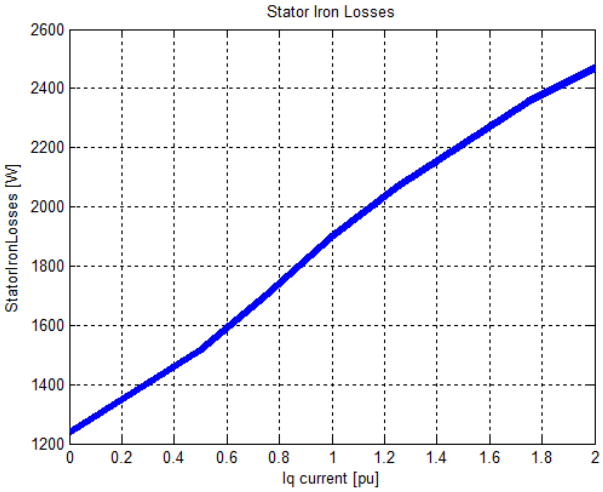

Figure 57.Stator iron losses vs I_q

3.2.3.3 No-load results for the two slots per pole per phase PMSM

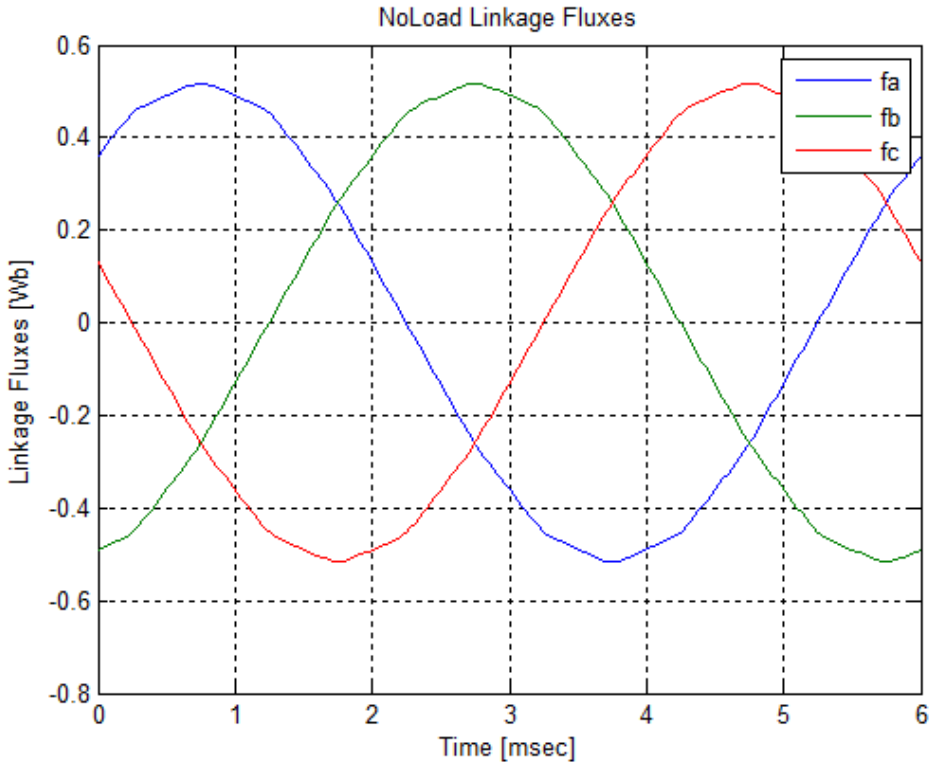

Figure 58.Linked fluxes for the three phases

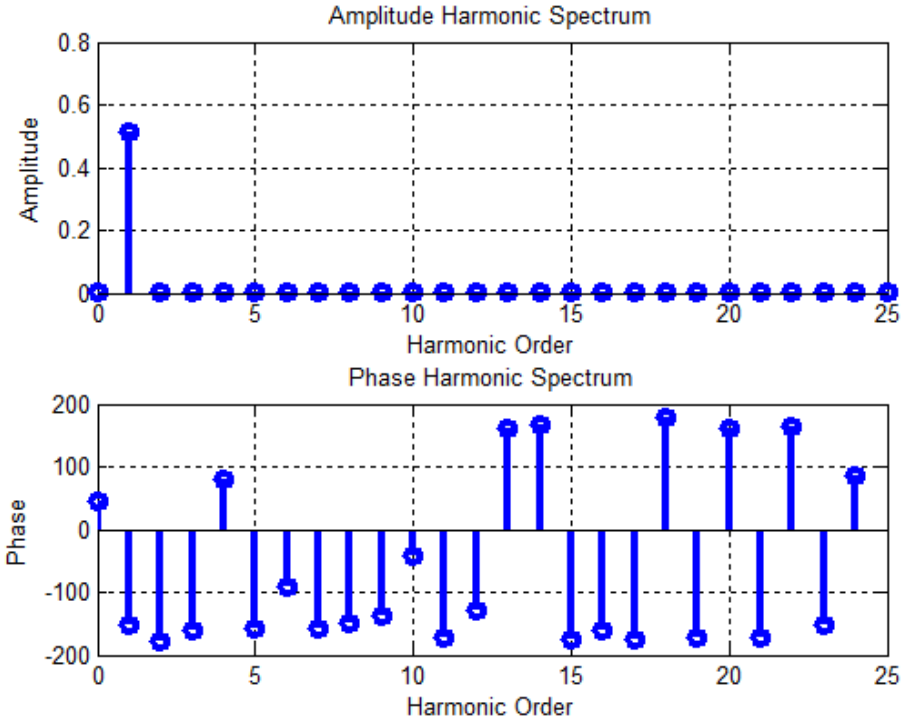

Figure 59.Linked fluxes amplitude and phase spectrum

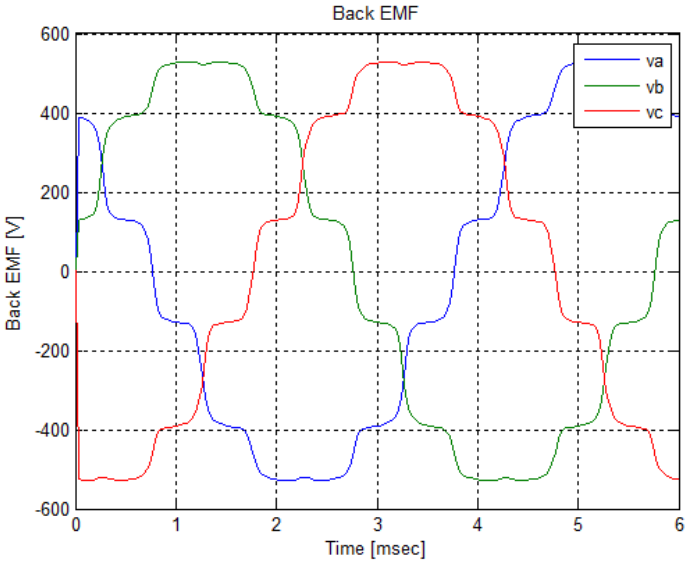

Figure 60.Back-EMFs in the three phases

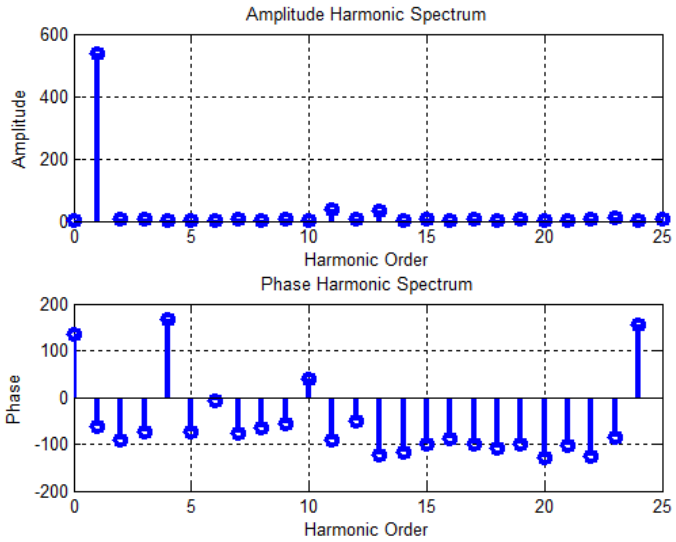

Figure 61.Back-EMFs amplitude and phase spectrum

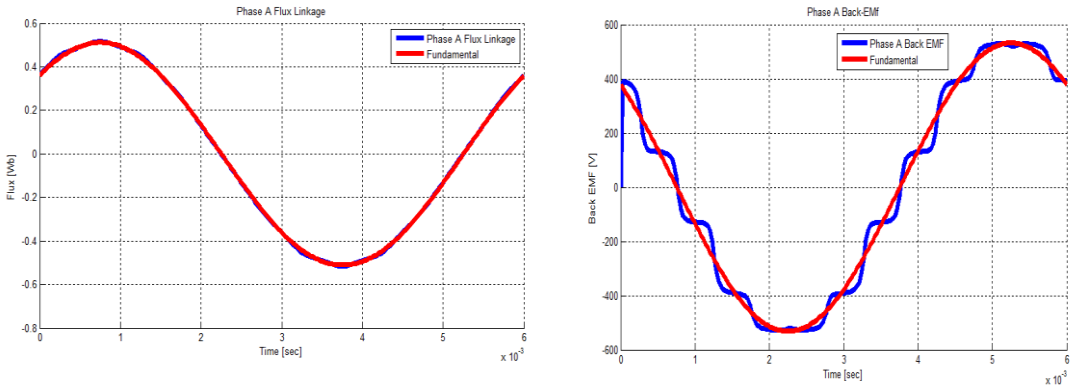

Figure 62.Fundamental harmonics of back-EMF and linked flux (phase A)

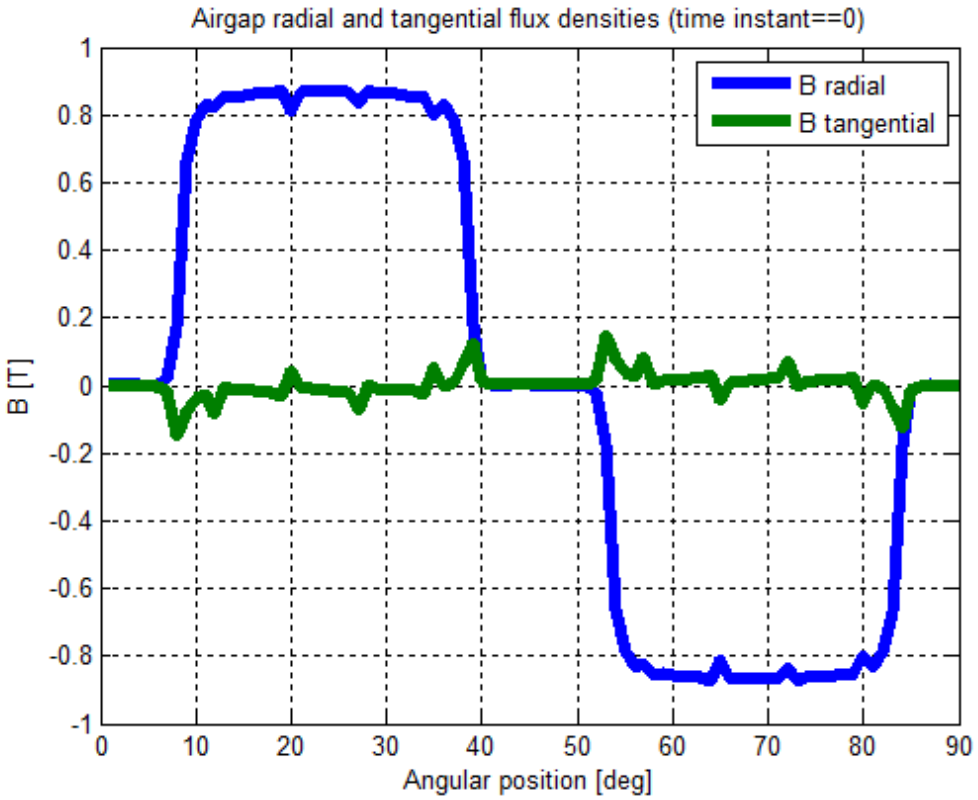

Figure 63.Radial and tangential air gap flux density

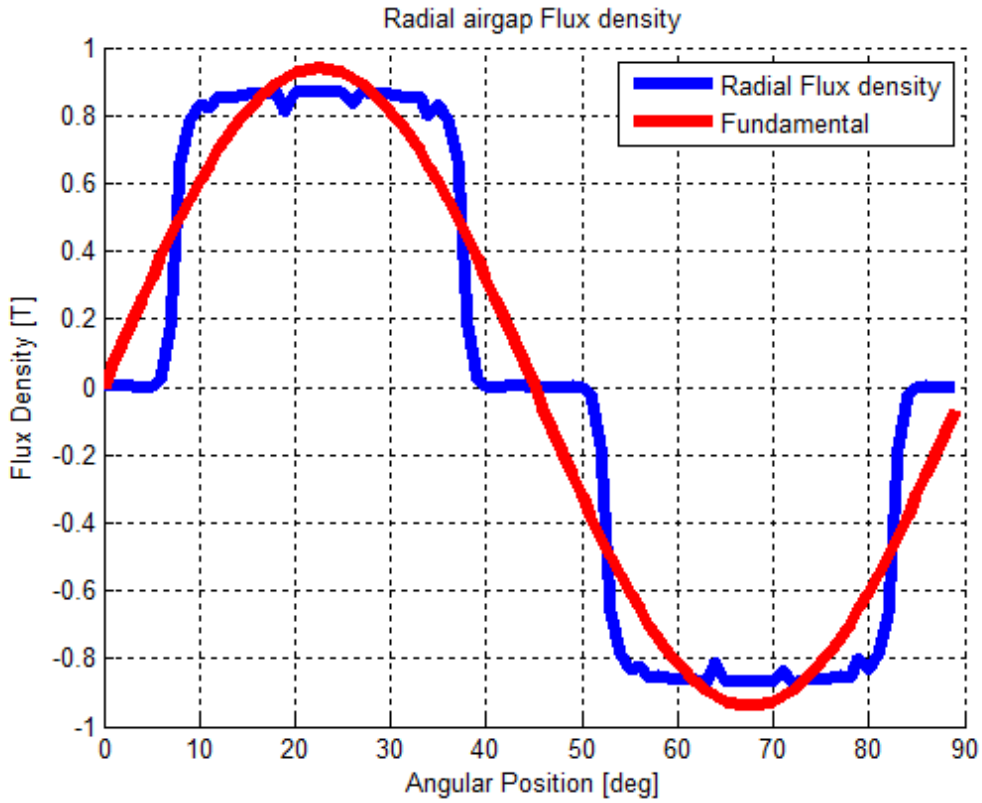

Figure 64.Fundamental harmonic of the air gap flux density

For the values of the flux densities in the teeth and in the stator yoke, as already observed with the no-load results for the one slot per pole per phase motor, the values are taken in the middle of the tooth and the yoke thickness in correspondence of the q-axis during one whole rotation of the rotor.

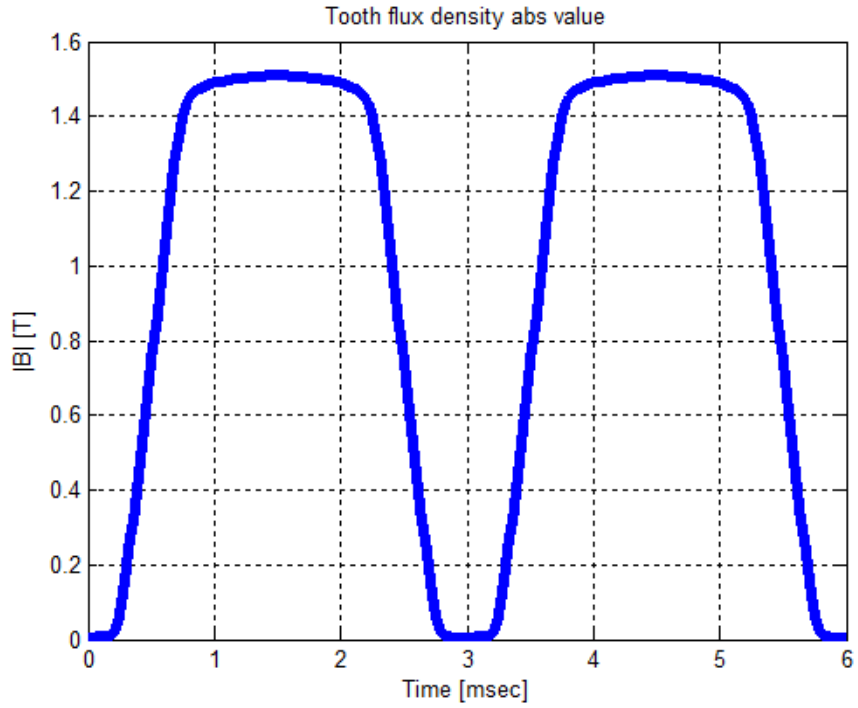

Figure 65.Flux density in the middle of a tooth

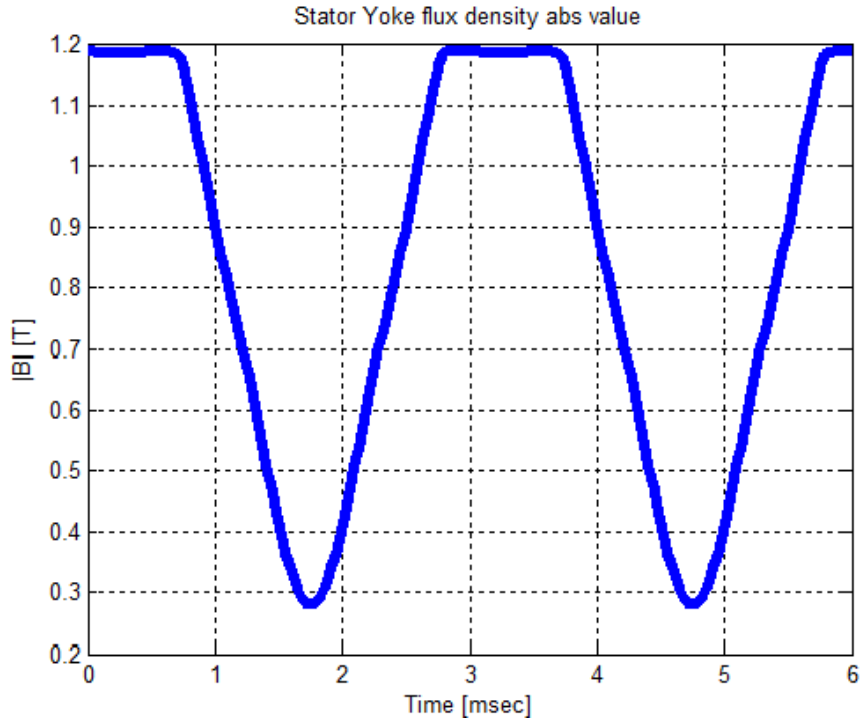

Figure 66.Flux density in the stator yoke

3.2.3.4 Load results for the two slots per pole per phase PMSM

The same considerations about the q-axis current supply, that we have done in the subsection 3.2.3.2 for the one slot per pole per phase machine, can be repeated for the under load simulations of the two slots per pole per phase motor.

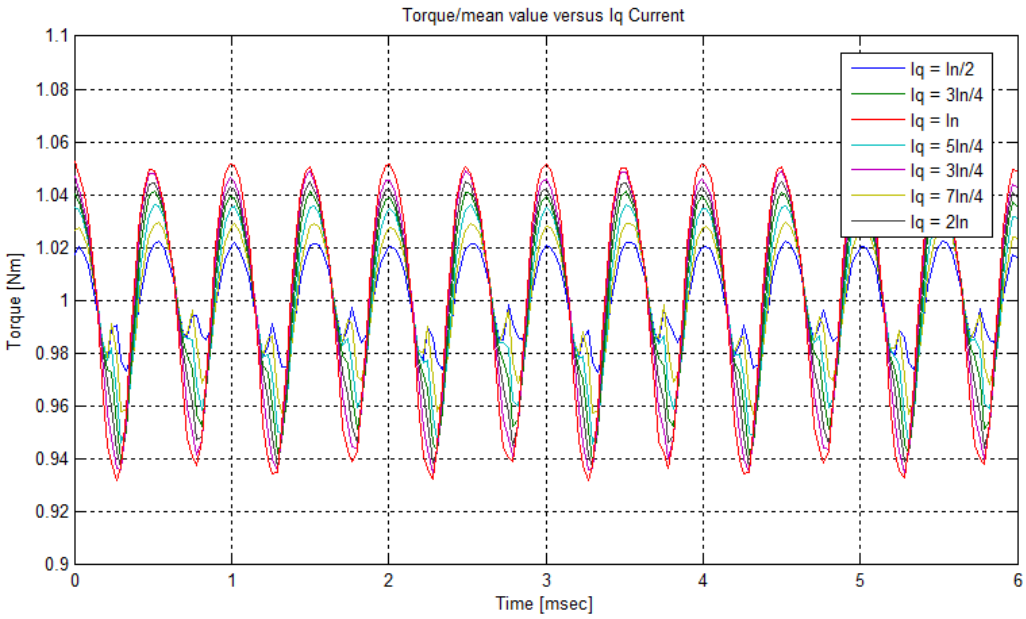

Figure 67.Torque ripples at different values of I_q

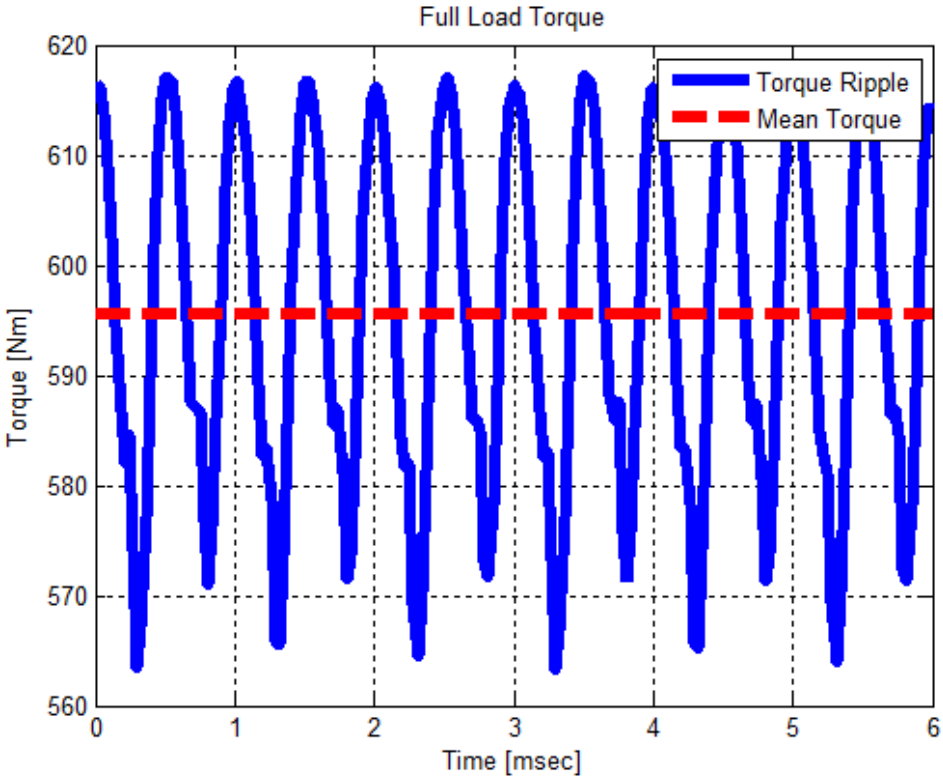

Figure 68.Torque ripple at full load ($I_q = I_n$)

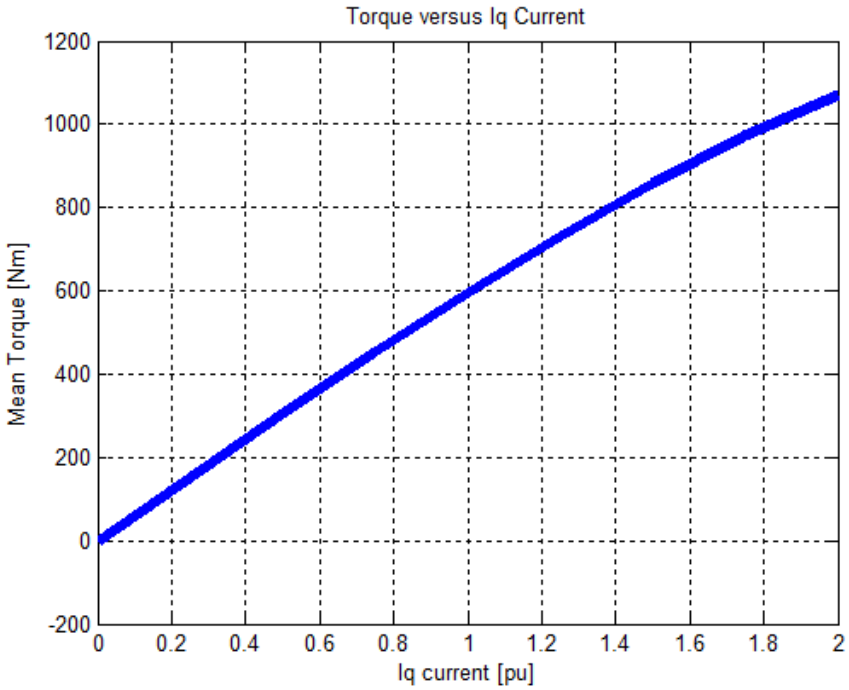

Figure 69.Torque vs I_q

Figures 68 and 69 show that the full torque now is very close to the calculated one: $T_n = 598.5\ Nm$ (by FEM) versus $T_n = 611.15\ Nm$ (by analytic way).
In next figures, the same quantities at load condition already shown in the case of the 1-slot-per-pole-per-phase PMSM are plotted below:

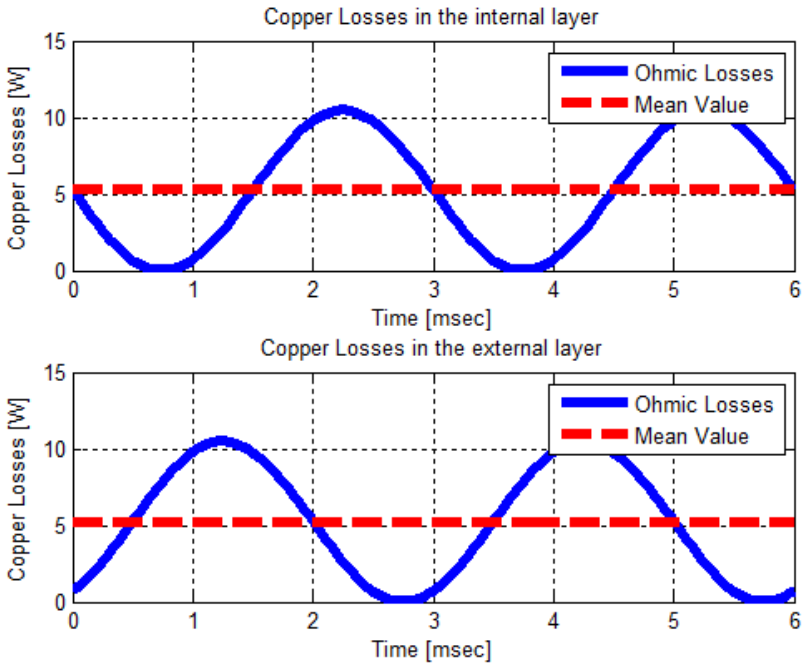

Figure 70.Joule losses in a slot (upper and lower layer)

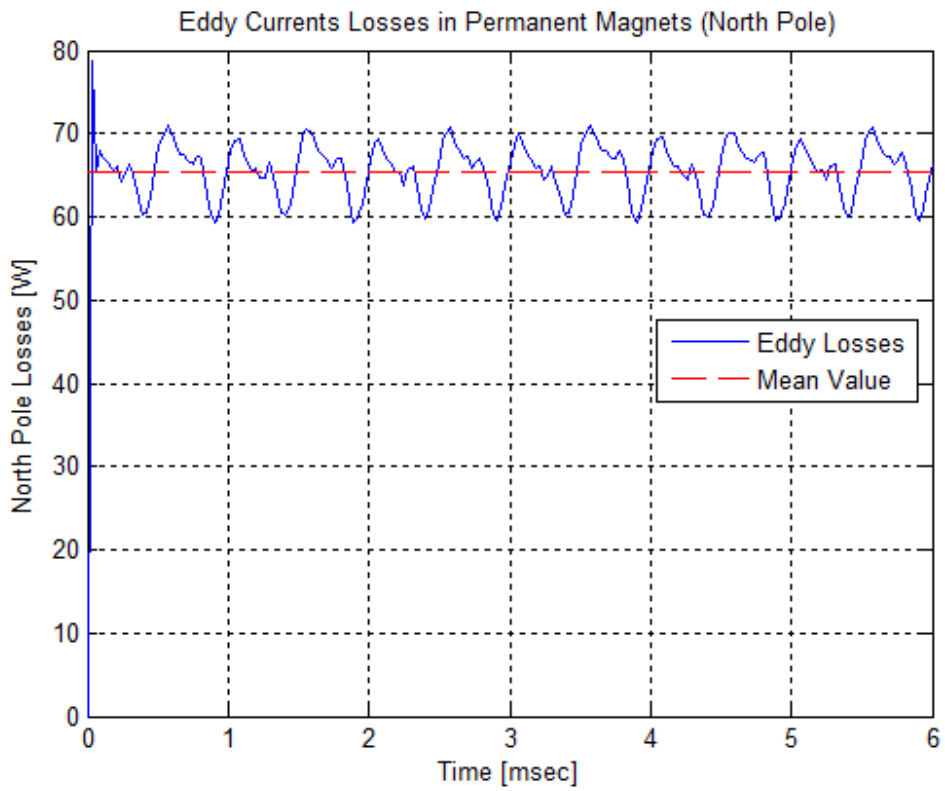

Figure 71.Eddy current losses in permanent magnets

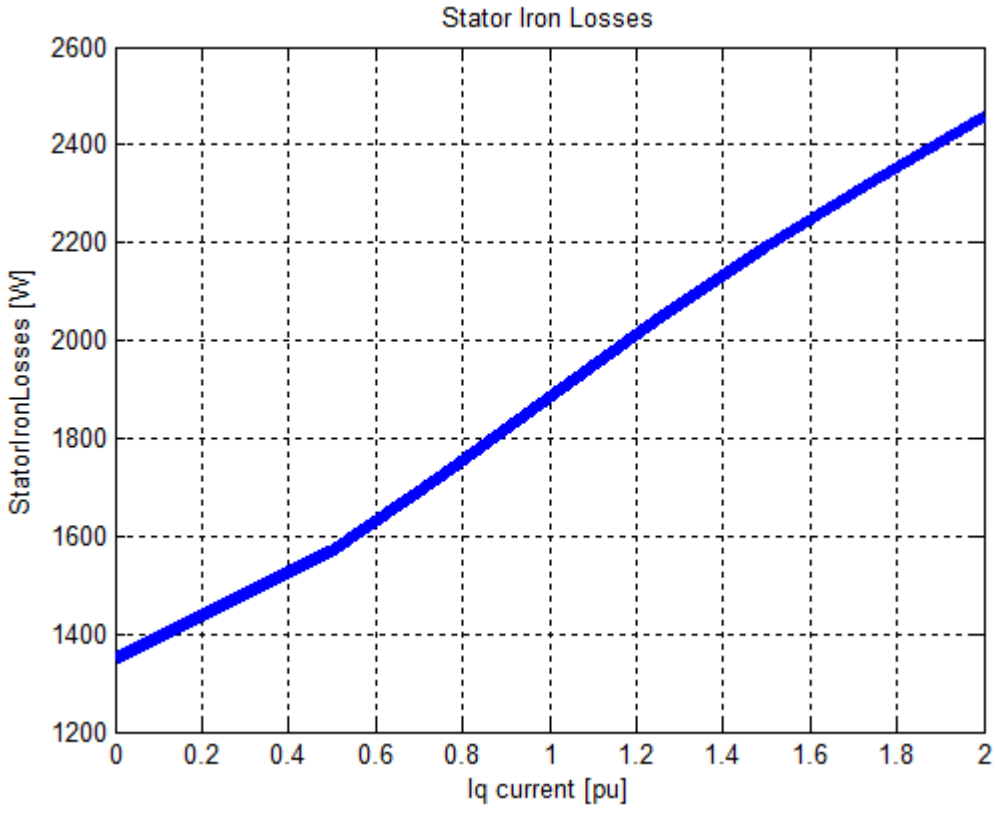

Figure 72.Stator core losses vs I_q

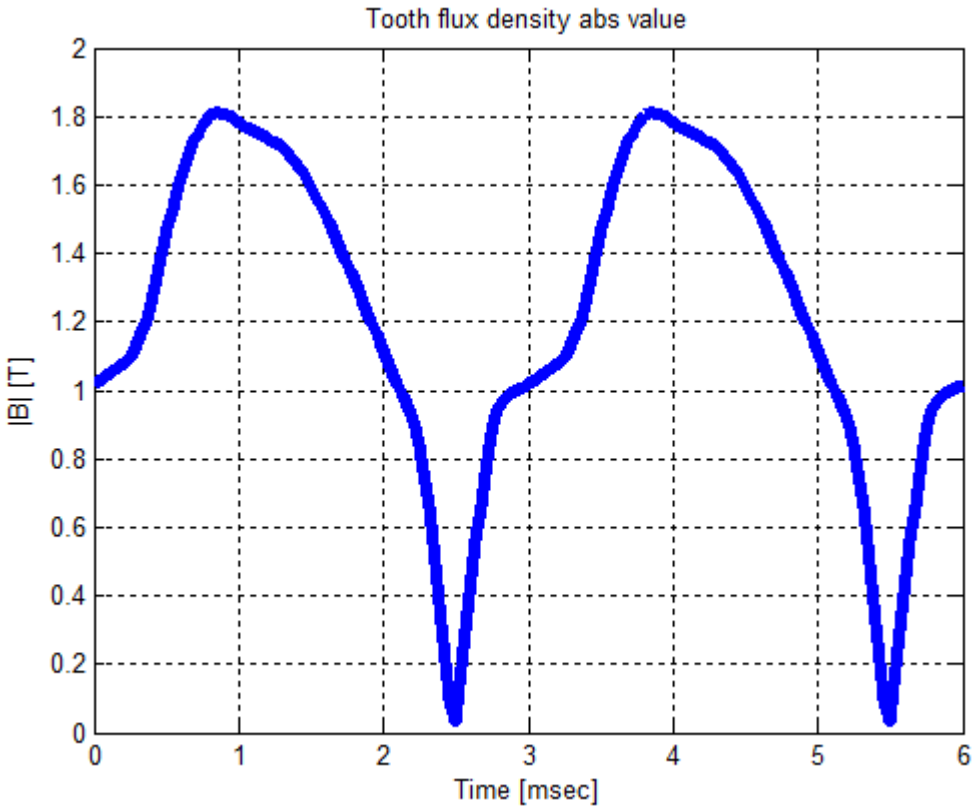

Figure 73.Flux density in the middle of a tooth

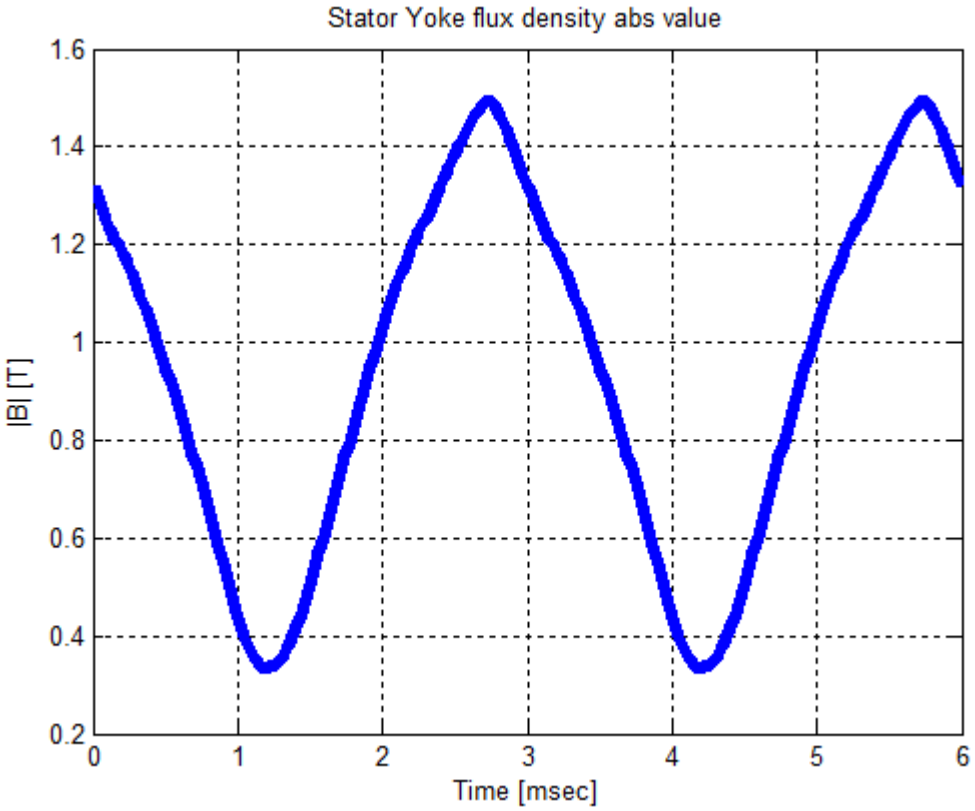

Figure 74.Flux density in the stator yoke

3.2.3.5 Comparison of results

Let us start from the consideration that some differences might appear since the preliminary sizing is based only on analytical equations which include a lot of approximations. With FEM some of the machine properties, such as magnetic flux densities and losses can be modelled more accurately. Therefore it is enough if the results are close to each other.

For the 1-slot-per-pole-per-phase machine it can be seen that FEM and dimensioning script results seem to be rather close to each other in terms of current density and back-EMF. In the case of the 2-slots-per-pole-per-phase PMSM the errors in back-EMF and current density are very small (1% circa). However, the leakage flux from a magnet to its neighbouring magnet is not taken into account by analytical dimensioning and can therefore be one explanation to the little difference in the back-EMF.

In the first case the rated torque disagree with an error more than 5%: the torque obtained by FEM is smaller than the analytically obtained value. It is possible that we are underestimating the current: one may observe in Figure 51 that the rated torque can be achieved considering a q-axis current $I_q = 1.1 I_n$. In the second case ($q = 2$), the error in torque calculation decreases (2.56%).

The efficiency and power factor are slightly different when calculated with Magnet 2D. However, in the preliminary design, efficiency and power factor are desired values imposed as inputs and they have not been calculated because of the difficulty in the estimation of core losses in an analytical way. Therefore also the iron losses obtained with Magnet 2D are also an approximation, although possibly somewhat more accurate. The accurate calculation of the iron losses is in any case rather difficult and requires modelling the physical phenomena in the iron.

In the case of efficiency, some difference occurs because the FEM software does not take into account the mechanical losses (windage and ventilator losses) and additional losses. Therefore Magnet 2D gives larger efficiency than the analytical dimensioning, in particular for the 2-slots-per-pole-per-phase motor. For this last design test case, the power factor is larger when calculated with FEM than the one obtained with the dimensioning script. When comparing the power factors it must be taken into account that the dimensioning tool assumes that the supply voltage is sinusoidal. This means that the harmonics created by for instance a frequency converter are not taken into account. In FEM calculation, this kind of assumption has not been made which may cause a difference between the power factors.

The flux density in the air gap is smaller when calculated with FEM in both cases. The greater differences in both test cases are related to the values of flux densities in the ferromagnetic structure: in FEM-based calculation are smaller than the typical values used in the dimensioning tool. For sure, the air gap flux density influences this values, but do not justifies the great errors. With standard sizing, there is a overestimation of

the teeth and stator yoke, even if the material seems to be well tapped at full load (see values in the tables below):

Table 2. 1-slot-per-pole-per-phase machine

Parameters	FEM	Analytical	Error %
Back-EMF	370.5947 V	378.4531 V	2.08 %
Air gap flux density	0.921 T	0.95 T	3.05 %
Tooth flux density at no-load	1.19 T	1.3 T	8.46 %
Stator yoke flux density at no-load	1.5 T	1.6 T	6.25 %
Tooth flux density at full-load	1.8 T	-	-
Stator yoke flux density at full-load	1.6 T	-	-
Current density	4.554 A/mm^2	4.5 A/mm^2	1.18 %
Rated torque	576.81 Nm	611.15 Nm	5.62 %
Efficiency	0.9624	0.95	1.29 %
Power factor	0.9053	0.91	0.52 %

Table 3. 2-slots-per-pole-per-phase machine

Parameters	FEM	Analytical	Error %
Back-EMF	387.3 V	381.8 V	1.41 %
Air gap flux density	0.915 T	0.95 T	3.68 %
Tooth flux density at no-load	1.21 T	1.3 T	6.92 %
Stator yoke flux density at no-load	1.53 T	1.6 T	4.38 %
Tooth flux density at full-load	1.81 T	-	-
Stator yoke flux density at full-load	1.55 T	-	-
Current density	4.525 A/mm^2	4.5 A/mm^2	0.56 %
Rated torque	595.5 Nm	611.2 Nm	2.56 %
Efficiency	0.982	0.95	3.23 %
Power factor	0.949	0.91	4.12 %

4 THERMAL DESIGN

4.1 Introduction

Heat transfer always occurs when there is a temperature difference in a system.
In electrical machines, the design of heat transfer is of equal importance as the electromagnetic design of the machine, because the temperature rise of the machine eventually determines the maximum output power with which the machine is allowed to be constantly loaded. Machine losses inevitably increase the temperature of all portions of the machine. The temperature rise in the machine, especially in its winding, must be limited in order to realize the expected lifetime. An elevated temperature deteriorates the mechanical and electrical strength of winding insulation and will lead to its premature failure.
The purpose of cooling is to limit the temperature increase by removing this heat: in most motors, adequate heat removal is ensured by convection in air, conduction through the fastening surfaces of the machine and radiation to ambient. In machines with a high power density, direct cooling methods can also be applied. Sometimes even the winding of the machine is made of copper pipe, through which the coolant flows during operation.
The most important factor in thermal design is, however, the temperature of ambient fluid, as it determines the maximum temperature rise with the heat tolerance of the insulation. The distribution of heat in the machine can be calculated when the distribution of losses in different parts of the machine and the heat removal power are exactly known. Moreover, one must is a good estimate of the properties of the cooling fluid and thermal characteristics of the magnetic, conductive and insulating portions of the machine.
The temperature rise of the winding of an electrical machine increases the resistance of the winding. A temperature rise of 50 K above ambient (20 °C) increases the resistance by 20% and a temperature rise of 135 K by 53%. If the current of the machine remains unchanged, the resistive losses increase accordingly. The average temperature of the winding is usually determined by the measurement of the resistance of the winding. At hot spots, the temperature may be 10–20 K above the average. As a matter of fact, thermal design in an electrical machine is a more difficult and complicated issue than the conventional electromagnetic design of an electrical machine. However, problems related to heat transfer can to some degree be avoided by utilizing empirical knowledge of the machine constants available. When creating completely new constructions, empirical knowledge is not enough,

and thorough modelling of the heat transfer is required. Finally, prototyping and measurements verify the successfulness of the design.

4.2 Heat removal

The heat is removed by convection, conduction and radiation. Usually, the convection through air, liquid or steam is the most significant method of heat transfer. Forced convection is, inevitably, the most efficient cooling method if we do not take direct water cooling into account.

The cooling design for forced convective cooling is also straightforward: the designer has to ensure that a large enough amount of coolant flows through the machine. This means that the cooling channels have to be large enough.

If the motor is flange mounted, a notable amount of heat can be transferred through the flange of the machine to the device operated by the motor. The proportion of heat transfer by radiation is usually moderate, yet not completely insignificant. However, in this work we disregard the heat removal by radiation.

With respect to the heat transfer by conduction, heat can be transferred between free electrons and by molecular interaction between higher energy molecules and lower energy ones. Fourier's law gives the heat flow transferred by conduction:

$$\Phi_{th} = -\lambda S \Delta \mathrm{T}$$

where Φ_{th} is the heat flow rate, λ the thermal conductivity, S the heat transfer area and $\Delta \mathrm{T}$ is the temperature gradient.

Thermal conductivity depends on the temperature; a typical property of metallic substances is that the thermal conductivity decreases as the temperature increases. On the other hand, an insulator's capability to transfer heat increases as the temperature rises. Often, materials are not isotropic but the conductivity varies in different directions. Materials are, however, usually considered isotropic in calculations. Materials with high electrical conductivity are, generally, also good thermal conductors. On the other hand, the insulators used in electrical machines are, unfortunately, usually poor thermal conductors.

Analogous to the electric resistance, defined as the ratio of the potential difference to the current, we can define the thermal resistance R_{th} as a ratio of the temperature difference Θ to the heat flow rate Φ_{th}.

$$R_{th} = \frac{\Theta}{\Phi_{th}} = \frac{l}{\lambda S} \tag{48}$$

Here l is the length of the conductor, λ is the thermal conductivity and S the conducting area.

The second form of heat transfer is due to radiation. It is an electromagnetic radiation, the wavelength of which lies in the range from 0.1 to $100\ \mu m$. This wavelength range includes visible light, infrared radiation and the long wavelengths of ultraviolet radiation ($0.1 - 0.4\ \mu m$). In contrast to the other two heat exchange phenomena, radiation does not require a medium for heat exchange. When radiation meets an object, part of it is absorbed into the object, some of it is reflected back from the surface of the object and some may transmit through the object.

The heat flow density q_{th} of radiation is defined by the Stefan–Boltzmann equation:

$$q_{th} = \frac{\Phi_{th}}{S} = \varepsilon_{th}\, \sigma_{SB}\, (T_1^4 - T_2^4)$$

In the equation above, T_1 is the temperature of the radiating surface, T_2 the temperature of the absorbing surface and σ_{SB} is the Stefan–Boltzmann constant ($\sigma_{SB} = 5.67 * 10^{-8}$). ε_{th} is the relative emissivity between the emitting and absorbing surfaces and depends on the characteristics of the surfaces and on the position of surfaces to each other.

In analogy to the conduction, the thermal resistance is defined as

$$R_{th} = \frac{T_1 - T_2}{\Phi_{th}} = \frac{1}{\alpha_r\, S} \tag{49}$$

where

$$\alpha_r = \frac{\varepsilon_{th}\, \sigma_{SB}\, (T_1^4 - T_2^4)}{(T_1 - T_2)}$$

is the heat transfer of radiation. It depends strongly on the temperatures of the emitting and absorbing surfaces. The temperature difference between the outer surface of an electrical machine and the surroundings is usually about $40\ K$ and the ambient temperature $20\ °C$. This leads to obtain $\alpha_r = 6\ W/m^2\, K$.

Convection is the third way to transfer heat. It is defined as the heat transfer between a region of higher temperature (here, a solid surface) and a region of cooler temperature (a coolant) that takes place as a consequence of motion of the cooling fluid relative to the solid surface. Knowledge of the boundary layers is essential in the analysis of the heat and mass transfer between the solid surface and the coolant flowing by the surface.

To facilitate the calculation process and minimize the number of parameters to be solved, certain dimensionless parameters have been generated. Of the numerous such parameters available in the literature, the three most important ones when

calculating heat transfer from solid surfaces to the coolant are the Nusselt number Nu, the Reynolds number Re and the Prandtl number Pr.
Convection heat transfer coefficient α can be found with the Nusselt number:

$$Nu = \frac{\alpha\, L}{\lambda}$$

Here L is the characteristic surface length and λ the thermal conductivity of the coolant.
The Nusselt number describes the effectiveness of convection heat transfer compared with conduction heat transfer.
The ratio between inertia and viscous forces is described by the Reynolds number Re and can be described by the equation

$$Re = \frac{v\, L}{\varsigma}$$

where v is the speed of the coolant on the surface, L is the characteristic length of the surface and ς is the kinematic viscosity of the coolant. The value of the Reynolds number at which the flow becomes turbulent is called the critical Reynolds number Re_{cr}.
The third dimensionless number is the Prandtl number, which describes the thickness ratio of velocity and the thermal boundary layers. The Prandtl number is described by the equation

$$\mathrm{Pr} = \frac{c_p\, \mu}{\lambda}$$

where c_p is the specific heat capacity, μ the dynamic viscosity and λ the thermal conductivity of the coolant. The Pr numbers depends on the temperature and pressure.
Convection can be divided into forced and natural convection. In forced convection, external instruments such as pumps or blowers assist the flow of coolant. Natural convection is caused by density variations resulting from temperature differences: as the coolant is heated, it changes its density, and the local changes in density in the coolant–solid interface result in buoyancy forces that cause currents in the coolant.
Newton's law of cooling defines the heat flow density q th created by convection:

$$q_{th} = \frac{\Phi_{th}}{S} = \alpha_{th}\, \Theta$$

Hence, the thermal resistance of convection is:

$$R_{th} = \frac{\Theta}{\Phi_{th}} = \frac{1}{\alpha_{th}\, S} \tag{50}$$

in which α_{th} is the heat transfer coefficient. The value of the heat transfer coefficient depends on the viscosity of the coolant, the thermal conductivity, specific heat capacity and flow velocity of the medium. Traditionally, the heat transfer coefficient has been defined by various empirical correlations.

For a typical radial flux electrical machine, there are three significant convection coefficients related to the frame, air gap and coil ends (the last two ones are very complex cases).

One may use the Miller relation in order to estimate the heat transfer coefficient for natural and forced convection in the air around a horizontally mounted, unfinned cylindrical motor of diameter D with ambient temperature close to room temperature can be calculated as

Natural convection	Forced convection
$\alpha_{th} \approx 1.32 \left(\frac{\Theta}{D}\right)^{0.25} \left[\frac{W}{m^2\, K}\right]$	$\alpha_{th} \approx 3.89 \left(\sqrt{\frac{v}{l}}\right) \left[\frac{W}{m^2\, K}\right]$

Here Θ is the temperature difference, v the air velocity and l the length of the machine frame.

To calculate the heat transfer coefficient from the rotor to the air-gap or from the stator to the air-gap the Nusselt number Nu is needed. According to (Pyrhonen, Tapani, & Hrabovcovà, 2008) it is:

$$\begin{aligned} Nu &= 2 && \text{for } Ta < 1700 \\ Nu &= 0.128\, Ta^{0.367} && \text{for } 1700 < Ta < 10^4 \\ Nu &= 0.409\, Ta^{0.241} && \text{for } 10^4 < Ta < 10^7 \end{aligned}$$

where

$$Ta = \frac{\rho^2\, \Omega^2 \delta^3\, r_m}{\mu_v^2}$$

where ρ is the mass density of the fluid, Ω the angular velocity of the rotor, r_m the average of the stator and rotor radii, δ the air gap, and μ_v the dynamic viscosity of the fluid. Hence, the heat transfer coefficient is:

$$\alpha_{th} = \frac{Nu\ \lambda}{\delta}$$

The heat transfer coefficient in the coil ends is more difficult to approximate. In the space between the rotor and the end winding the heat transfer coefficient is determined by the rotation speed of the rotor. In the space between the end winding and the frame the speed of the air stream is much smaller than in the space between the rotor and the end winding. The flow may be assumed to be laminar which means that the convection is natural and also radiation has to be taken into account.
Figure 75 represents the different types of heat transfer in a permanent magnet synchronous machine. Convection is presented with green arrows, radiation with purple arrows and conduction with red arrows. The radiation inside the machine is not taken into account in the figure.

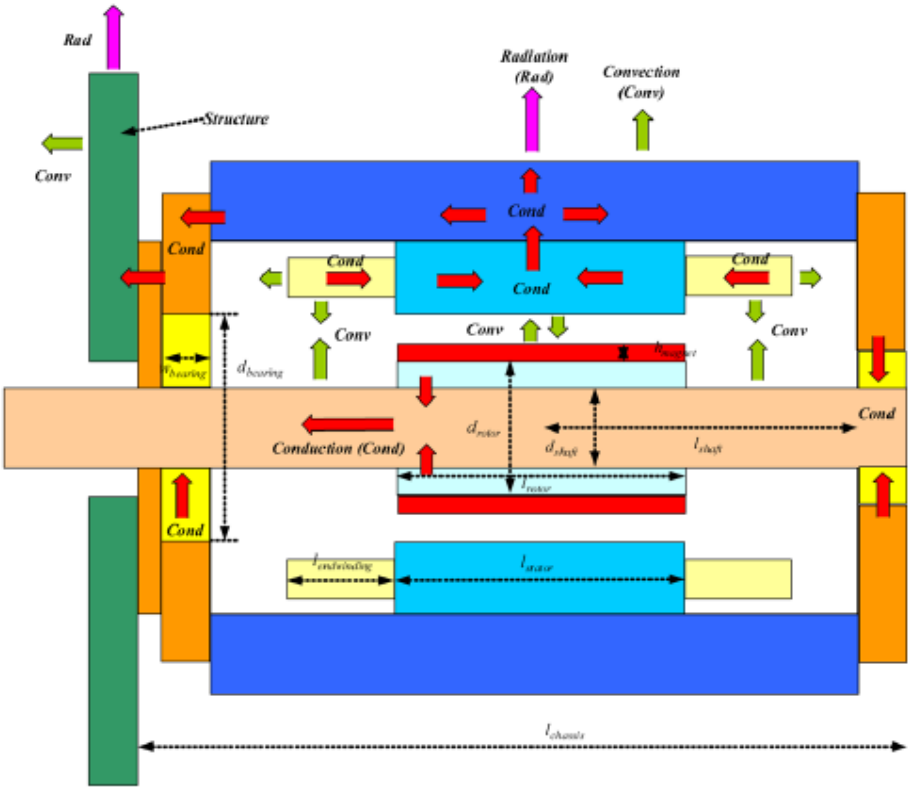

Figure 75.Heat transfer in a surface mounted permanent magnet motor

4.3 Thermal equivalent circuit

The heat-removal calculation only tells us whether enough heat can be removed from the machine surface in the stationary state. However, when considering the operation of the machine, it is essential to define the internal temperature distribution, which is regulated by the flux densities, frequencies and current densities in the machine parts.

To determine the internal temperature distribution, a lamped-parameter thermal network is used for modelling the heat transfer of the machine. Heat transfer analysis is the counterpart to electrical-network analysis with the following equivalences: temperature to voltage, power to current and thermal resistances to electrical resistances. In the heat-transfer network, a thermal resistance circuit describes the main paths for power flow, enabling the temperatures of the main components within the machine to be predicted for a given loss distribution.

As is well known, in a thermal network, it is possible to lump together components that have similar temperatures and to represent each as a single node in the network. Nodes are separated by thermal resistances that represent the heat transfer between components. Inside the machine, a set of conduction thermal resistances represents the main heat-transfer paths, such as from the winding copper to the stator tooth and back iron (in this case, the heat transfer is through the winding insulation consisting of a combination of enamel, impregnation, and slotliner materials), from the tooth and stator back iron nodes to the stator bore and housing interface, etc. In addition, internal convection and radiation resistances are used for heat transfer across the air gap and from the end windings to the endcaps and housing. External convection and radiation resistances are used or heat transfer from the outside of the machine to ambient.

In the past, due to limited computational capabilities, simple thermal networks with few thermal resistances, capacitances, and sources were adopted [12]. Nowadays, much more detailed thermal and flow networks can be quickly solved, including a high number of thermal and flow elements [6].

As an example of this approach, the thermal model shown in figure 76 has been used to analyze the design test cases. Analytical lumped-circuit techniques are also very useful in determining the thermal model's required discretization level. This refers to the number of sections used to model the electrical machine as a whole, or some of the more critical components, both in the axial and radial directions. For this work purpose, the thermal behavior only in the radial direction has been modelled, with particular attention being given to the winding area. Due to its low thermal conductivity [2–3 $W/(m\,°C)$], this area is of great thermal significance and has to be analyzed with care. In the real winding, the heat generation is distributed over the section, and this work highlights the impact upon accuracy of specifying such a loss in the discrete nodes. Concentrating all loss in one node in the network results in an

unrealistic gradient between the wall and the winding center. Thus, using lower levels of discretization reduces the accuracy of the results, while increasing the node numbers unnecessarily complicates the thermal model. Moreover, the thermal conductivity of the system winding, impregnation and insulation depends on several factors, such us material and quality of the impregnation, residual air quantity after the impregnation process and so on. If the equivalent thermal conductivity k_{Cu} is known, the thermal resistance between the winding and the stator lamination can be easily computed. According to [5]

$$k_{Cu,eq} = 0.2749\ [(1 - k_{Cus})S_{Cus}\ l]^{-0.4471} \tag{51}$$

where k_{Cus} is the slot fill factor, S_{Cus} is the slot area (see equation 39) and l is the axial core length.

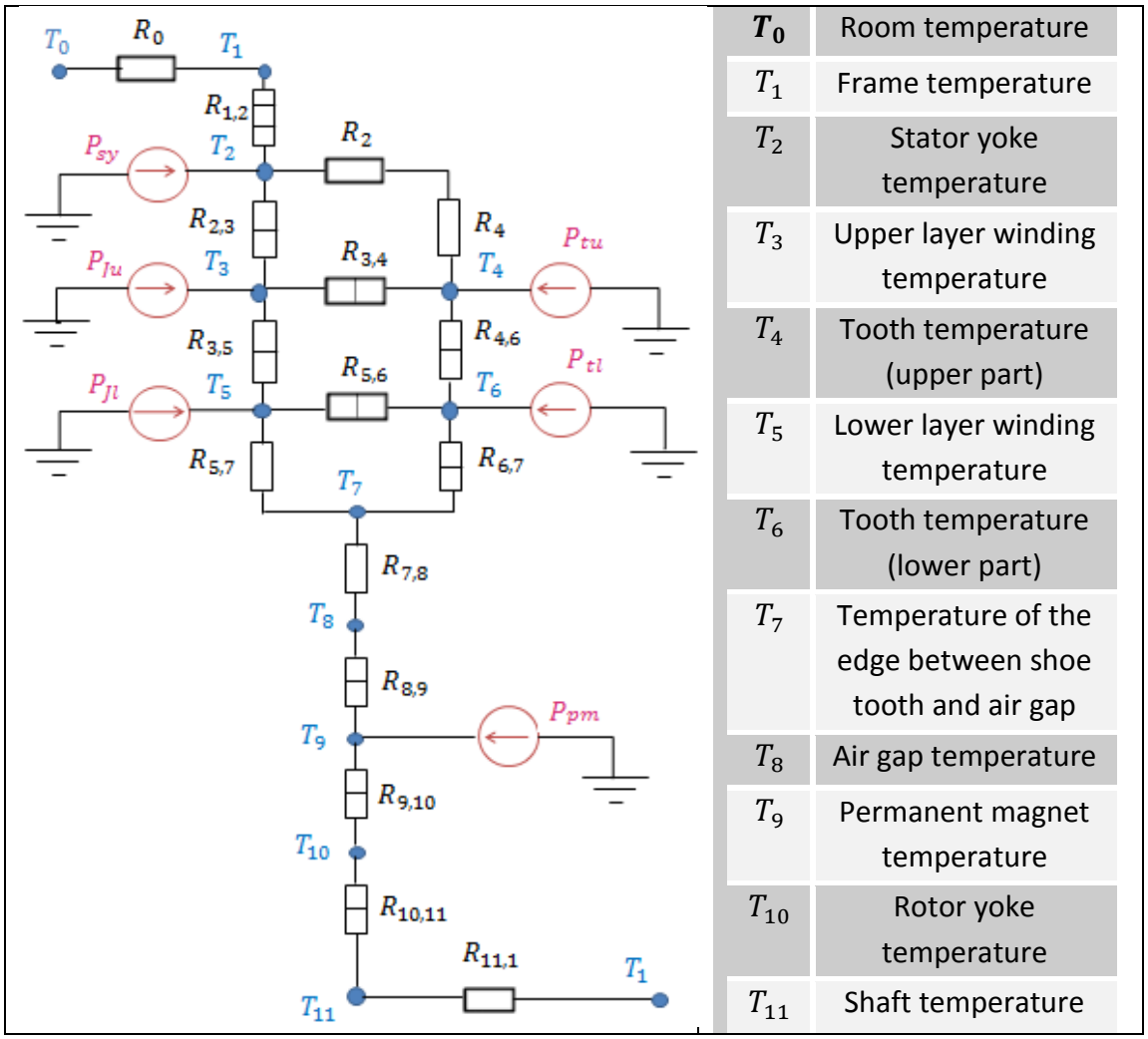

T_0	Room temperature
T_1	Frame temperature
T_2	Stator yoke temperature
T_3	Upper layer winding temperature
T_4	Tooth temperature (upper part)
T_5	Lower layer winding temperature
T_6	Tooth temperature (lower part)
T_7	Temperature of the edge between shoe tooth and air gap
T_8	Air gap temperature
T_9	Permanent magnet temperature
T_{10}	Rotor yoke temperature
T_{11}	Shaft temperature

Figure 76.Thermal network and explanation of nodes temperatures

Note that it has been considered the worst case: the radiation heat transfer is neglected, a constant ambient temperature is assumed and the external frame is not

finned. Finned structures allow to notably increase the heat transfer surfaces and thus to improve the heat flow towards the external ambient.
The temperatures in the nodes of the network can be solved by writing equations for the heat flows. The equations are written in matrix form

$$\boldsymbol{G\,T = P}$$

$$\begin{vmatrix} G_1 & -G_{1,2} & 0 & 0 & 0 & 0 & 0 & 0 & 0 & 0 & -G_{1,11} \\ -G_{1,2} & G_2 & -G_{2,3} & -G_{2,4} & 0 & 0 & 0 & 0 & 0 & 0 & 0 \\ 0 & -G_{2,3} & G_3 & -G_{3,4} & -G_{3,5} & 0 & 0 & 0 & 0 & 0 & 0 \\ 0 & -G_{2,4} & -G_{3,4} & G_4 & 0 & -G_{4,6} & 0 & 0 & 0 & 0 & 0 \\ 0 & 0 & -G_{3,5} & 0 & G_5 & -G_{5,6} & -G_{5,7} & 0 & 0 & 0 & 0 \\ 0 & 0 & 0 & -G_{4,6} & -G_{5,6} & G_6 & -G_{6,7} & 0 & 0 & 0 & 0 \\ 0 & 0 & 0 & 0 & -G_{5,7} & -G_{6,7} & G_7 & -G_{7,8} & 0 & 0 & 0 \\ 0 & 0 & 0 & 0 & 0 & 0 & -G_{7,8} & G_8 & -G_{8,9} & 0 & 0 \\ 0 & 0 & 0 & 0 & 0 & 0 & 0 & -G_{8,9} & G_9 & -G_{9,10} & 0 \\ 0 & 0 & 0 & 0 & 0 & 0 & 0 & 0 & -G_{9,10} & G_{10} & -G_{10,11} \\ -G_{1,11} & 0 & 0 & 0 & 0 & 0 & 0 & 0 & 0 & -G_{10,11} & G_{11} \end{vmatrix}$$

$$\boldsymbol{P^T} = \begin{vmatrix} 0 & P_{sy} & P_{Ju} & P_{tu} & P_{Jl} & P_{tl} & 0 & 0 & P_{pm} & 0 & 0 \end{vmatrix}$$

in which P_{sy} are the iron losses in the stator yoke, P_{tu} and P_{tl} are the iron losses in the upper and lower parts of a tooth ($P_{tu} = P_{tl}$), P_{Ju} and P_{Jl} are the Joule losses respectively in the upper and lower layers and P_{pm} are the Eddy current losses in the permanent magnets.
In the matrix $\boldsymbol{G}$, the thermal conductances are

$$G_1 = G_o + G_{1,2} + G_{1,11}$$

$$G_2 = G_{1,2} + G_{2,3} + G_{2,4}$$

$$G_3 = G_{2,3} + G_{3,4} + G_{3,5}$$

$$G_4 = G_{2,4} + G_{3,4} + G_{4,6}$$

$$G_5 = G_{3,5} + G_{5,6} + G_{5,7}$$

$$G_6 = G_{4,6} + G_{5,6} + G_{6,7}$$

$$G_7 = G_{5,7} + G_{6,7} + G_{7,8}$$

$$G_8 = G_{7,8} + G_{8,9}$$

$$G_9 = G_{8,9} + G_{9,10}$$

$$G_{10} = G_{9,10} + G_{10,11}$$

$$G_{11} = G_{10,11} + G_{1,11}$$

where $G_0 = 1/R_0$ and $G_{m,n}$ are the thermal conductances of the network $G_{m,n} = 1/R_{m,n}$.
The thermal resistances of the network consist of the thermal resistances of the different machine parts:

$$R_0 = \frac{1}{\alpha\, A_0} \qquad R_{1,2} = R_{fr} + R_{ig} + R_{sy,u}$$

$$R_{2,3} = R_{sy,l} + R_{w,u} \qquad R_{2,4} = R_{sy,t} + R_{t,u}$$

$$R_{3,4} = R_{w,tu} + R_{t,tu} \qquad R_{3,5} = R_{w,mu} + R_{w,ml}$$

$$R_{4,6} = R_{t,mu} + R_{t,ml} \qquad R_{5,7} = R_{w,l}$$

$$R_{6,7} = R_{t,l} + R_{t,sh} \qquad R_{7,8} = R_{\delta,u}$$

$$R_{8,9} = R_{\delta,l} + R_{pm,u} \qquad R_{9,10} = R_{pm,l} + R_{ry,u}$$

$$R_{10,11} = R_{ry,l} + R_{sh,r} \qquad R_{1,11} = R_{sh,a}$$

Next the methods to calculate the thermal resistances of the different machine parts are explained. R_{fr} is the thermal resistance of the frame, R_{ig} is related to the interface gap between frame and lamination; the stator yoke has two thermal resistances in the radial direction and one resistance that is representative of the heat flow in the tangential direction. The resistance of the frame is

$$R_{fr} = \frac{\left[\ln\left(\frac{D_{se}}{2} + h_{ig} + h_{fr}\right) - \ln\left(\frac{D_{se}}{2} + ig\right)\right]}{sp\; k_{Al}\; l}$$

Here h_{ig} is the interface gap thickness and h_{fr} is the frame thickness; $sp = 2\pi/Q$ is the slot pitch in $[rad/s]$ and k_{Al} is the aluminum thermal conductivity, which is $k_{Al} = 209\ W/mK$ for electro-technical aluminum. All the thermal resistances in radial direction are calculated in the same way in the other parts of the motor, simply by putting the right dimensions (calculated in the preliminary design) at numerator and by changing the thermal conductivity at denominator; in the stator back iron, the space factor k_{Fe} has to be taken into account, while in the slot the total slot pitch sp has to be substituted by an its fraction because a slot does not fill the whole slot pitch. In the air gap, at low speed, the same equation may be used: this means that the convection heat flow may be neglected and only conduction is taken into account [11]. However, also a convection resistance has been calculated by using the convection coefficient α_{th} introduced in the section 4.1. The results have not shown great differences in terms of temperatures. In the iron and the shaft, the thermal conductivity $k_{iron} = 74.7\ W/mK$ has been used, in permanent magnets $k_{pm} = 9\ W/mK$ and for the winding the equivalent thermal conductivity k_{eq} introduced in Equation 51.

Other formulas have been used for the thermal resistances of the tooth ($R_{t,u}$, $R_{t,mu}$, $R_{t,ml}$, $R_{t,l}$) and the interface gap between lamination and external frame (R_{ig}); also the resistances related to the tangential heat flow in the stator yoke ($R_{sy,t}$), in the tooth ($R_{t,tu}$, $R_{t,tl}$) and in the winding ($R_{w,tu}$, $R_{w,tl}$) are computed in a different way; there is also a thermal resistance in the axial direction that is referred to half length of the motor shaft ($R_{sh,a}$):

$$R_{t,u} = R_{t,mu} = R_{t,ml} = R_{t,l} = \frac{h_c/4}{k_{iron}\, k_{Fe}\, l\, b_d}$$

$$R_{ig} = \frac{h_{ig}\, Q}{\pi\, D_{se} k_{air} l}$$

$$R_{sy,t} = \frac{(\pi D_{ys})/2Q}{k_{iron} k_{Fe} l\, h_{ys}}$$

$$R_{t,tu} = R_{t,tl} = \frac{b_d/2}{k_{iron}\, k_{Fe}\, l\ (h_c/2)}$$

$$R_{w,tu} = \frac{(3b_{sb} + b_{st})/4}{k_{Cu,eq}\ l\ (h_c/2)}$$

$$R_{w,tu} = \frac{(3b_{st} + b_{sb})/4}{k_{Cu,eq}\ l\ (h_c/2)}$$

$$R_{sh,a} = \frac{l/2}{k_{iron}\ (\pi\ D_{ri}^2/4)}$$

The idea is to calculate a suitable convection thermal resistance between frame (node 1) and ambient in order to estimate the convection-heat-transfer coefficient α by keeping the temperatures in the winding (T_3 and T_5) lower than 120°. In this way one may make an idea about the most suitable cooling method to adopt. Also the temperature rise of the magnets is important to know, because the permanent magnets can easily demagnetize in high temperatures.
Next, the tables of results are shown:

Table 4.Temperatures distribution in the 1-slot-per-pole-per-phase motor

α	$42.56\ W/m^2°C$
T_1	$109.39\ °C$
T_2	$115.68\ °C$
T_3	$118.68\ °C$
T_4	$118.52\ °C$
T_5	$119.98\ °C$
T_6	$119.08\ °C$
T_7	$118.59\ °C$
T_8	$92.82\ °C$
T_9	$84.36\ °C$
T_{10}	$54.36\ °C$
T_{11}	$47.59\ °C$

Table 5. Temperatures distribution in the 2-slots-per-pole-per-phase motor

α	$32.64\ W/m^2°C$
T_1	$112.45\ °C$
T_2	$117.49\ °C$
T_3	$118.29\ °C$
T_4	$118.88\ °C$
T_5	$119.98\ °C$
T_6	$119.52\ °C$
T_7	$119.14\ °C$
T_8	$91.01\ °C$
T_9	$67.55\ °C$
T_{10}	$48.35\ °C$
T_{11}	$41.41\ °C$

Because of the greater Joule losses in winding and the Eddy currents losses in permanent magnets, the 1-slot-per-pole-per-phase PMSM needs a cooling system more efficient than that one to which the 2-slots-per-pole-per-phase motor needs. This statement is justified by the higher value of the convection-heat-transfer coefficient in the first design test case. From the tables above, one may note that the temperatures in permanent magnets are quite safe with respect to the demagnetization. This last result has been also verified through Magnet 2D, in which the presence of points subjected to possible demagnetization can be predicted.

CONCLUSIONS

This thesis deals with the electromagnetic and thermal sizing and design refinement of permanent magnet synchronous motors.

A preliminary theoretical study has been described in order to better understand the model, the performances and the design space of the PMSMs. Then, an analytical sizing preliminary procedure has been carried out starting from free parameters and required rated quantities. Besides the rated parameters, such as torque, speed and supply voltage, there are a considerable number of free parameters that, when aiming for an optimal solution, is somehow limited because otherwise the task becomes extremely complicated. It has to be also highlighted that the machine design process has multiple properties that have to be optimized. This means that the best solutions are always compromises between different criteria.

The optimal solution also depends on the application that the machine is intended for. The preliminary design implementation does not take into account a specific application, but the design results can be modified to meet different requirements for different applications. It is easy to test how the results can be modified by changing different parameters. It is rather easy to obtain a number of possible design solutions for a given design situation by changing the free parameters, such as the materials to be used (both hard and soft ferromagnetic materials), the number of pole pairs, the number of slots per pole per phase, the number of layers in a slot and so on. The outputs are the dimensions of the machine; all main dimensions have been obtained by computing the magnetic voltages in all magnetic paths of the motor and, by defining the total magnetic voltage over the machine, it may be possible to calculate the permanent magnets height. Also the efficiency and the power factor are imposed as initial required values and they have to be verified a-posteriori.

Possible future developments of this thesis may involve different aspects: on one hand new optimization inputs and new cost functions (as the core losses, the constant power speed ratio, etc.) can be introduced according the requirements of the specific application under study; on the other hand, a reverse approach could be used by implementing in a spreadsheet an approximated analytical model of the machine which could be used to quickly check the performances of the machine for different combinations of the design parameters. Furthermore, more complex machine structures may be considered, such as interior permanent magnet motors, keeping anyway in mind the possible greater inaccuracy of analytical results.

An exact analytical solution of the field problem is rarely achieveble, because usually the structure under study is geometrically complex and the materials are non-linear and therefore only a numerical solution is possible. Therefore, in this thesis FEM

analysis was used to validate and refine the design process. Hence, after a preliminary sizing of two design test cases (a 1-slot-per-pole-per-phase motor with a single-layer winding and a 2-slots-per-pole-per-phase machine with a short pitch double-layer winding), the FEM analysis was used to reduce the cogging torque. After a brief recall about the cogging torque and the techniques presently considered as the state of the art to minimize it, different values of the magnet span and the slot opening have been simulated in order to find the best combination that minimize the cogging torque. The results highlighted that cogging torque has an almost linear dependence with the slot opening and this means that the narrower the slot opening, the smaller the cogging torque becomes. The slot opening range of simulation varies between the minimum acceptable from a manufacturing point of view and the value after which the slot becomes an open slot. More interesting is the dependence with the magnet width that highlights a clear minimum for both test cases.

The values obtained for such parameters as the best one able to minimize the cogging torque were used to get new values for the dimensions of the other parameters through the implemented analytical design and then the behavior of both design test cases at no-load and load conditions was simulated in order to validate the preliminary design.

For the 1-slot-per-pole-per-phase machine it can be seen that results provided by FEM analysis and by the analytical sizing procedure seem to be rather close each other in terms of current density and back-EMF. Yet, the rated torque disagree with an error more than 5%: the torque obtained by FEM is smaller than the analytically obtained value and this means that the analytical sizing overestimates the performances of the machine. In the 2-slots-per-pole-per-phase motor, the errors in back-EMF, current density and torque calculation decrease.

The efficiency and power factor are slightly different when calculated with FEM model rather than with the analytical models. With respect to efficiency, some difference occurs because the FEM software does not take into account the mechanical losses (venting losses) and additional losses. Therefore FEM analysis gives larger efficiency than the analytical dimensioning, in particular for the 2-slots-per-pole-per-phase motor. For this last case, the power factor is larger when calculated with FEM. When comparing the power factors it must be taken into account that the preliminary design assumes that the supply voltage is sinusoidal. This means that the harmonics created by for instance a frequency converter are not taken into account. In FEM calculation, this kind of assumption has not been made which may cause a difference between the power factors.

The amplitude of the fundamental component of the flux density in the air gap is smaller when calculated with FEM in both cases. The greatest differences in both test cases are related to the values of flux densities in the ferromagnetic structure: in FEM-based calculation they are smaller than the initial values used in the

analytical sizing. For sure, the air gap flux density level affects these values, although such aspect seems not enough to justify the errors. With standard sizing, there is an overestimation of the teeth and stator yoke thickness because the worst case is hypothesized, but the ferromagnetic materials seem to be well tapped at full load.

However, these differences do not represent great problems because FEM optimizations are always possible: for instance, in order to better exploit the ferromagnetic materials, higher flux density values may be achieved by reducing the widths of the stator and rotor yokes.

The accurate calculation of the iron losses is in any case rather difficult and requires modelling the physical phenomena in the iron. Empirical equations have to be applied in order to analytically estimate them and for this reason their computation has been entrusted to FEM. However, also the iron losses obtained with FEM models are indeed an approximation, although somewhat more accurate.

The calculated losses are the inputs of the thermal design: a lumped-parameters circuit has been applied to the design test cases in order to estimate the best cooling system by the definition of the most suitable convection-heat-transfer coefficient between external frame and ambient air. The results highlighted that the 1-slot-per-pole-per-phase motor needs a cooling system more efficient than the 2-slots-per-pole-per-phase one.

In summary, the employ of windings featuring double layer and short pitch allowed to obtain a smaller harmonic content in several quantities such as air gap flux density, back-EMF, etc.. This brings to get smaller errors in terms of back-EMF, flux densities and full-load torque between the preliminary sizing and FEM analysis. Moreover, the 2-slots-per-pole-per-phase motor has lower losses than the 1-slot-per-pole-per-phase, in particular those concerning the permanent magnets.

The above considerations lead to the conclusion that an optimized design produces benefits from both electromagnetic and thermal points of view.

Future possible developments may be aimed towards the creation of a loop that combines both the electromagnetic and thermal designs within an iterative process.

APPENDIX 1

Dimensions and other parameters of the design test cases before cogging torque minimization

Two models have been validated. The shaft power have been set to $160\ kW$, rotational speed to $2500\ rpm$, phase voltage to $690\ V$ and the number of pole pairs to $p = 4$ for both design test cases. The initial value of relative magnet width has been imposed to $\alpha_{PM} = 0.8$ and the slot opening to $b_o = 3\ mm$. The first design has 1 slot-per-pole-per-phase and the second one 2 slots-per-pole-per-phase. The dimensions given by the preliminary sizing are given below for the models.

Table 6. 1-slot-per-pole-per-phase PMSM

δ	$1.6\ mm$
l	$118.2\ mm$
Q	24
z_q	14
S_{cs}	$31.32\ mm^2$
b_d	$21.1\ mm$
b_{sb}	$30.1\ mm$
b_{st}	$21.3\ mm$
h_{sh}	$5.1\ mm$
h_c	$34.1\ mm$
h_{PM}	$5.1\ mm$
D_{ro}	$299.3\ mm$
D_{ri}	$236.7\ mm$
D_{se}	$453.8\ mm$
h_{sy}	$31.3\ mm$
h_{ry}	$31.3\ mm$
E_{PM}	$386.42\ V$
I_s	$140.92\ A$
R_{DC}	$0.88\ \Omega$
L_{md}	$0.001\ H$

Table 7. 2-slots-per-pole-per-phase PMSM

δ	$1.6\ mm$
l	$118.2\ mm$
Q	48
z_q	14
S_{cs}	$31.32\ mm^2$
b_d	$10.6\ mm$
b_{sb}	$18.2\ mm$
b_{st}	$10.2\ mm$
h_{sh}	$2.6\ mm$
h_c	$37.9\ mm$
h_m	$20.7\ mm$
h_{PM}	$5.3\ mm$
D_{ro}	$298.6\ mm$
D_{ri}	$235.9\ mm$
D_{se}	$503.8\ mm$
h_{sy}	$31.4\ mm$
h_{ry}	$31.4\ mm$
E_{PM}	$374.47\ V$
I_s	$140.92\ A$
R_{DC}	$0.94\ \Omega$
L_{md}	$0.0012\ H$

- **No-load and load results for the 1-slot-per-pole-per-phase motor**

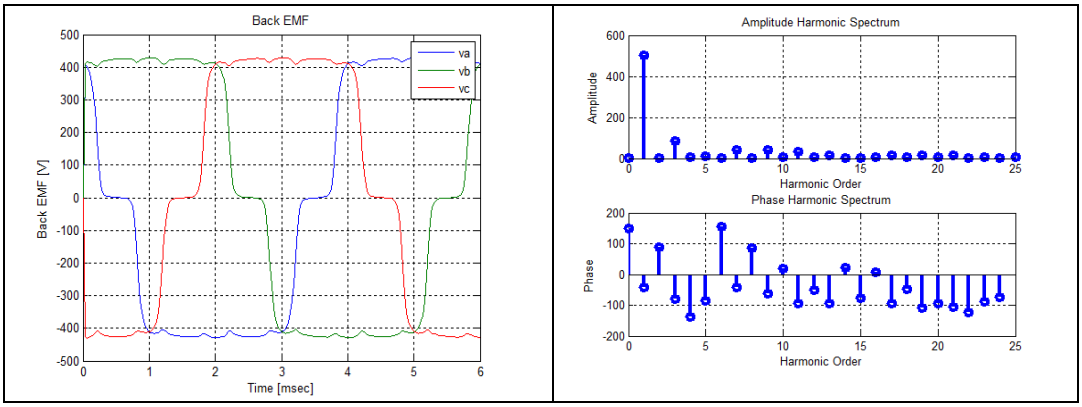

Figure 77.Back-EMFs and related amplitude and phase spectrums

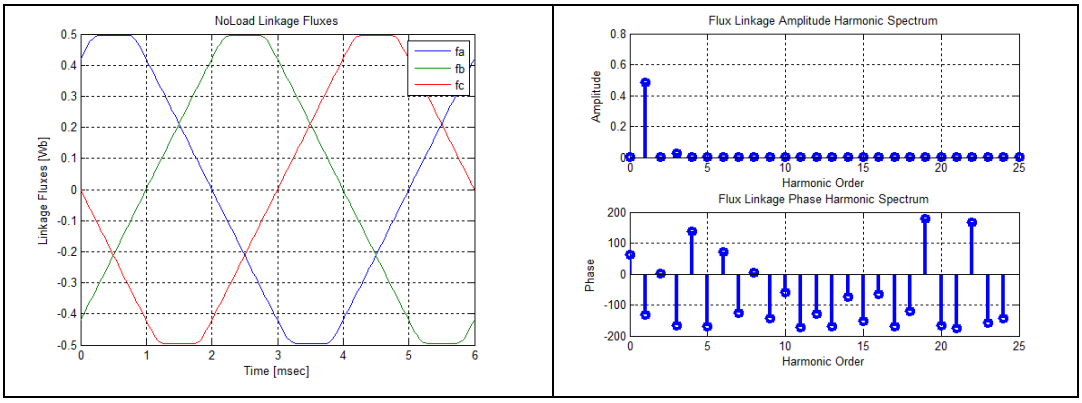

Figure 78.No-load linked fluxes and related amplitude and phase spectrums

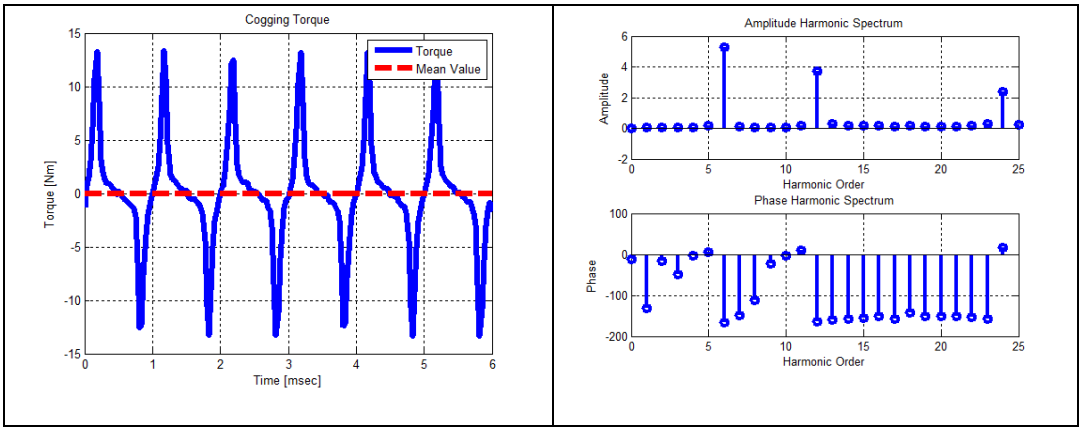

Figure 79.Cogging torque and related amplitude and phase spectrums

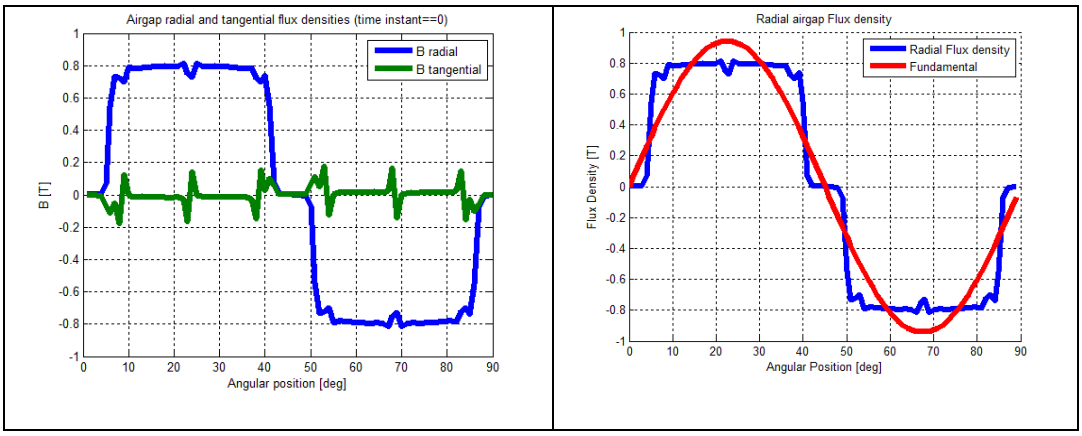

Figure 80.Tangential and radial air gap flux density with its fundamental

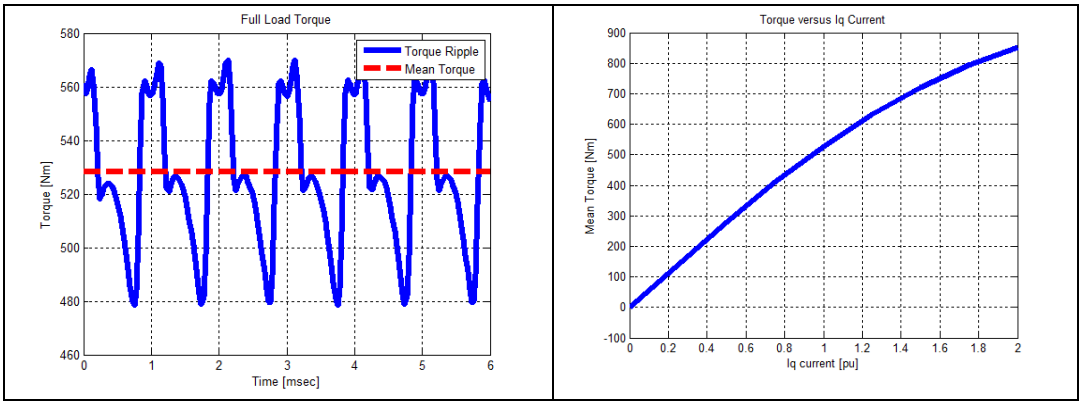

Figure 81.Full-load torque; torque vs I_q characteristic

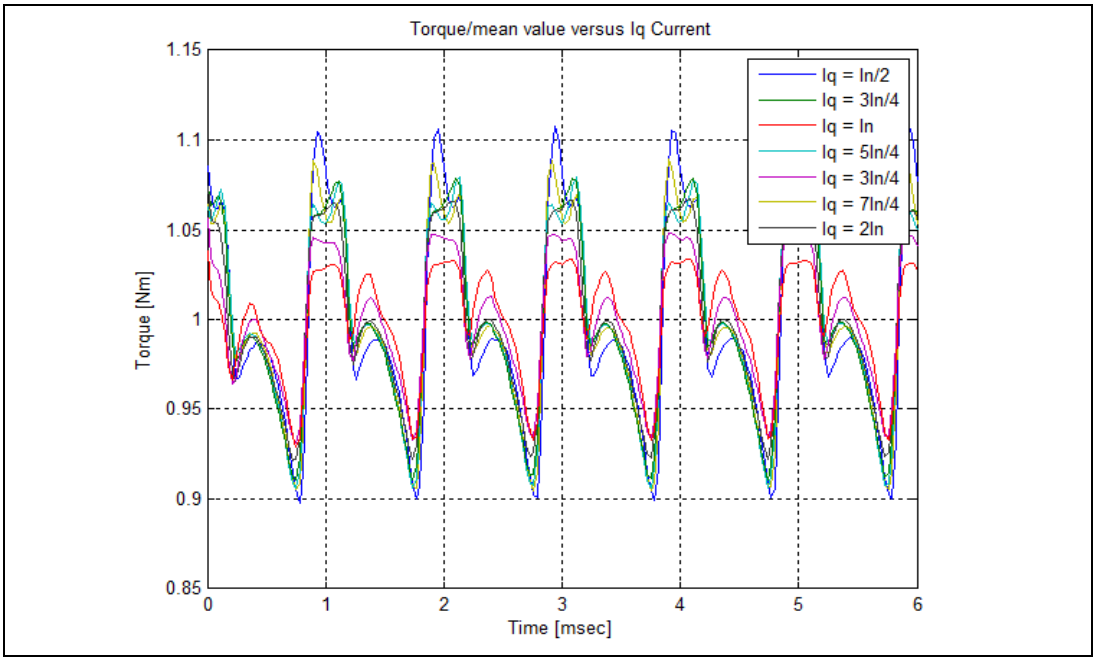

Figure 82.p.u torque profile vs mean value, for different values of I_q

- **No-load and load results for the 2-slots-per-pole-per-phase motor**

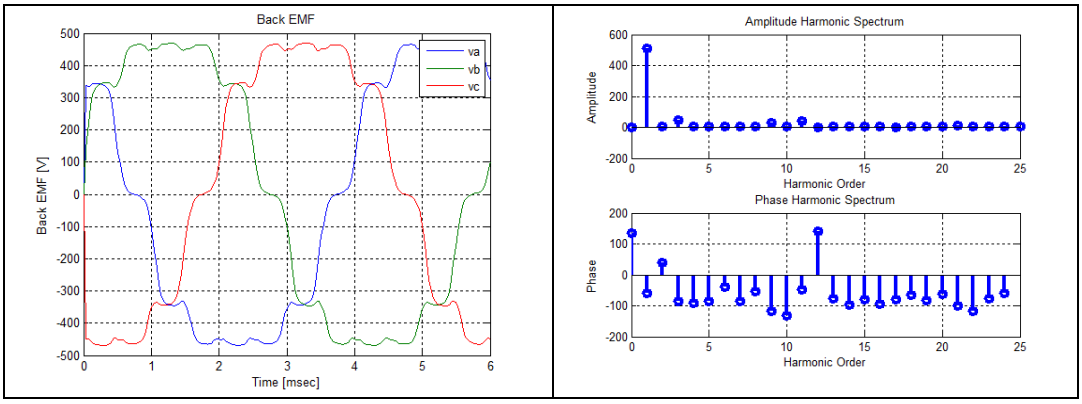

Figure 83.Back-EMFs and related amplitude and phase spectrums

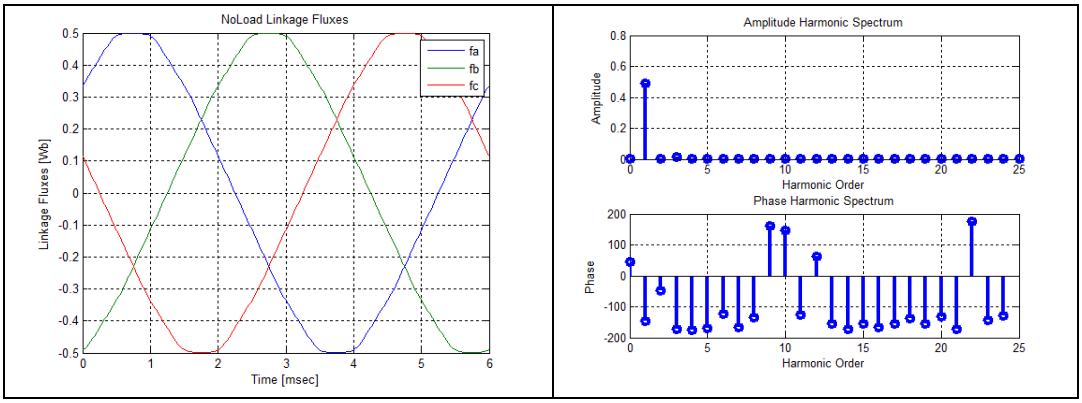

Figure 84.No-load linked fluxes and related amplitude and phase spectrums

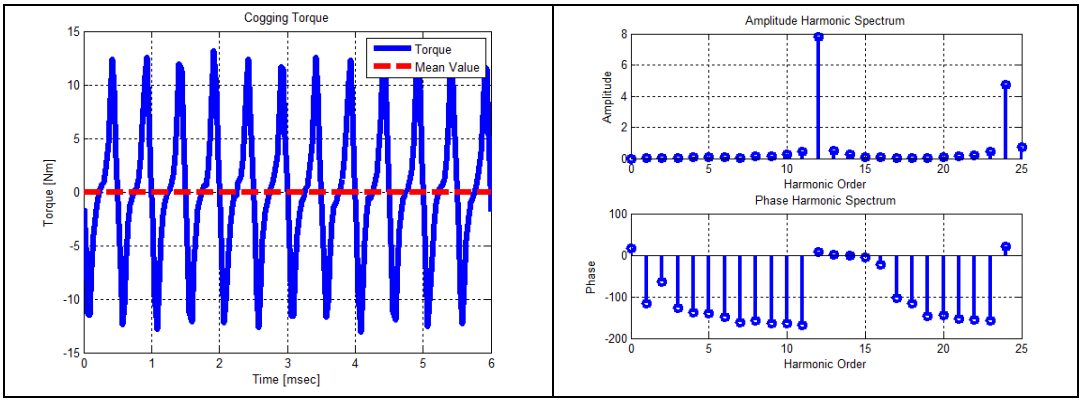

Figure 85.Cogging torque and related amplitude and phase spectrums

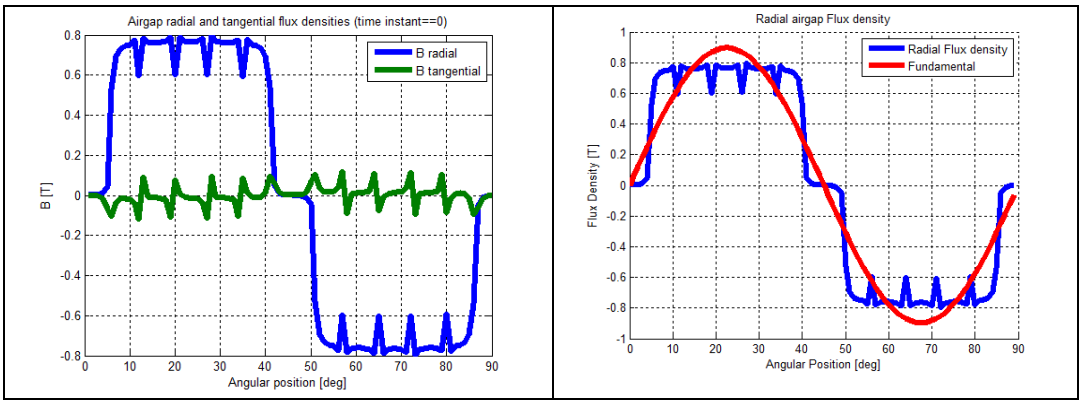

Figure 86.Tangential and radial air gap flux density with its fundamental

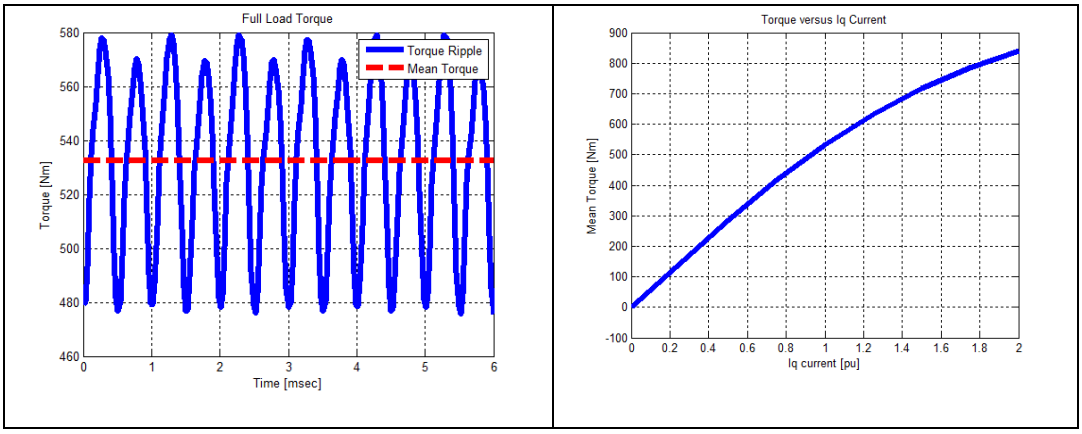

Figure 87.Full-load torque; torque vs I_q characteristic

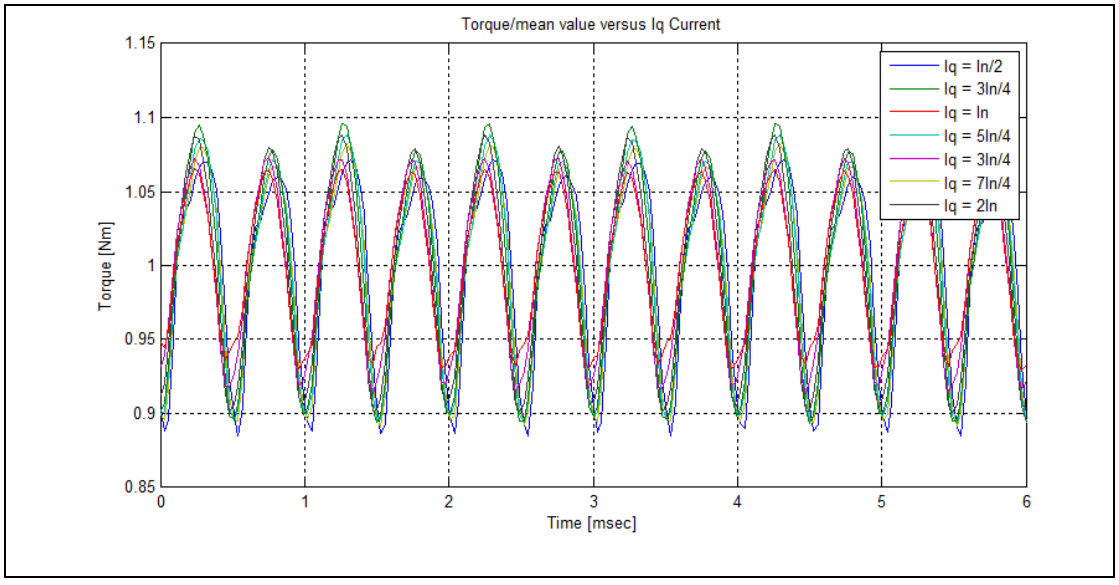

Figure 88.p.u torque profile vs mean value, for different values of I_q

APPENDIX 2

Dimensions and other parameters of the design test cases after cogging torque minimization

Shaft power ($160\ kW$), rotational speed ($2500\ rpm$), phase voltage ($690\ V$) and the number of pole pairs ($p = 4$) have been set. Now, the magnet widths are different for the two designs ($\alpha_{PM} = 0.7$ and $\alpha_{PM} = 0.68$ respectively) and the slot opening is the same for both test cases ($b_o = 3\ mm$). The first design has 1 slot-per-pole-per-phase and the second one 2 slots-per-pole-per-phase. The dimensions given by the preliminary sizing are given below for the models.

Table 8. 1-slot-per-pole-per-phase PMSM

δ	$1.6\ mm$
l	$118.2\ mm$
Q	24
z_q	15
S_{cs}	$31.32\ mm^2$
b_d	$22.1\ mm$
b_{sb}	$29.9\ mm$
b_{st}	$20.1\ mm$
h_{sh}	$5.1\ mm$
h_c	$37.5\ mm$
h_{PM}	$5.8\ mm$
D_{ro}	$297.6\ mm$
D_{ri}	$240.4\ mm$
D_{se}	$454.9\ mm$
h_{sy}	$28.6\ mm$
h_{ry}	$28.6\ mm$
E_{PM}	$378.45\ V$
I_s	$140.92\ A$
R_{DC}	$0.95\ \Omega$
L_{md}	$0.0014\ H$

Table 9. 2-slots-per-pole-per-phase PMSM

δ	$1.6\ mm$
l	$118.2\ mm$
Q	48
z_q	8
S_{cs}	$31.32\ mm^2$
b_d	$11.6\ mm$
b_{sb}	$14.7\ mm$
b_{st}	$9.2\ mm$
h_{sh}	$2.5\ mm$
h_c	$41.8\ mm$
h_m	$23.3\ mm$
h_{PM}	$7.1\ mm$
D_{ro}	$295.0\ mm$
D_{ri}	$236.9\ mm$
D_{se}	$459.3\ mm$
h_{sy}	$29.0\ mm$
h_{ry}	$29.0\ mm$
E_{PM}	$382.44\ V$
I_s	$140.92\ A$
R_{DC}	$1.22\ \Omega$
L_{md}	$0.0012\ H$

APPENDIX 3

In the following tables, the values of thermal resistances referred to the lamped-parameters circuit of figure 76 are shown:

Table 10. 1-slot-per-pole-per-phase PMSM

$R_{1,2}$	0.074 °C/W
$R_{2,3}$	0.218 °C/W
$R_{2,4}$	0.164 °C/W
$R_{3,4}$	0.848 °C/W
$R_{3,5}$	0.403 °C/W
$R_{4,6}$	0.099 °C/W
$R_{5,6}$	0.709 °C/W
$R_{5,7}$	0.218 °C/W
$R_{6,8}$	0.065 °C/W
$R_{7,8}$	6.57 °C/W
$R_{8,9}$	6.67 °C/W
$R_{9,10}$	0.114 °C/W
$R_{10,11}$	0.410 °C/W
$R_{1,11}$	0.035 °C/W
R_0	1.28 °C/W

Table 11. 2-slots-per-pole-per-phase PMSM

$R_{1,2}$	0.148 °C/W
$R_{2,3}$	0.394 °C/W
$R_{2,4}$	0.162 °C/W
$R_{3,4}$	0.291 °C/W
$R_{3,5}$	0.722 °C/W
$R_{4,6}$	0.212 °C/W
$R_{5,6}$	0.238 °C/W
$R_{5,7}$	0.395 °C/W
$R_{6,8}$	0.122 °C/W
$R_{7,8}$	13.13 °C/W
$R_{8,9}$	13.37 °C/W
$R_{9,10}$	0.261 °C/W
$R_{10,11}$	0.823 °C/W
$R_{1,11}$	0.036 °C/W
R_0	2.535 °C/W

BIBLIOGRAPHY

1) An, Y., An, H., Sun, D., Zhao, W., & Xue, L. (2012). *Study on Cogging Torque in PM motor with Pole Width Modulation Rotor.* Shenyang: IEEE.

2) Barcaro, M., Bianchi, N., & Magnussen, F. (2010). *Design Considerations to maximize Performance of an IPM Motor for a Flux-Weakening Region.* International Conference on Electrical Machines.

3) Bianchi, N. (2005). *Electrical Machines Analysis using finite elements.* Taylor & Francis Group.

4) Bianchi, N., Bolognani, S., Consoli, A., Jhans, T., Lorentz, R., Lovelance, E., et al. (2004). *Design, Analysis and Control of Interior PM Synchronous Machines.* Seattle: IEEE IAS Tutorial Course Notes.

5) Boglietti, A., Cavagnino, A., & Staton, D. (2008). *Determination of Critical Parameters in Electrical Machine Thermal Model.* New Orleans: IEEE.

6) Boglietti, A., Cavagnino, A., Staton, D., Shanel, M., Mueller, M., & Mejuto, M. (2009). *Evolution and Modern Approaches for Thermal Analysis of Electrical Machines.* IEEE.

7) Bramerdorfen, G., Silber, S., Marth, E., Jungmayr, G., & Wolfgang, A. (2012). *Analytic Determination of Cogging Torque Harmonics of Brushless Permanent Magnet Machines.* Linz: Internetional Symposium on Power Electronics, Electrical Drives, Automation and Motion.

8) Gieras, J. F., & Wing, M. (2002). *Permanent Magnet Motor Technology - Design and Applications.* Marcel Dekker, Inc.

9) Guru, B., & Hiziroğlu, H. (2001). *Electric Machinery and Transformers, 3rd ed.* Oxford University Press.

10) Hanselman, D. (2006). *Brushless Permanent Magnet Motor Design.* Orono: Magna Phisics Publishing.

11) Lipo, T. (2007). *Introduction to AC Machine Design.* Wisconsin.

12) Mellor, P., Roberts, D., & Turner, D. (1991). *Lumped parameter thermal model for electrical machines of TEFC design.* Sheffield: IEE Proceedings.

13) Morimoto, S. (2007). *Trends of Permanent Magnet Synchronous Machines, Vol.2.* Transactions on Electrical and Electronic Engineering.

14) Pyrhonen, J., Tapani, J., & Hrabovcovà, V. (2008). *Design of Rotating Electrical Machines.* Chicester, UK: John Wiley & Sons, Ltd.

15) Wang, D., Wang, X., & Jung, S.-Y. (2013). *Cogging Torque Minimization and Torque Ripple Suppression in Surface-Mounted Permanent Magnet Synchronous Machines Using Different Magnet Widths.* Jinan: IEEE Transactions on magnetics.